DEBONDING FAILURE OF FIBER REINFORCED POLYMERS

Bhavna Sharma

and

Ian N. Robertson

Research Report UHM/CEE/06-03

August 2006

UNIVERSITY OF HAWAII
COLLEGE OF ENGINEERING

DEPARTMENT OF CIVIL AND ENVIRONMENTAL ENGINEERING

Abstract

The use of Fiber Reinforced Polymer (FRP) is becoming more common in the construction industry for repair and retrofitting of concrete structures. The material has many advantages for an externally retrofitted member. Research into FRP has found that the typical failure modes are premature debonding or delamination, rupture of the FRP, and failure at the anchorage point. Debonding failure occurs when the FRP is no longer adhered to the member due to a crack or separation of the fiber-matrix and bond interface resulting from increased strain in the strip. Through varying the substrate material strength and surface preparation, this thesis investigates the FRP-concrete interface to develop a better understanding of FRP debonding behavior.

This thesis explores FRP debonding through three different experiments. The first employs a steel plate substrate to eliminate the effects of the concrete and understand the debonding behavior. In the second experiment the surface preparation of concrete specimens is varied to determine the effect of the surface on the debonding process. Finally, the anchorage zone is investigated through a series of pullout tests. Based on these experiments, the factors and limits involved in Fiber Reinforced Polymer (FRP) debonding failure are determined.

Acknowledgements

This report is based on a Masters Thesis prepared by Bhavna Sharma under the direction of Dr. Ian Robertson. The authors would like to thank Drs. H. Ronald Riggs, Si-Hwan Park, and Gregor Fischer for their contributions during the course of this project.

All FRP materials used in this study were graciously donated by SIKA Inc. The specimens were constructed by the staff of the University of Hawaii at Manoa Structural Testing Laboratory. Thanks are extended to Miles Wagner and Gaur Johnson for their assistance throughout the project.

This research was supported by funding from the Federal Highway Administration (FHWA) and the Hawaii Department of Transportation (HDOT) research contract No. 47770. This contents of this report reflect the views of the authors, who are responsible for the facts and accuracy of the data presented herein. The contents do not necessarily reflect the official views or policies of the State of Hawaii, Department of Transportation or the Federal Highway Administration. This report does not constitute a standard, specification or regulation.

Table of Contents

Tables

Figures

Chapter 1: Introduction

1.1 Project Summary

Infrastructure in the United States will require significant maintenance and rehabilitation in the next ten to thirty years due to the lifespan of pre-stressed and reinforced concrete structures. The Salt Lake Boulevard Bridge, in the City and County of Honolulu, is a 3-span pre-stressed concrete girder bridge, built in 1968, over the Halawa stream. A recent bridge inspection and evaluation found the shear capacity of some bridge girders to be inadequate (Riggs et al., 2002). Visual inspections also found hairline diagonal shear cracks in some girders. An external retrofit was designed and proposed with Fiber Reinforced Polymer (FRP) composites to strengthen the bridge girders. The project included preliminary research conducted at the University of Hawaii at Manoa's Civil and Environmental Engineering Structural Testing Laboratory.

The *Instrumentation and Monitoring the Performance of the FRP Shear Strengthening of the Salt Lake Boulevard Bridge* project investigated the application of FRP to externally strengthen pre-stressed girders. The objective of the project is to obtain benchmark data for use in developing a remote monitoring system for the FRP using fiber optic instrumentation (Riggs et al., 2002). Research previously conducted includes large-scale pre-stressed T-beam tests, as well as smaller specimens that investigated the failure of the FRP. The study presented in this thesis is comprised of single-face and double-face shear specimens that will further explore the FRP – concrete bond interface and the debonding failure mode of the FRP.

1.2 Introduction

The use of Fiber Reinforced Polymer (FRP) is becoming more common in the construction industry for repair and retrofit of concrete structures. The material has many advantages for an externally retrofitted member. The studies presented here explore the behavior and factors involved in the debonding failure mode of the FRP, including the concrete strength, surface preparation and the significance of anchorage.

Research into FRP has found that the typical failure modes are premature debonding or delamination, rupture of the FRP, and failure at the anchorage point. Debonding failure occurs when the FRP is no longer adhered to the member due to a crack or separation of the fiber-matrix and bond interface resulting from increased strain in the strip. This failure mode is often referred to as intermediate crack (IC) debonding. IC debonding failure usually initiates at a crack in the concrete and propagates along the FRP laminate, which produces interfacial shear stress between the FRP and the adhesive as well as between the adhesive and the concrete substrate. A more detailed investigation has shown that the interfacial bond strength is a critical factor in debonding failure.

Applications of FRP are typically bonded to concrete, which is a substrate that has an unpredictable and varying effect on the FRP – concrete interface. Concrete strength and surface preparation can also influence the bond interface, however the impact of these parameters continues to be investigated. Anchorage zones also continue to be researched, as the behavior of the material differs greatly from that of steel. The FRP typically fails before reaching the ultimate strength due to premature debonding. The major factors involved in anchorage zone failure are the FRP bond design and anchorage length. Further investigations of the FRP-concrete bond interface, by varying the substrate material strength and surface preparation, are used here to study the debonding behavior, and determine the factors that affect debonding.

1.3 Literature Review

Fiber reinforced polymers (FRP) are appealing to civil engineers due to their high strength to weight ratio and resistance to corrosion. The use of composites for engineering applications has been researched globally and continues to be explored. Research topics on FRP include efficiency, performance of both internal and externally applied reinforcement, and the failure modes of FRP. The literature review of prior research presented here will focus on the debonding failure of externally applied FRP. Reinforced concrete (RC) beams that are externally strengthened with FRP have six categories of failure: FRP rupture and steel yielding; concrete compressive failure; concrete shear failure; debonding of the concrete layer along rebar; delamination of FRP plate; and peeling due to shear crack (Buyukozturk and Hearing, 1998). Debonding failure can be influenced by various factors.

Investigation of FRP retrofit of reinforced concrete beams mainly utilizes experiments in bending, which provides information about the overall performance of the reinforced concrete – FRP system. For study of the debonding failure of FRP, the experiments usually attempt to replicate the tension face of the beam to gather the most information on the concrete–FRP bond interface. To eliminate any bending effects, tension tests are used with direct shear type specimens.

Ueda and Dai, reviewed the prior research conducted on FRP and noted test methods and specimens used to determine interfacial bond behavior with shear type specimens as: (a) single lap, (b) double lap, (c) inserted and (d) bending (Fig. 1.1). The authors also noted the three major failure modes of FRP retrofits are plate-end failure, anchorage failure and mid-span debonding (Ueda and Dai, 2005).

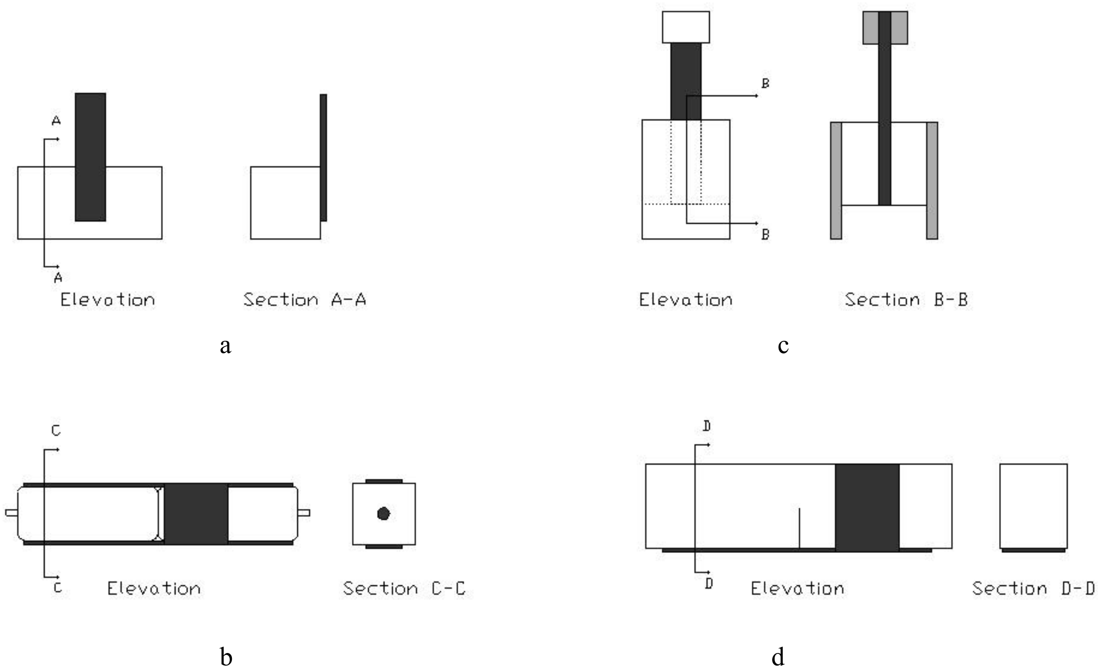

Figure 1.1: Shear Type Specimens: (a) single lap; (b) double lap, (c) inserted; (d) bending.

The bending mid-span debonding failure mode has been extensively investigated. Typically failure is initiated by an intermediate crack, which causes a mode II, or shearing failure, to occur within the concrete-FRP interface. Investigation of the concrete-FRP bond has provided additional factors that influence debonding. The type of FRP system, surface preparation, epoxy, and concrete strength have been varied to determine their significance (Arduini and Nanni, 1997; Bizindavyi and Neale, 1999;

Brena et al., 2005; Chajes et al., 1995, 1996; De Lorenzis et al., 2001; Wu, 2003). Research has found that the surface preparation and concrete strength affect the bond shear transfer (Chajes et al., 1996; De Lorenzis et al., 2001; Harmon et al., 2003; Nakaba et al., 2001). Authors have found little difference between mechanical abrasion and grinding of the surface, however both types of preparation provide a good bond in comparison to no preparation. The research work on the significance of the concrete strength, i.e. low vs. high strength, also has not provided definitive results. The FRP systems are varied and in general can be categorized into wet lay-up, pre-preg, and pre-cured systems. All of these systems can be used for beam retrofits and perform well providing additional strength to the beam. Additional factors that are investigated are related to the bond stress-slip relationship (Kanakubo et al., 2005; Nakaba et al., 2001; Yuan et al., 2004).

Nakaba et al. (2001) investigated the bond strength and stress-slip relationship using a pure tensile experiment. These authors used mathematical and numerical analysis to determine the bond stress-slip model, and subsequently the strain in the FRP and bond stress distributions. They illustrated three types of stress-slip bond models: (a) cutoff type, (b) bilinear type, and (c) tensile softening type (Fig. 1.2). Slip is defined as the

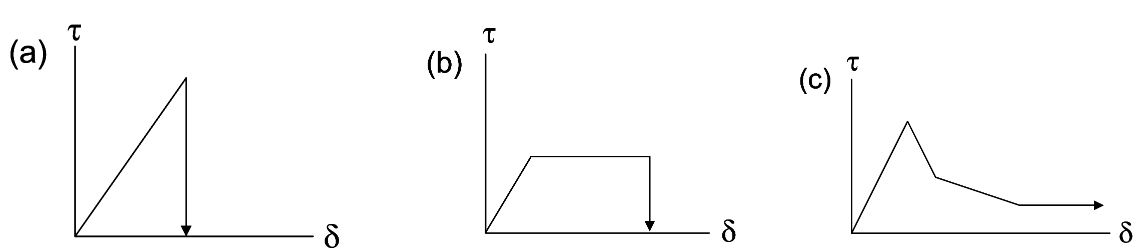

Figure 1.2: Stress-slip bond models: (a) cutoff; (b) bilinear; (c) tensile softening

sum of the difference between the elongation of the FRP and elongation of the equivalent section of concrete, epoxy and reinforcement from the loaded end of the specimen to the free end of the FRP. Nakaba et al. (2001) found that the bond stress is limited to the area surrounding the crack. These authors determined that delamination of the FRP caused the bonded area to shift, until the entire strip delaminates.

To further quantify the impact of the factors affecting debonding failure of the FRP, fracture mechanics and computational analysis can be used to provide additional information. The use of Finite Element Analysis (FEA) has provided modeling techniques which attempt to quantify the significance of these factors (Alfano et al., 2005; Leung, 2004; Wu and Yin, 2003). Theoretical framework has also been utilized to further understand the behavior of debonding failure. These investigations provide information on the interfacial shear stresses, fracture energy and behavior of crack induced debonding (Lau et al., 2001; Leung, 2001; Rasheed and Pervaiz, 2002; Yuan et al., 2004). The significance of these factors facilitates a better understanding of the behavior of FRP failure.

New guidelines on design and analysis of FRP-strengthened beams, based on the above investigations, are providing additional information to improve the efficiency and use of FRP in civil engineering (Chen and Teng, 2003; Harmon et al., 2003; Oehlers et al., 2005). The American Concrete Institute Committee 440 (ACI 440) is responsible for providing guidelines for the use of FRP in civil engineering applications. The ACI 440R-02 guide notes a need for accurate methods of prediction for debonding failure of

FRP. The guidelines provides surface preparation and anchorage methods to help prevent debonding failure. The surface preparations are abrasive or water blasting techniques that achieve a concrete surface profile (CSP) of 3. The CSP is defined by the International Concrete Repair Institute guidelines for surface preparation (ICRI, 1997). The ACI 440R-02 design guidelines cover flexural and shear applications, including coefficients to account for potential debonding failure. The calculations account for the fact that laminates with a greater stiffness are more likely to delaminate.

The ACI 440R-02 guidelines present three types of FRP wrapping schemes for shear strengthening as shown in Figure 1.3: (a) complete wrap, (b) u-shaped, and (c) two-sided bonding. The most efficient scheme is complete wrapping and the least efficient is two-sided bonding. Two-sided bonded face plates are noted to delaminate before loss of aggregate interlock of the concrete. The guide suggests analysis of bond stresses to determine efficiency of the FRP system and the effective strain that can be achieved in the FRP prior to delamination. The active bond length, L_e, is the length over which the majority of the bond stress is transferred into the FRP.

a b c

Figure 1.3: FRP Shear Wrapping Schemes: (a) complete wrap; (b) u-shaped; (c) two-sided bonding

The ACI guidelines note that mechanical anchorage helps to develop larger tensile forces, and also is effective at increasing stress transfer in the bond interface. (As noted earlier, the bond interface is vital to delamination failure and is further complicated by the cracking of the concrete substrate.) According to the ACI guide, debonding usually results when the substrate is unable to maintain the interfacial shear and normal stress in the bond, which results in the FRP debonding with a relatively thin layer of concrete attached to it. The research discussed here has helped to develop the use of FRP in civil engineering applications, however the need for long-term field data is one area of research necessary for the prediction of lifespan of FRP systems (ACI 440R-02).

1.4 Project Objectives

The objective of this study is to explore debonding failure through three different experimental approaches. The first test utilizes a steel plate substrate to eliminate the effects of the concrete substrate and to provide a better understanding of the debonding behavior. In the second experiment, the surface preparation and strength of the concrete specimens are varied to determine the effect on the bond interface and the debonding process. Finally, the anchorage zone is investigated through a series of pullout tests. These three sets of experiments will be used to determine the factors and limits involved in Fiber Reinforced Polymer (FRP) debonding failure.

Chapter 2: Steel Debonding Specimens

2.1 Introduction

The majority of FRP debonding specimens in the literature have a reinforced concrete substrate, which provides an accurate model for the typical application of FRP. Delamination typically occurs due to failure of the surface concrete bonded to the FRP. To eliminate concrete failure as a mechanism, a specimen with a steel substrate was tested. The specimen was designed as a benchmark for comparison with the other specimens in this study.

2.2 Experimental Setup

2.2.1 Specimens

The first two identical specimens, S1A and S1B, each consisted of a pre-cured CFRP strip bonded to the surface of two ¼ inch thick steel plates as shown in Figure 2.1. The

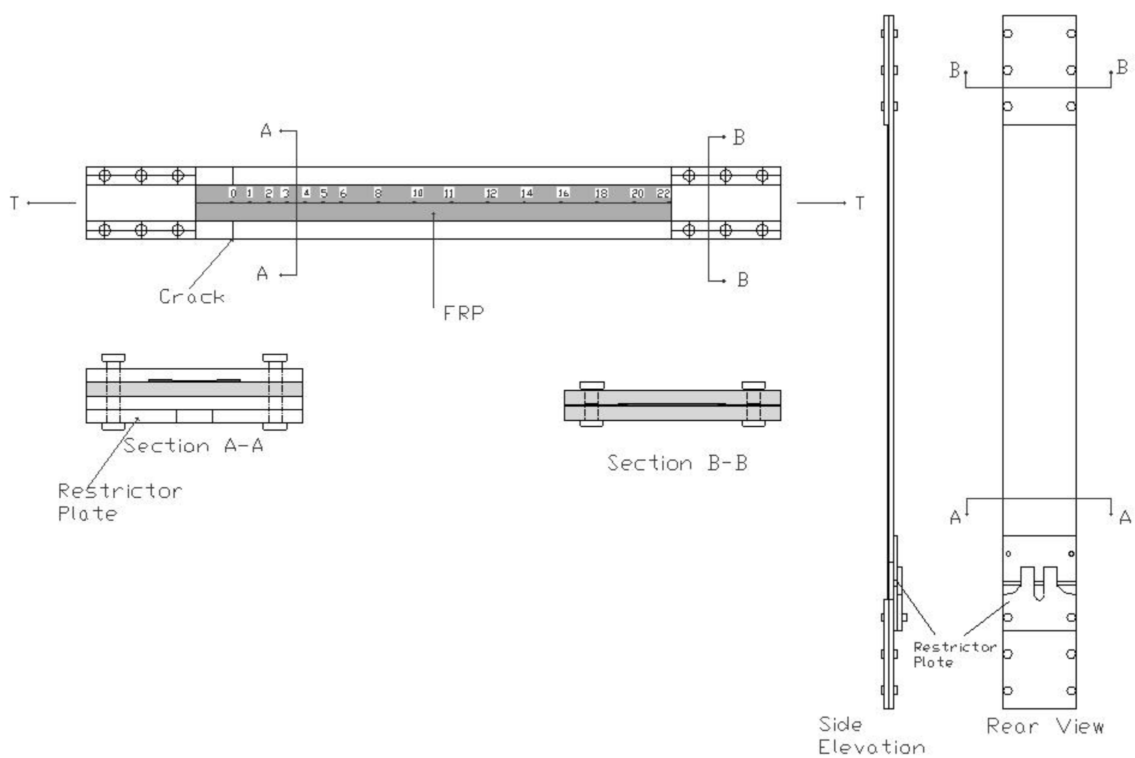

Figure 2.1: Steel Plate Specimens, S1A and S1B

two plates were temporarily bolted together, by two bracing plates on the back of the bonded side of the specimen, to create a simulated crack. The bolts were removed prior to testing. Preliminary tests showed that the increased stiffness of one side of the specimen, due to the single FRP laminate, caused a shearing failure. A restrictor plate

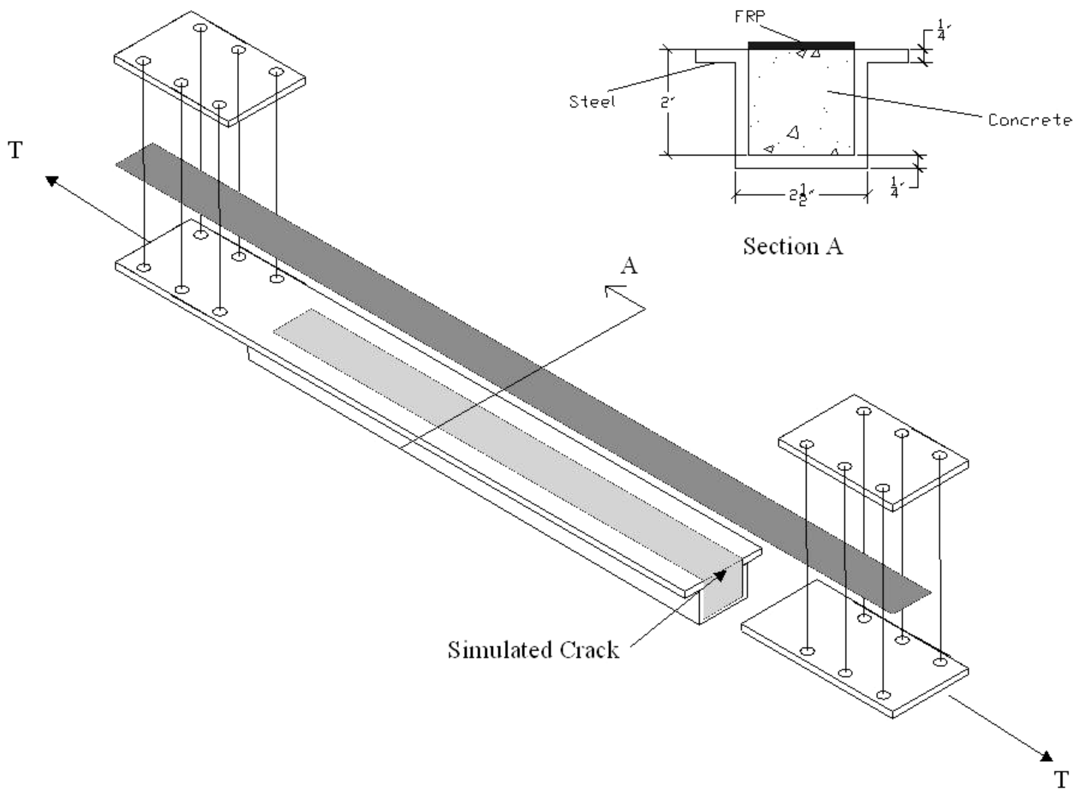

Figure 2.2: Steel—Concrete Specimen, SC1

was added to ensure that the specimen was loaded axially (Fig. 2.1). The specimen also had additional steel clamping plates at either end to serve as anchorage for the FRP. The third specimen, SC1, was a modified version of specimens S1A and S1B with a u-shaped trough filled with concrete (Fig. 2.2). The FRP was bonded to the concrete surface and anchored at each end with additional steel clamping plates. The specimen was designed so that the applied tension force, T, was applied directly to the bond interface between the FRP and the concrete.

2.2.2 Material Properties

A Sika Carbodur S512 pre-cured pultruded CFRP laminate (Table 2.1) with an epoxy resin matrix was used for both specimens, along with the manufacturer recommended Sikadur 30, a two-component, structural epoxy paste adhesive (Table 2.2). The SC1 specimen had a low strength normal weight concrete substrate, with material properties as listed in Tables 2.3 and 2.4.

Table 2.1. Sika CarboDur S 512 Design Properties

Tensile Strength	37.8 x 10^3 lbs (168 kN)
Modulus of Elasticity	23.9x10^6 psi
Elongation at Break	1.69%
Thickness	0.047 in (1.2mm)
Width	1.97 in (50mm)
Cross Sectional Area	0.093 sq. in. (60mm^2)

Table 2.2. Sikadur 30 Design Properties

Tensile Strength	3,600psi (24.8 MPa)
Modulus of Elasticity	6.5 x 10^5 psi (4,482 MPa)
Elongation at Break	1%
Recommended Surface Preparation	ICRI CSP 3

Table 2.3. Concrete Mixture Design Proportions

Material	Mix 1
Coarse Aggregate [lb/yd^3]	1576
Maui Dune Sand [lb/yd^3]	431
Concrete Sand [lb/yd^3]	825.6
Cement [lb/yd^3]	683.7
Water [lb/yd^3]	307.7
W/C ratio	0.45
Daratard [oz/sk]	3
Darex [oz/sk]	2

Table 2.4. Concrete Compressive Strengths

Cylinder	Area [in^2]	Compressive Strength [psi] Mix 1
1	28.27	6260
2	27.34	6543
3	28.27	6207
Average Strength		6337

2.2.3 Surface Preparation

Specimens S1A and S1B were prepared using a sandblaster to clean the steel surface. The plate was then cleaned to remove dust particles before applying the FRP. The concrete surface had no surface preparation and was cleaned using an air hose to remove loose particles from the surface.

2.2.4 Installation

The Carbodur strip was cut into a 38-inch strip and cleaned using MEK solvent. The two-part epoxy was mixed following manufacturer instructions. The steel surface was cleaned using acetone before applying the epoxy. The epoxy was applied to the Carbodur strip in a thin layer (less than 1/32 in). The strip was then centered on the steel plate and pressed on to squeeze out excess epoxy. At the ends of the specimen, epoxy was placed on both sides of the strip to adhere the clamping plates to the specimen. Excess epoxy was wiped clean from the edges of the FRP strip using acetone. The concrete in the SC1 specimen was poured and allowed to cure before applying the Carbodur strip. The FRP was installed using the same procedure for the S1A and S1B specimens. All specimens were allowed to cure for at least 3 days before instrumentation and 7 days before testing.

2.2.5 Crack Gage Instrumentation

An Epsilon clip-on gage with a gage length of 3 mm was used to monitor the crack width as the load was applied.

2.2.6 Strain Gage Instrumentation

The CFRP strip was instrumented with electric resistance strain gages (ERSG), placed along the strip to monitor longitudinal strain. The strain gages were applied according to the manufacturer's instructions. The gages had a 2.105 strain gage factor and a resistance of 350 ohms. One strain gage was placed at the crack. Six gages were installed at intervals of 1 inch for the first 6 inches from the crack, and then at intervals of two inches for the remainder of the strip (Figure 2.1).

2.2.7 Test Setup

The specimen was placed in a 2 Post MTS universal test frame. A National Instruments system, running Labview software, was used to monitor the applied load, frame displacement, crack gage and strain gages during the experiment. To capture post peak response and strain changes in the FRP strip during delamination, the test was run in displacement control. This mode maintains the displacement while the load fluctuates during the experiment. The loading rate for the experiment was 0.168 mm/min.

2.3 Results

The results show that by measuring the strain in the FRP strip, it was possible to detect the initiation of debonding and subsequent failure. Both steel specimens, S1A (Fig. 2.3) and S1B failed in the adhesive layer. The steel specimens provided information on the behavior of the FRP-substrate bond interface in the debonding failure. Analysis of the results from each of the steel specimens are outlined below. The notation used in the results correspond to the distance of the point of measurement from the crack. For example, Strain0 is located at the crack and Strain14 is located fourteen inches from the crack. During the experiment, some strain measurements were lost due to malfunction of the gage, and are noted in the legend key without a symbol. The dashed line indicates the initiation of debonding failure.

Figure 2.3: Photo of S1A Specimen with debonding failure in the adhesive

2.3.1 <u>Specimen S1A</u>

Figure 2.4 shows the strain gage measurements for all gages during the test of specimen S1A. The strain at the crack (Strain0) increases, as the specimen is loaded, followed by the increase in strain of the next gage (Strain1) and so on. Debonding is observed when the strain in the second gage equals that of the first gage, i.e. there is no longer any bond transfer between the two gage locations. Debonding occurs between Strain0 and Strain1 at 3500 microstrain., as indicated by the dashed line Soon after, Strain2 increases to match Strain1 at approximately 4000 microstrain. This debonding continued in a controlled manner as each subsequent gage reached the same strain as the gages on the

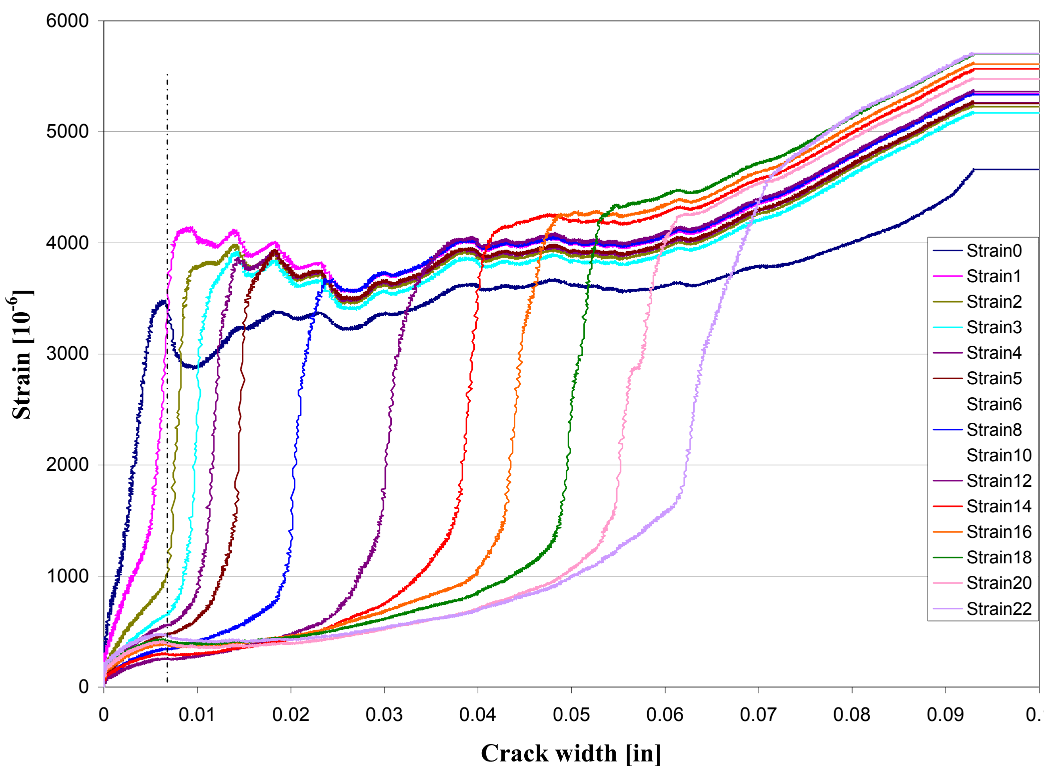

Figure 2.4: Strain vs. Crack width for Specimen S1A

delaminated section. The final readings indicate the strip is no longer bonded and is transferring the load directly from one end anchorage to the other.

Figure 2.5 shows the effect of debonding on the load and crack mouth opening displacement (CMOD). The maximum load of 7.4 kips occurs at a CMOD of 0.006 inches, which corresponds to the initial debonding of the area around the crack. As the CMOD increased, the load continued to decrease from the maximum. The fluctuations in the load correspond to debonding of subsequent segments of the strip. The increase in load after 0.06 crack opening is the result of the fully debonded CFRP transferring the load from one anchorage end to the other.

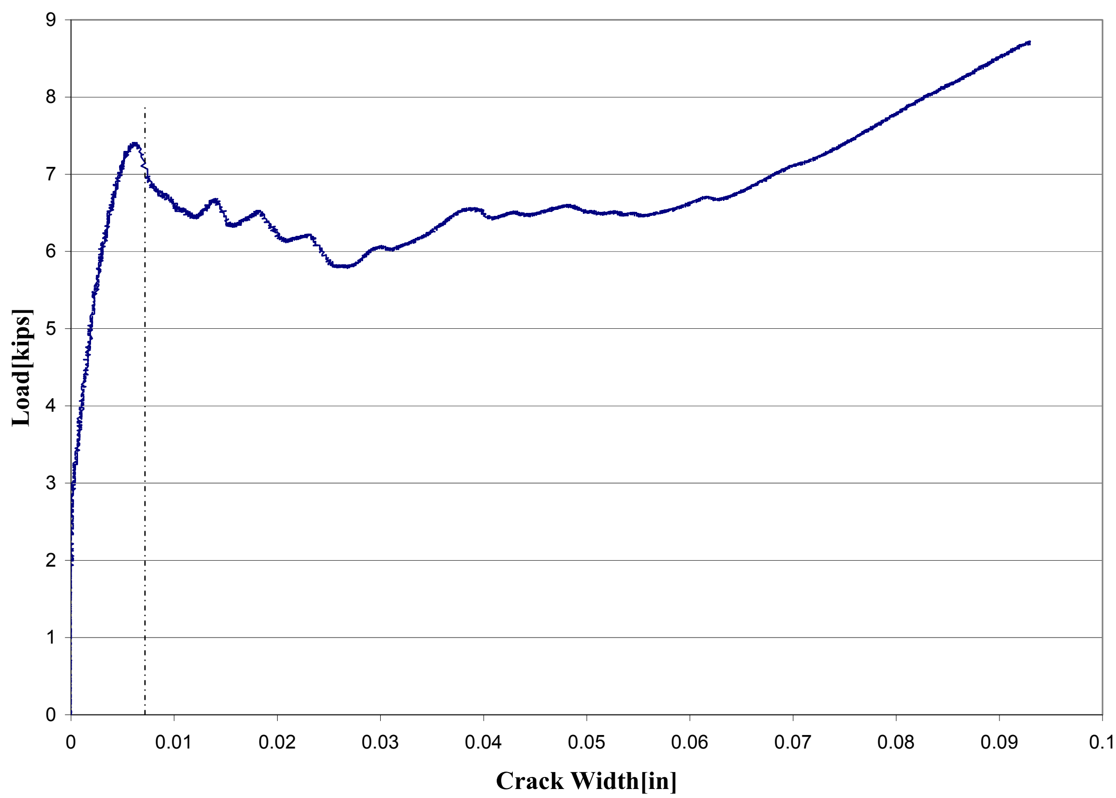

Figure 2.5: Load vs. Crack Width for Specimen S1A

Figure 2.6 shows the strain profile along the length of the FRP strip corresponding to the maximum shear stress in the epoxy between two gages. The dashed lines are profiles measured at every 500th increment. The notation is reading line number, followed by the location of the reading and the maximum shear stress at that location. Gages in the debonded region record high strain, with a sharp decrease in strain, to the remaining bonded area which remains at a low strain. As the test progresses, the strain in the strip remains uniformly high, this is an indication of debonding. The maximum shear stress, 2814 psi, was observed between 1-2 inches from the crack. The sandblasted surface preparation and anchorage helped to increase the bond transfer between the FRP and the steel substrate.

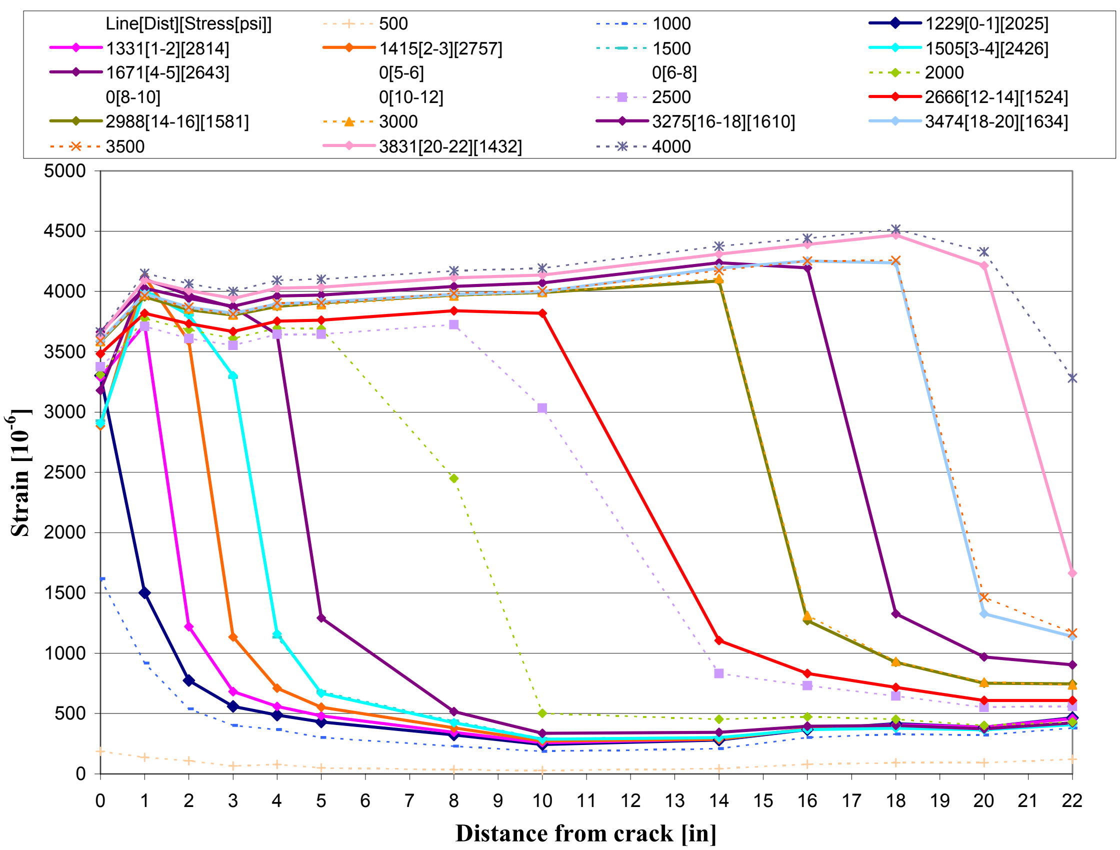

Figure 2.6: Strain vs. Distance from the Crack for Specimen S1A

Shear Stress– Crack Width

An additional method to analyze the shear stress is to calculate the average bond shear stress using the measured strain in the strip. The equation for the average interfacial bond shear stress was derived using the following equations:

$$\Delta\varepsilon = \varepsilon_n - \varepsilon_{n+1}$$
$$\sigma_n = \varepsilon_n E_{FRP}$$
$$\tau \cdot w_{FRP} \cdot \Delta x_i = \sigma_n \cdot w_{FRP} \cdot t_{FRP} - \sigma_{n+1} \cdot w_{FRP} \cdot t_{FRP}$$
$$\tau \cdot w_{FRP} \cdot \Delta x_i = (\sigma_n - \sigma_{n+1}) \cdot w_{FRP} \cdot t_{FRP}$$
$$\tau \cdot w_{FRP} \cdot \Delta x_i = E_{FRP}(\varepsilon_n - \varepsilon_{n+1}) \cdot w_{FRP} \cdot t_{FRP}$$
$$\tau = \frac{E_{FRP}(\varepsilon_n - \varepsilon_{n+1}) \cdot w_{FRP} \cdot t_{FRP}}{w_{FRP} \cdot \Delta x_i}$$

which results in the equation below:

$$\tau = \frac{(\varepsilon_n - \varepsilon_{n+1}) \cdot E_{FRP} \cdot t_{FRP}}{\Delta x_i} \quad \text{at limit} \frac{\Delta\varepsilon}{\Delta x_i} \qquad [1]$$

τ – average interfacial bond stress; ε_n – strain at n; ε_{n+1} – strain at n+1; Δx_i – the distance between the two gages; E_{FRP} – modulus of elasticity of the CFRP; w_{FRP} - width of the FRP strip; and t_{FRP} – thickness of the FRP strip.

The interfacial shear stress is calculated using two adjacent strain gages. The bond shear stress obtained is at the limit and the error is proportional to the size of the bond area or the distance between two gages. The FRP strip is instrumented with strain gages at intervals of 1 inch for the first 6 inches from the crack, and then at intervals of 2 inches for the remainder of the strip (Figure 2.1). The distance between the gages provides an approximate measure of bond shear stress. This approximation does not capture the maximum shear stress developed in the bond.

Figure 2.7 displays the increase and decrease of shear stress along the strip as the crack propagates, which was calculated using equation [1]. The notation represents the interfacial shear stress between two measurement points, i.e. c0-1 is the interfacial shear stress in the area one inch away from the crack. As the crack opening increases, the shear stress one inch from the crack begins to increase, illustrated by the linearly ascending branch to a peak shear stress. The peak stress is followed by a linearly descending branch, which represents interface softening.

As the shear stresses on a particular 1 inch long segment passes its peak value, delamination has begun for that section. Delamination is complete when the shear stress

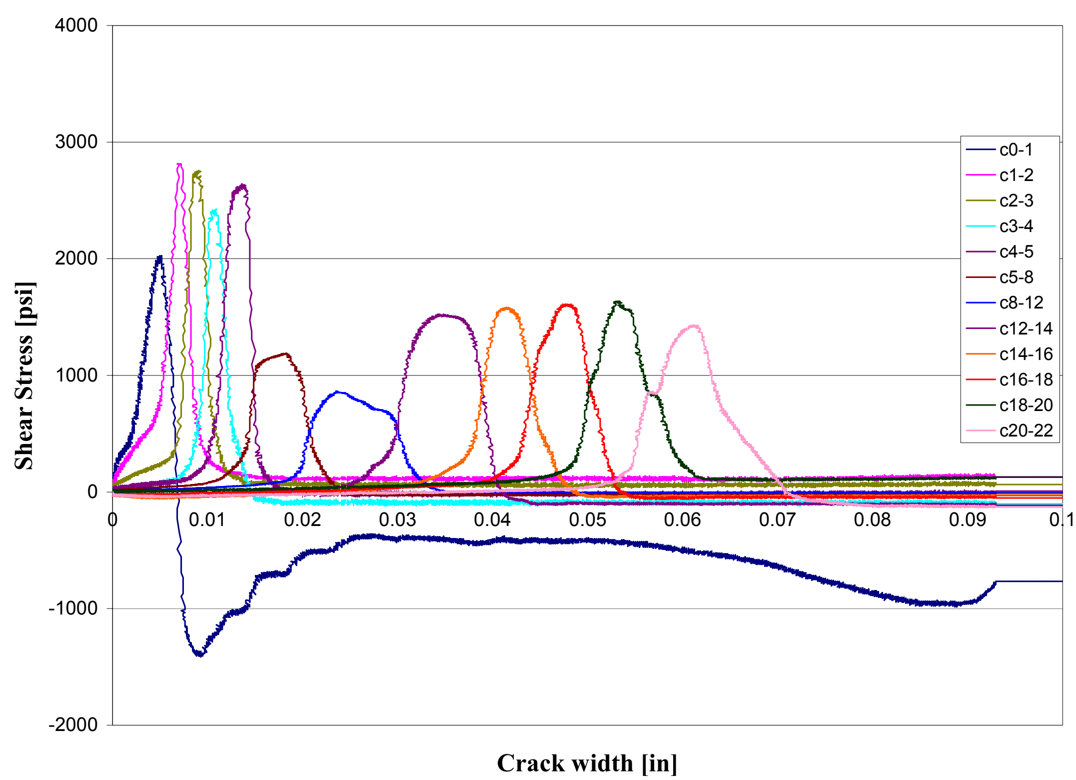

Figure 2.7: Shear Stress vs. Crack Width for Specimen S1A

drops to zero, at which time the adjacent segments are reaching their peak shear stress. The shear stress in the first inch of the crack, c0-1, reached a lower value due to the local effects of the anchorage clamping plates. The shear stress is averaged over the gage length, which is 1 inch for the first six inches of the strip and 2 inches for the remaining gages. By averaging the bond shear stress over the gage length, there is a loss of the peak shear transfer. The deviation in shear stress from the first six inches and the remaining FRP strip is attributed to the averaging of the stresses.

2.3.2 Specimen S1B

The results show again that by measuring the strain in the FRP strip, it is possible to

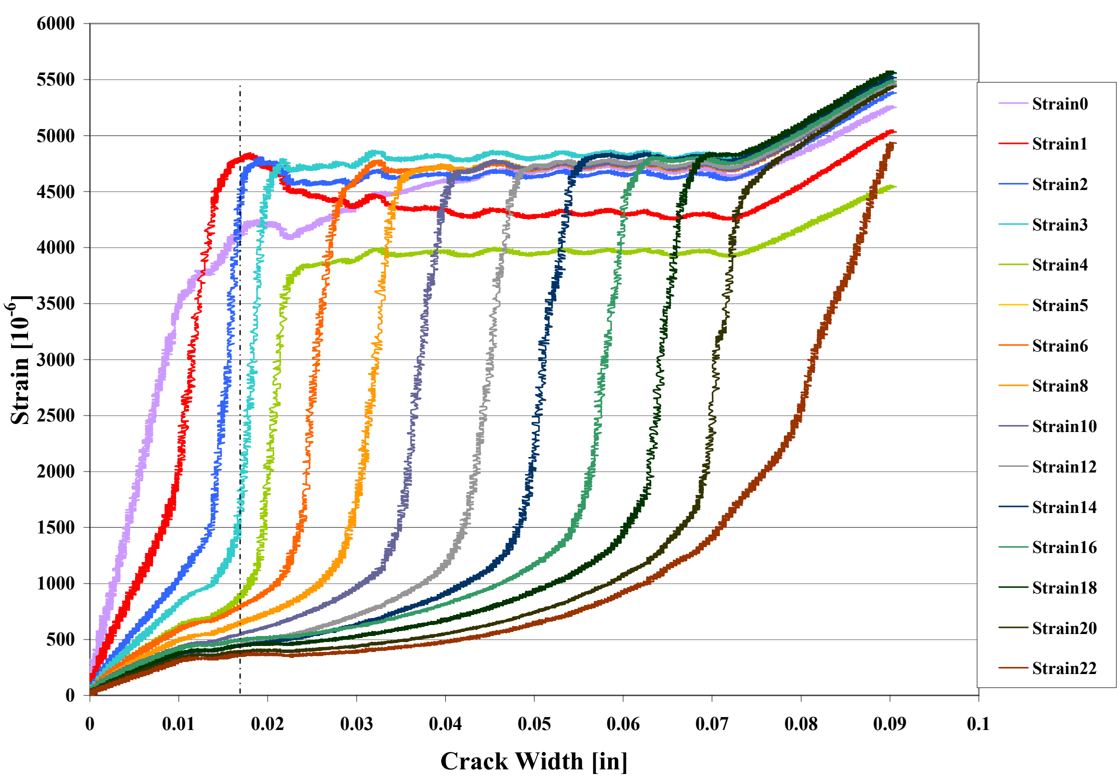

Figure 2.8: Strain vs. Crack Width for Specimen S1B

detect the initial debonding and subsequent failure. The S1B results are similar to the S1A specimen. Figure 2.8 shows the strain gage measurements for all of the gages during the test of specimen S1B. The strain at the crack, Strain0, increases immediately as the crack opens, followed by Strain1, one inch away. Debonding failure is observed when Strain0 and Strain1 are equal in strain, at approximately 3750 microstrain, indicating there is no longer any bond transfer between the two gages. Briefly after the first inch of the FRP strip has debonded, Strain2 increases and debonds at approximately 4750 microstrain. Debonding continued to propogate the length of the strip in a controlled manner. The gradual failure indicated a ductile bond and a peeling failure. The final readings indicate the FRP strip is no longer bonded and is transferring the load

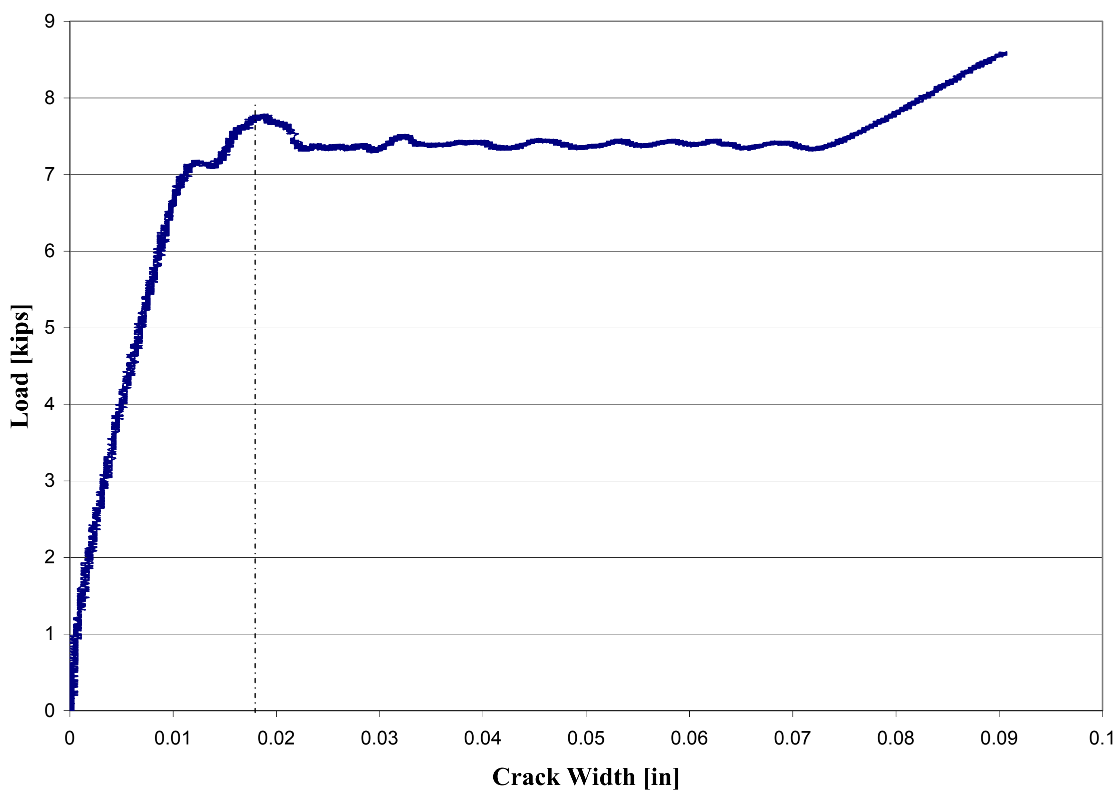

Figure 2.9: Load vs. Crack width for Specimen S1B

directly from one end anchorage to the other.

Figure 2.9 shows the maximum load of 7.8 kips occurred at a crack width of 0.016 inches. The crack mouth opening displacement (CMOD) is maintained as the load fluctuated due to debonding of subsequent segments of the strip. The first plateau in the load corresponds to the debonding of the area around the crack, which occurred at a crack opening of 0.01 inches. The load continued to increase to the maximum load, until the region four inches away from the crack debonded. The load increase at a crack opening of 0.07 inches is due to the completely debonded FRP transferring the load from one end anchorage to the other.

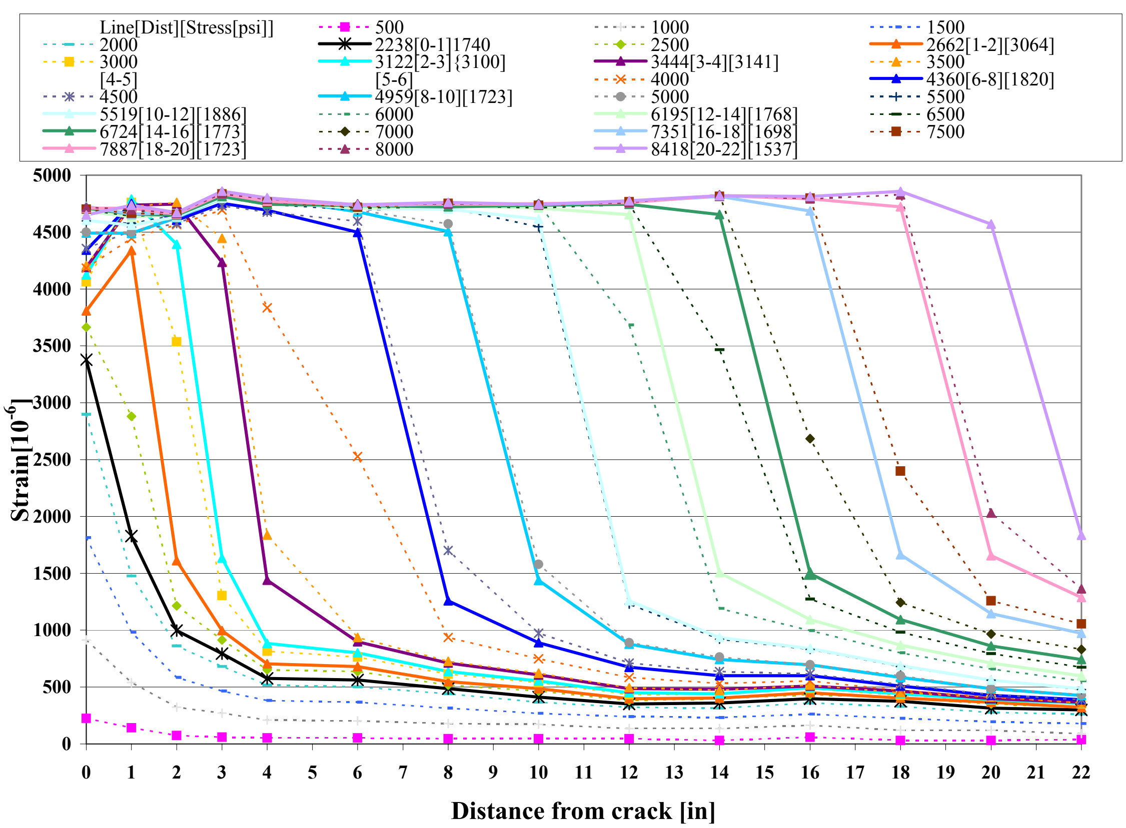

Figure 2.10: Strain vs. Distance from the Crack for Specimen S1B

In Figure 2.10, the strain profile along the length of the FRP strip shows the maximum shear stress in the adhesive bond between two gages. The dashed lines are profiles at every 500th increment. The notation is the reading number, followed by the location and the maximum shear stress at that location. The profile again shows the debonding failure through a maintained high strain in the debonded region, followed by a sudden sharp decrease to the bonded area that remains at a lower strain. The maximum shear stress, 3141 psi, was observed between 3-4 inches from the crack. The surface preparation of sandblasting and mechanical anchorage increased the bond transfer.

Debonding failure and the propagation of the bond stress in the adhesive along the

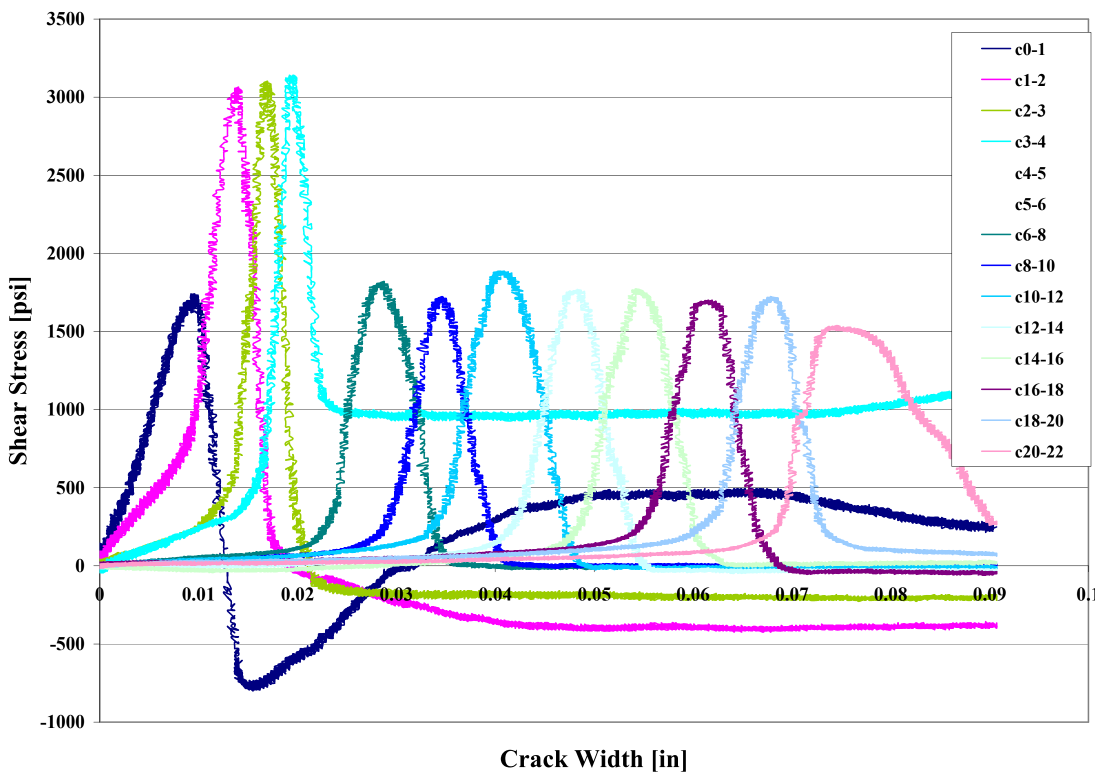

Figure 2.11: Shear Stress vs. Crack Width for Specimen S1B

length of the strip is also visible in Fig. 2.11. The notation indicates the bond stress between two gages, calculated using equation [1]. As the crack opens the shear stress in the first inch of the bond begins to increase, illustrated by the linearly ascending branch to a peak shear stress. Once the peak shear stress has been reached, debonding has begun for that segment, indicated by the linearly descending branch, which represents an interface softening. The next section begins to increase in shear stress when the previous section reaches the peak shear stress. Debonding is complete when the shear stress reduces to zero. The shear stress in the first inch of the strip, c0-1, becomes negative due to the difference in the strain measurements between Strain0 and Strain1. The lower reading for the strain at the crack, Strain0, is due to the local effects of the anchorage clamping plates near the crack. The approximate measurement of shear stress is averaged over the bond length, i.e. 1 inch for the first 6 inches and 2 inches for the remaining 16 inches. The average bond stress creates a loss of peak shear stress and does not capture the maximum shear stress in the FRP-concrete interface.

2.3.3 Test Results for Specimen SC1

The results for the concrete specimen, SC1, differed significantly from the previous results for the steel specimens (S1A and S1B). Debonding occurred in the concrete surface paste and resulted in a brittle failure. Figure 2.12 shows the strain gage readings as the crack opened. The strain at the crack, Strain0, increases as the specimen is loaded, followed by the strain one inch away, Strain1. The first debonding occurs in the first 12 inches of the strip at a crack opening of 0.02 inches, indicated by the dashed line. Strain14, the strain 14 inches away from the crack, shows a partial debonding through the sudden increase in strain, however it continues to increase indicating the region between Strain12 and Strain14 was bonded. The second debonding led to

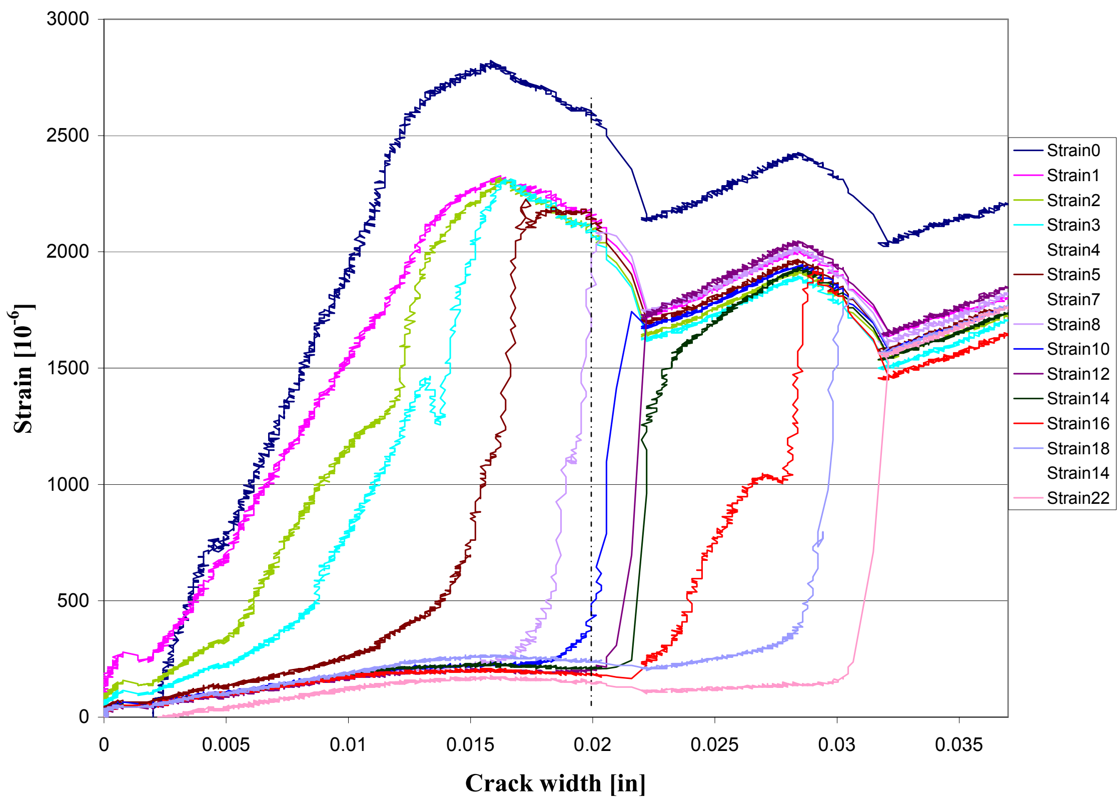

Figure 2.12: Strain vs. Crack Width for Specimen SC1

complete debonding failure of the strip at a crack opening of 0.035 inches. The final increase in strain readings represents the fully debonded CFRP strip spanning between the end anchorages.

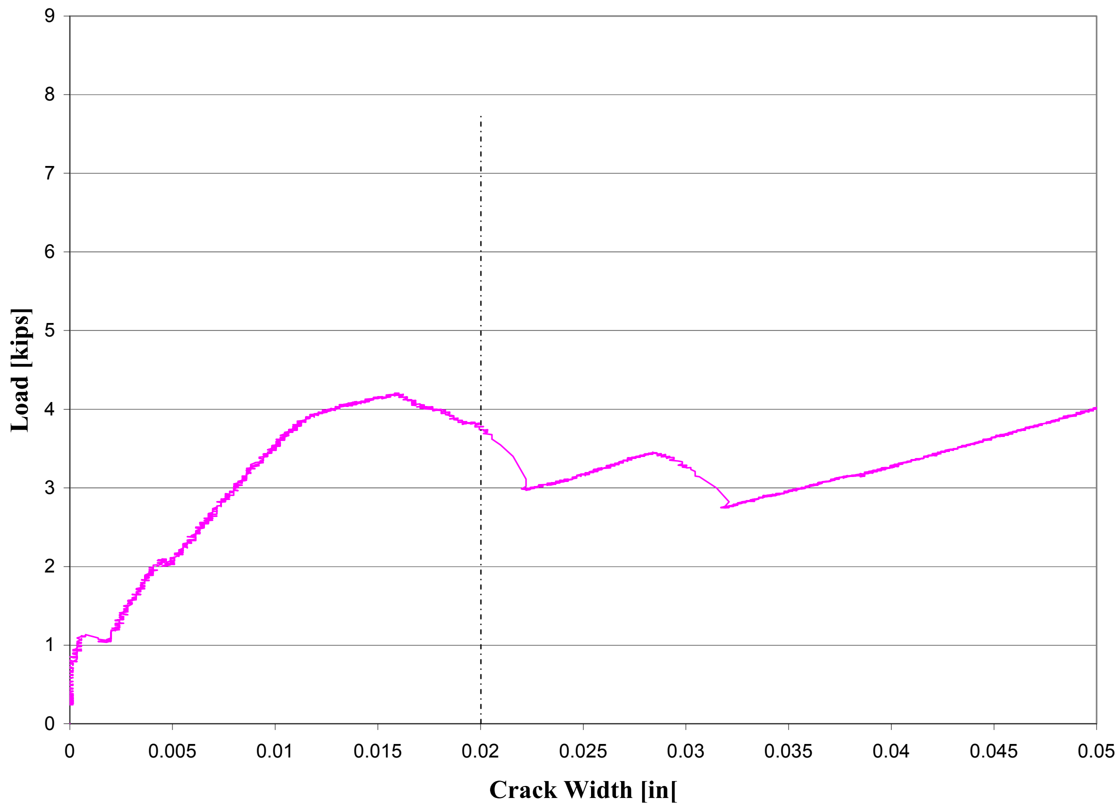

Figure 2.13: Load vs. Crack Width for Specimen SC1

Figure 2.13 shows the relationship between the applied load and crack width. The maximum load, 4.2 kips, occurs at a crack width of 0.015 inches immediately prior to the debonding of the first 12 inches of the FRP strip at a crack width of 0.02 inches. The fluctuations in the applied load indicate small debonding events before the first major debonding. As the crack width increases, the FRP attempts to carry additional load, but fails with the second debonding failure at a crack width of 0.033 inches. The

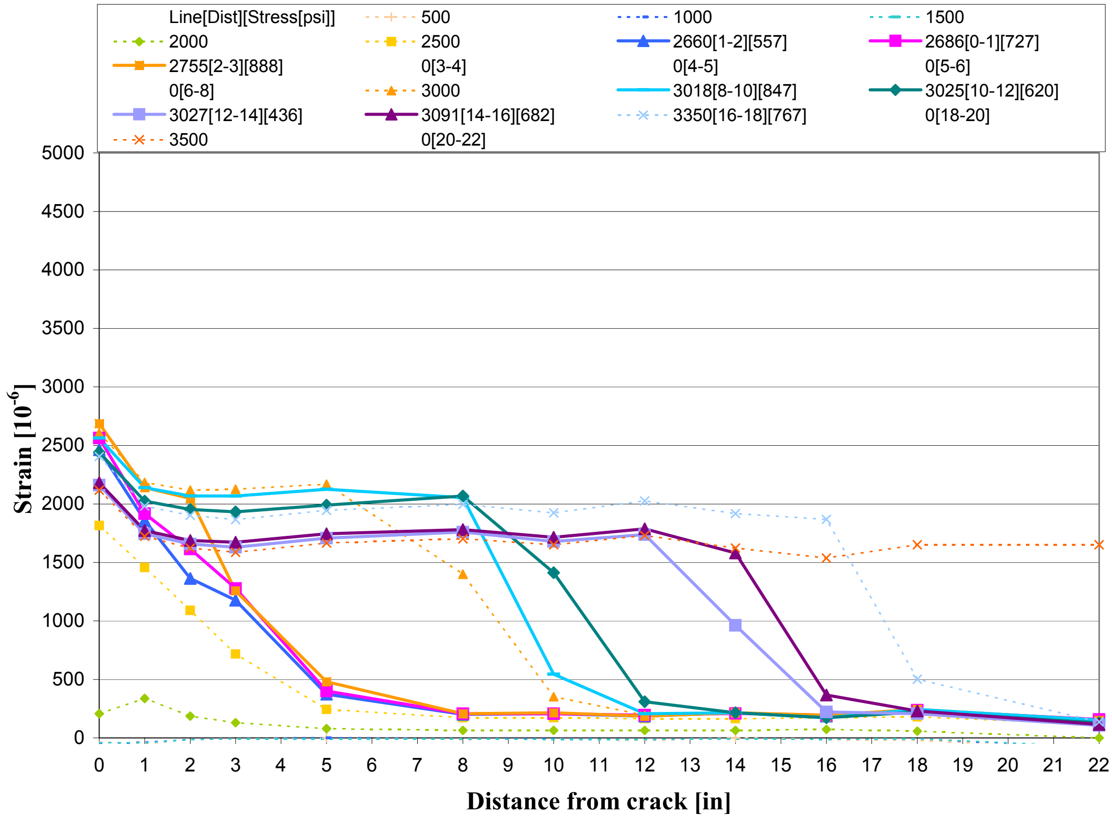

Figure 2.14: Strain vs. Distance from the Crack for Specimen SC1

final increase in load is the result of the CFRP spanning between end anchorages.

Figure 2.14 shows the strain profile along the FRP strip at selected intervals during the test of specimen SC1. The solid line strain profiles displays the maximum shear stress in the bond observed between two adjacent gages. The maximum shear stress of 888 psi was observed between 2-3 inches from the crack, when the crack opening was 0.018 inches. This low level stress may be due to lack of concrete surface preparation leading to poor bond transfer.

Figure 2.15 shows that the shear stress peaks are not as clearly defined as in the previous steel specimen tests. The results, however, indicate the same behavior of bond shear

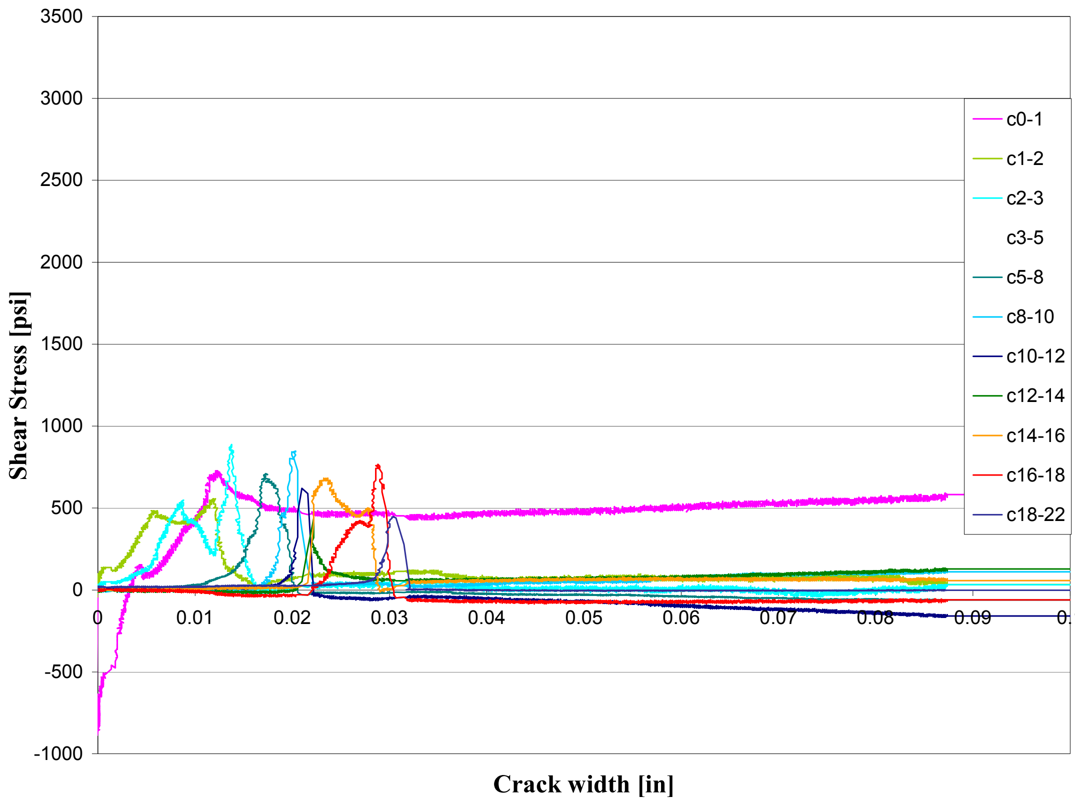

Figure 2.15: Shear Stress vs. Crack Width for Specimen SC1

stress increasing and decreasing, propagating the delamination along the strip. The concrete substrate creates an unpredictable surface, for instance, multiple sections of the strip delaminating simultaneously (due to fracture of the concrete matrix). The brittle fracture of the concrete is noted by multiple peaks of shear stress that overlap, opposed to the gradual and defined peaks of the steel specimens (Fig. 2.11). The overlapping signifies the fracture of the bond interface instead of a peeling failure. The maximum shear stress of 888 psi occurs at 2-3 inches from the crack.

2.4 Comparison

2.4.1 Comparison of the results of specimens S1A and S1B

The experiments demonstrated that debonding can be detected through measurement of the strain in the FRP. Both steel specimens, S1A and S1B, had a gradual, ductile failure in the adhesive, as debonding progressed from the crack along the length of the FRP (Figs. 2.4 and 2.8). The strain at the crack in both specimens increased immediately and reached a crack width of 0.006 to 0.016 inches, approximately 3500 – 4250 microstrain before debonding. The maximum crack width prior to delamination for S1B was larger than S1A (Figs. 2.5 and 2.9), suggesting that the bond strength of the second specimen was greater than the first. This also results in a larger load for specimen S1B than S1A.

The data indicate a stronger bond in the S1B specimen which allowed the FRP to reach higher values in strain, load and crack width. The cause for the discrepancy between the specimens is unknown. Both were prepared with the same process, with the thickness of the epoxy as the only unknown variable. Based on the weaker of the two specimens, the ultimate strain, at the maximum shear stress, is approximately 3500 microstrain for the CFRP on the steel substrate (Figs. 2.6 and 2.10). This is considered to represent the upper limit for strain in the FRP before debonding occurs for the CFRP and epoxy used in this study.

2.4.2 Comparison of the SC1 and S1 specimens

The concrete specimen presented a very different behavior than the steel specimens. The debonding failure was a brittle failure in the concrete paste with long sections of FRP debonding simultaneously. The results summary for each of the specimens is found in Table 2.5. The ultimate load of the SC1 specimen was approximately half of the steel specimens S1A and S1B, which was attributed to the lack of concrete surface

Table 2.5 Summary of the Results of Steel Specimen Tests

	Initial Debonding					
Specimen	Maximum Load [kips]	Crack Width [in]	FRP Strain at the crack [με]	Initial Debonding Length [in]	Average Shear Stress over Debonding Length [psi]	Maximum Shear Stress for limit ($\Delta\varepsilon/\Delta x_i$) [psi]
S1A	7.4	0.006	3500	—	—	2814
S1B	7.8	0.016	4250	—	—	3141
SC1	3.8	0.02	2500	8	267	888

preparation and lower strength of the concrete substrate. The strain in the FRP for SC1 was approximately 2500 microstrain (Fig. 2.12), at a crack width of 0.02 inches, before debonding occurred. It appeared that the first four inches from the crack are critical to the performance of the FRP-to-concrete bond. Specimen SC1 highlighted several factors that affect debonding: concrete surface preparation, the bond interface between the concrete and FRP, and the critical region four to five inches from the crack.

Chapter 3: Concrete Debonding Specimens

3.1 Introduction

To study the effect of the concrete substrate on the debonding failure of the FRP, two sets of experiments were conducted. Test variables included the concrete strength and surface preparation. The experiments provided information on the effect of the concrete surface and strength on the behavior of the debonding failure.

3.2 Experimental Setup

3.2.1 <u>Specimen design</u>

The specimens were double lap shear type specimens. Each specimen was constructed in two pieces, each with an inserted steel bar welded to a square steel end plate (Fig. 3.1). The two end plates fit together creating a simulated crack. The two pieces were placed in a prism mold and bolted together temporarily using a small steel plate. The mold formed two concrete prisms; the longer piece for the instrumented section of FRP, and the shorter section as the anchorage area of the FRP, restrained using a FRP fabric wrap. For each test set, four specimens were constructed simultaneously with the same concrete mixture.

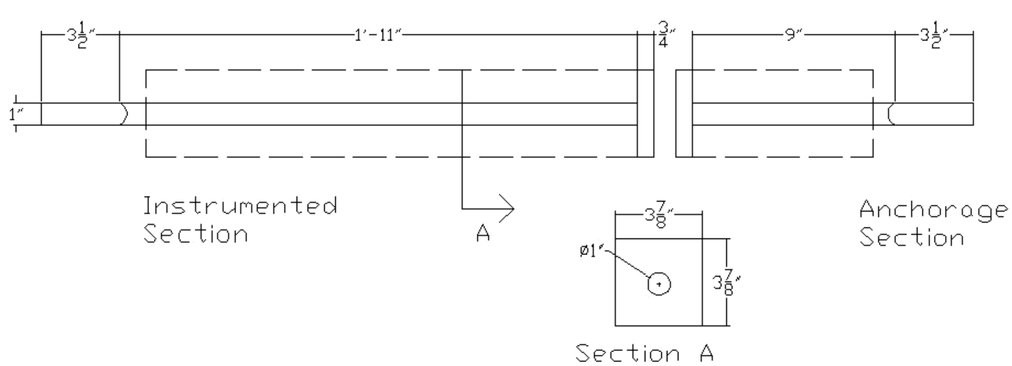

Figure 3.1: Double lap shear specimen steel reinforcement diagram

3.2.2 Material Properties

A Sika Carbodur S512 pre-cured pultruded carbon fiber reinforced polymer (CFRP) laminate with an epoxy resin matrix was used for all specimens, along with the manufacturer recommended Sikadur 30 two-component, structural epoxy paste adhesive. Tables 3.1 and 3.2 summarize the deign properties of Sika CarboDur S 512 and Sikadur 30, respectively.

Table 3.1. Sika CarboDur S 512 Design Properties

Tensile Strength	37.8 x 10^3 lbs (168 kN)
Modulus of Elasticity	23.9x10^6 psi
Elongation at Break	1.69%
Thickness	0.047 in (1.2mm)
Width	1.97 in (50mm)
Cross Sectional Area	0.093 sq. in. (60mm^2)

Table 3.2. Sikadur 30 Design Properties

Tensile Strength	3,600psi (24.8 MPa)
Modulus of Elasticity	6.5 x 10^5 psi (4,482 MPa)
Elongation at Break	1%
Recommended Surface Preparation	ICRI CSP 3

The anchored section utilized SikaWrap Hex 103C, a high strength unidirectional carbon fiber fabric (Table 3.3). The fabric was impregnated with Sikadur 300, a two-component, high strength, and high modulus epoxy (Table 3.4), and wrapped around the anchorage zone in two layers.

Table 3.3. SikaWrap Hex 103C Design Properties

Tensile Strength	5.5 x 10^5 psi (3,793 MPa)
Tensile Modulus	34 x 10^6 psi (234,500 MPa)
Elongation at Break	1.5%
Density	0.065 lbs/in^3 (1.8g/cc)
Width	25 in

Table 3.4. Sikadur 300 Design Properties

Tensile Strength	8,000 psi (55 MPa)
Tensile Modulus	2.5×10^5 psi (1,724 MPa)
Elongation at Break	3%
Recommended Surface Preparation	ICRI CSP 3

The first group of four specimens, designated DBL, were cast using a low strength normal weight concrete, and the second group, designated DBH, were cast using a high strength normal weight concrete (Tables 3.5 and 3.6).

Table 3.5. Concrete Mixture Design Proportions

Material	Mix 1, DBL	Mix 2, DBH
Coarse Aggregate [lb/yd^3]	1576	1576
Maui Dune Sand [lb/yd^3]	431	431
Concrete Sand [lb/yd^3]	825.6	825.6
Cement [lb/yd^3]	683.7	786.1
Water [lb/yd^3]	307.7	275.1
W/C ratio	0.45	0.35
Daratard [oz/sk]	3	3
Darex [oz/sk]	2	2

Table 3.6. Concrete Compressive Strengths at 28 days

Cylinder	Area [in^2]	Compressive Strength [psi] Mix 1, DBL	Compressive Strength [psi] Mix 2, DBH
1	28.27	6260	8596
2	27.34	6543	8560
3	28.27	6207	8727
Average Strength		**6337**	**8628**

3.2.3 Surface Preparations

The concrete specimens were prepared using four different surface preparations. The surface preparations followed International Concrete Repair Institute (ICRI) Technical Guidelines (1997) that are summarized in Table 3.7. The four preparations were sandblasting, grinding, needle gun and a control specimen with no preparation. The

Figure 3.2: ICRI CSP and corresponding prepared concrete surfaces

preparations range from a concrete surface profile (CSP) of 1-4 (Figure 3.2 and Table 3.8). The FRP manufacturer specifications for application of the CFRP strip required a surface preparation with a minimum ICRI surface profile of 3 and therefore only specimens DBL2, DBL3, DBH2 and DBH3 complied (Table 3.8).

Table 3.7. ICRI Technical Guidelines (1997)

Surface Preparation	ICRI CSP	Uses
No Preparation		
Sand Blasting	2-4	sealers, thin film coatings, high build coatings, etc.
Grinding	1-3	reduce or smooth slight surface irregularities and to remove mineral deposits and thin coatings
Needle gun scaling	5-8	for preparing concrete surfaces for high build coatings, self-leveling and broadcast applications, and thin overlays

Table 3.8. Concrete Prism Specimen Identification

Surface Preparation	DBL	DBH
No Preparation	DBL1	DBH1
Sandblasting	DBL2	DBH2
Grinding	DBL3	DBH3
Needle Gun Scaling	DBL4	DBH4

3.2.4 Installation

The Carbodur strip was cut into a 38-inch strip and cleaned using MEK solvent. The epoxy was mixed according to the manufacturer's instructions. The concrete surface was cleared of loose particles with an air hose before applying the epoxy. The epoxy was applied using a spatula to the Carbodur strip in a thin layer (less than 1/32 in). No epoxy was placed on the concrete specimen. The epoxy-covered strip was then centered on the concrete specimen and pressed down to squeeze out excess epoxy. Excess epoxy was wiped clean from the edges using acetone. At the anchorage end of the specimen, epoxy was placed on both sides of the strip and along the exposed concrete to adhere the anchorage fabric wrap to the specimen. The anchorage fabric was cut into a 8 inch wide strip and impregnated with Sikadur 300 epoxy. The fabric was wrapped tightly around the prism twice. All specimens were allowed to cure for at least 3 days before instrumentation and 7 days before testing.

3.2.5 Strain Gage Instrumentation

The CFRP strip was instrumented with electric resistance strain gages (ERSG), placed along the strip to monitor the longitudinal strain. The strain gages were applied following the manufacturer's instructions. The gages had a 2.105 strain gage factor and a resistance of 350 ohms. Strain gages were placed at the crack, at intervals of 1 inch for a distance of 6 inches from the crack, and then at intervals of every two inches (Fig. 3.3).

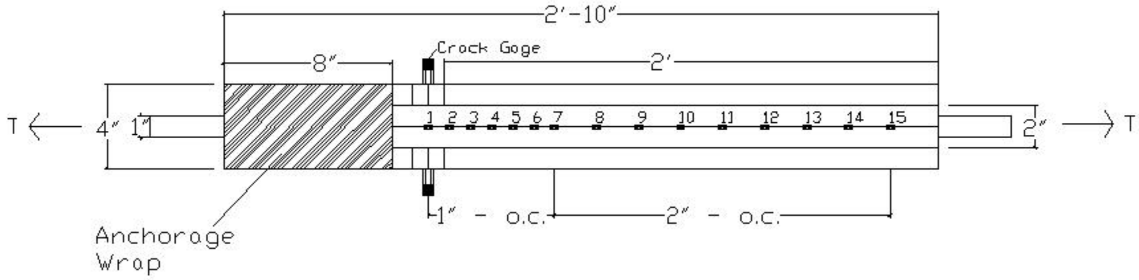

Figure 3.3: Concrete Prism Specimen with Instrumentation Diagram

3.2.6 Crack Gage Instrumentation

Two Epsilon clip on gages, with a gages length on 3 mm, were used on either side of the simulated crack to measure crack opening as the load was applied.

3.2.7 Test Setup

The specimen was placed in a 2 Post MTS universal test frame. A National Instruments system running Labview software was used to monitor the applied load, frame displacement, crack gage and strain gages during the experiment. To capture post peak response and strain changes in the FRP strip during delamination, the test was run in displacement control. This mode maintains the displacement while the load fluctuates during the experiment. The loading rate for the experiment was 1.68 mm/min.

3.3 **DBL Specimen Results**

Of the four specimens tested, three delaminated in the non-instrumented FRP strip while DBL3 delaminated in the instrumented strip (Fig. 3.4). The notation used in the results correspond to the distance of the point of measurement from the crack. The dashed line indicates the initiation of debonding failure.

a

b

c

d

Figure 3.4: Photo of Debonded DBL Specimens: (a) DBL1; (b) DBL2; (c) DBL3; (d) DBL4

3.3.1 Test results for specimen DBL1

In DBL1, the non-instrumented strip delaminated. The failure occurred in the concrete surface paste. Figure 3.5 shows the strain gage readings for the instrumented strip as the crack opened. The strain at the crack, Strain0, increased immediately as the crack width increased, followed by the Strain1, one inch away. The strain gage readings indicate that the first two inches from the crack were debonded before the delamination of the non-instrumented strip at a crack width of 0.009 inches. The failure caused 8 inches of the instrumented FRP strip to debond.

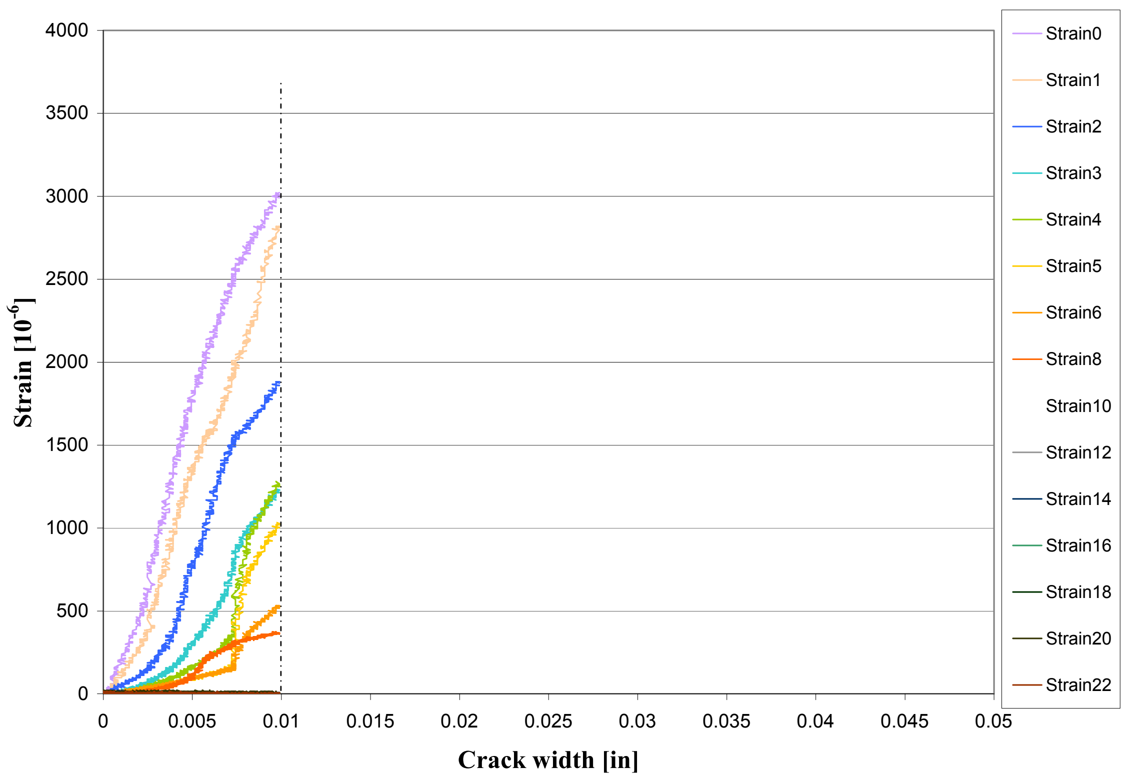

Figure 3.5: Strain vs. Crack Width for Specimen DBL1

Figure 3.6 shows the relationship of the applied load and crack width. Two crack gages were used to ensure balanced opening of the crack and were averaged. The maximum load of 12.62 kips occurs at an average crack width of 0.009 inches. The load increased until failure of the non-instrumented strip. After the failure, the specimen is unable to recover the load.

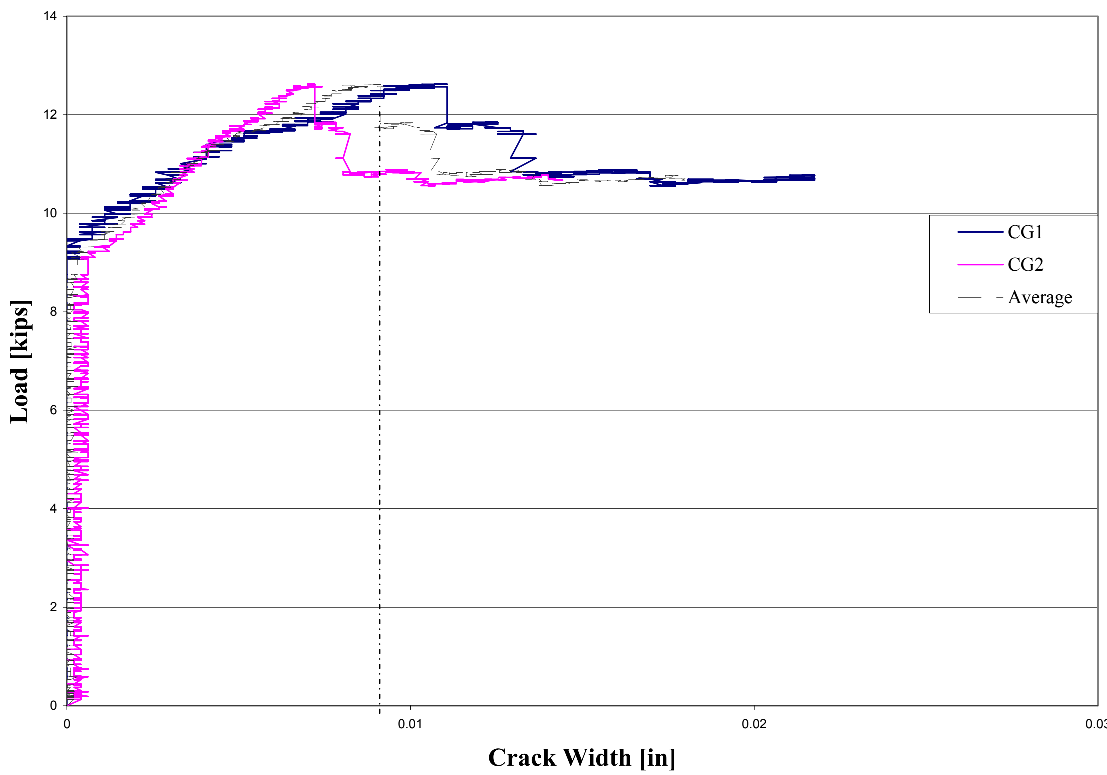

Figure 3.6: Load vs. Crack Width for Specimen DBL1

Figure 3.7 shows the strain profile along the FRP strip until just before the delamination of the non-instrumented strip. The profile lines represent the maximum shear stress in the bond observed between two adjacent gages. The maximum shear stress, 715 psi, was observed between 1-2 inches from the crack. The low level stress may be due to the lack of concrete surface preparation leading to poor bond transfer. Also, the premature failure of the non-instrumented strip may have prevented the shear stresses in the bond from fully developing.

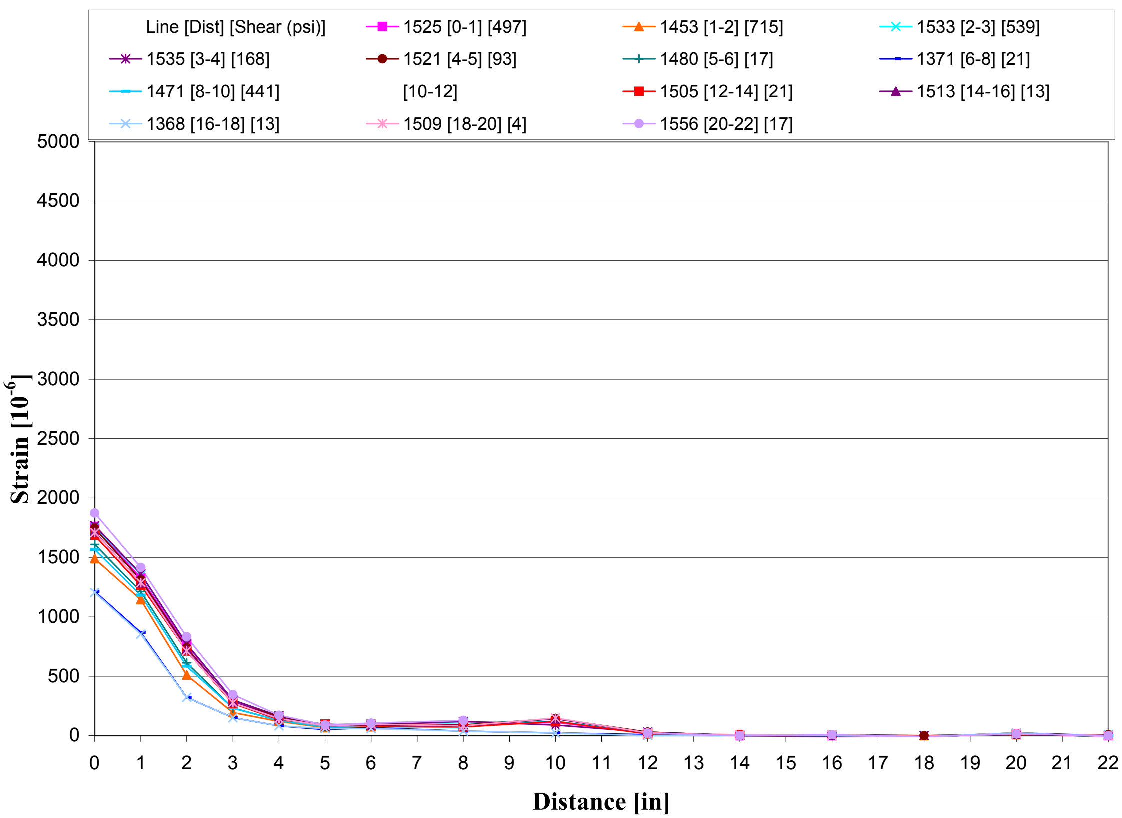

Figure 3.7: Strain vs. Distance from the Crack for Specimen DBL1

Figure 3.8 shows the shear stress peaks that developed in the specimen. The delamination of the non-instrumented strip limited the ability to observe the peak shear stress develop throughout the FRP strip. As the crack width increased the shear stress in the first two inches, c0-1 and c1-2, increased simultaneously. The shear stress three inches away from the crack increases shortly after. The simultaneous increase of bond shear stress in the first two one-inch segments from the crack indicates a brittle fracture of the concrete interface. This is comparable to the simultaneous fracture seen in specimen SC1.

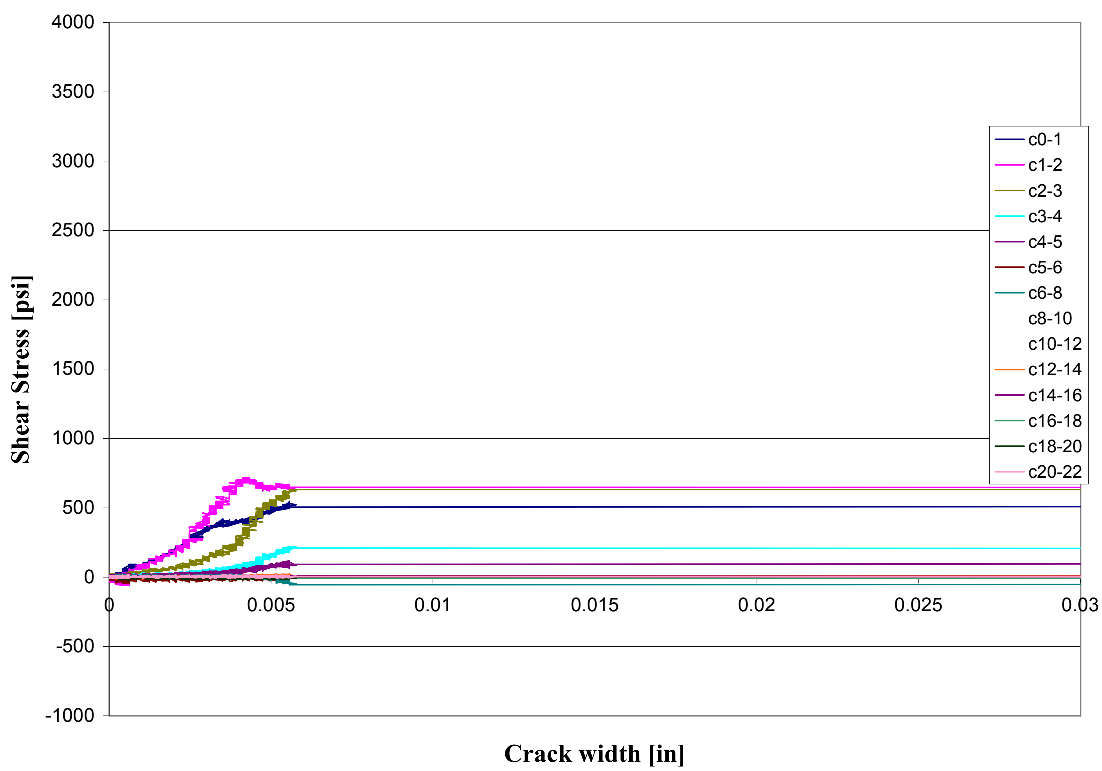

Figure 3.8: Shear stress vs. Crack Width for Specimen DBL1

3.3.2 Test results for specimen DBL2

Figure 3.9 shows the strain gage measurements for all gages during the test of specimen DBL2. Debonding failure occurred in the non-instrumented strip. The strain at the crack, Strain0, increases as the crack width increases, followed by Strain1, one inch away. The strain 2 and 3 inches away, Strain2 and Strain3, were also increasing when delamination of the non-instrumented strip occurred. The failure caused 6 inches of the instrumented FRP strip to debond, visible in the sudden increase in strain.

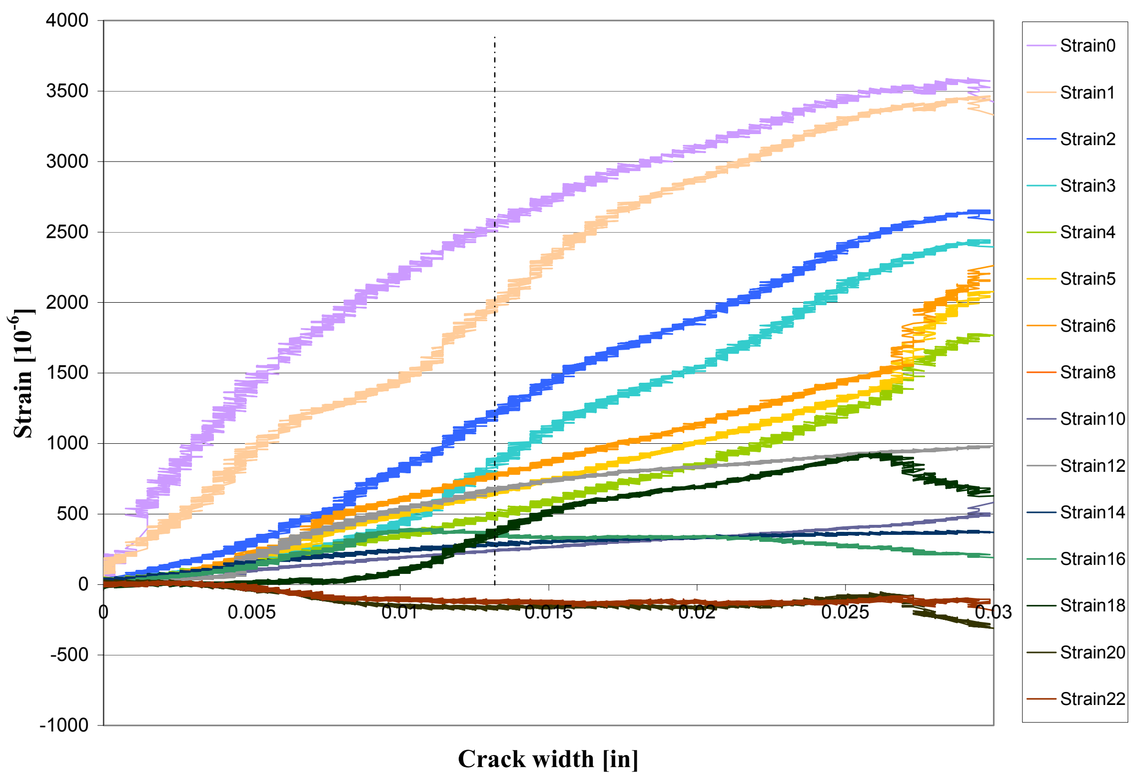

Figure 3.9: Strain vs. Crack Width for Specimen DBL2

Figure 3.10 shows the maximum load of 13.43 kips occurs at an average crack width of 0.013 inches. The initial readings indicate the crack opened evenly, however the gages deviate, which indicates some bending may have occurred. The premature failure of the non-instrumented strip may have caused uneven loading of the specimen due to a weaker bond strength of the non-instrumented strip.

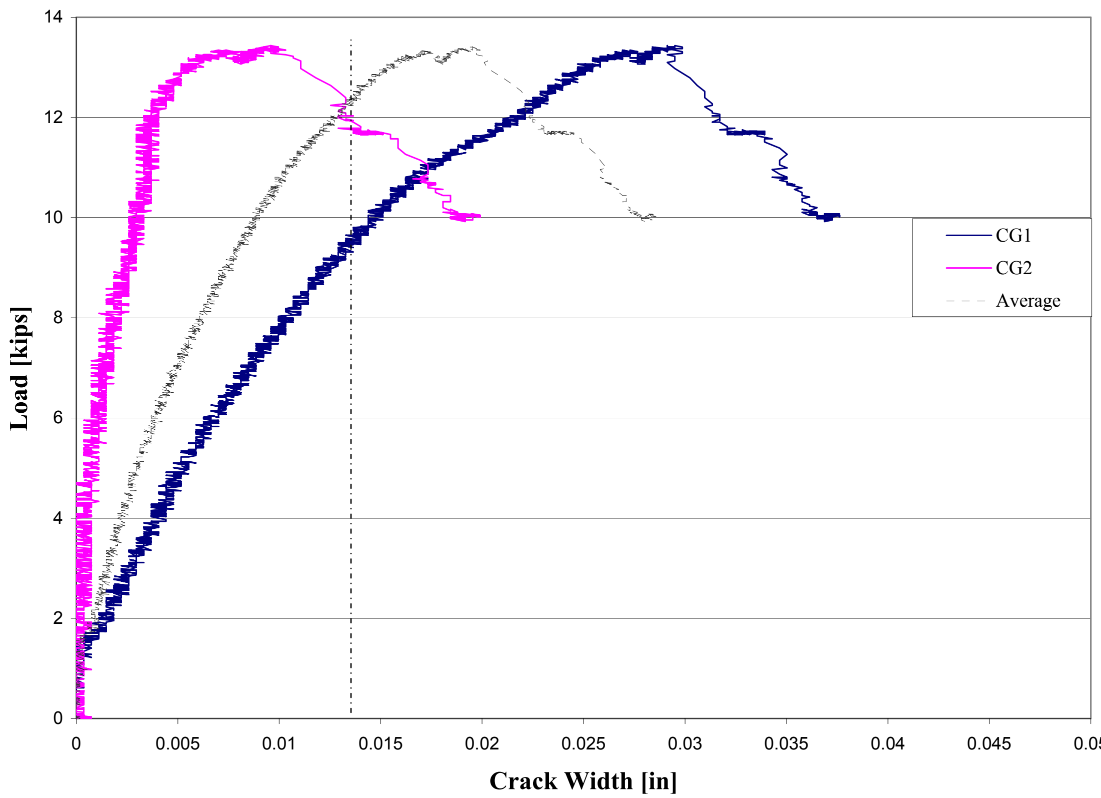

Figure 3.10: Load vs. Crack Width for Specimen DBL2

The strain profile, Figure 3.11, displays the maximum shear stress in the bond observed between two adjacent gages. The profiles indicate that the first inch of the strip had debonded when failure of the non-instrumented strip occurred. The maximum shear stress, 1138 psi, was observed between 1-2 inches from the crack. The maximum shear stress occurred at a crack width of approximately 0.013 inches. The increased strain in the FRP 6-16 inches away from the crack are due to the debonding of the non-instrumented strip.

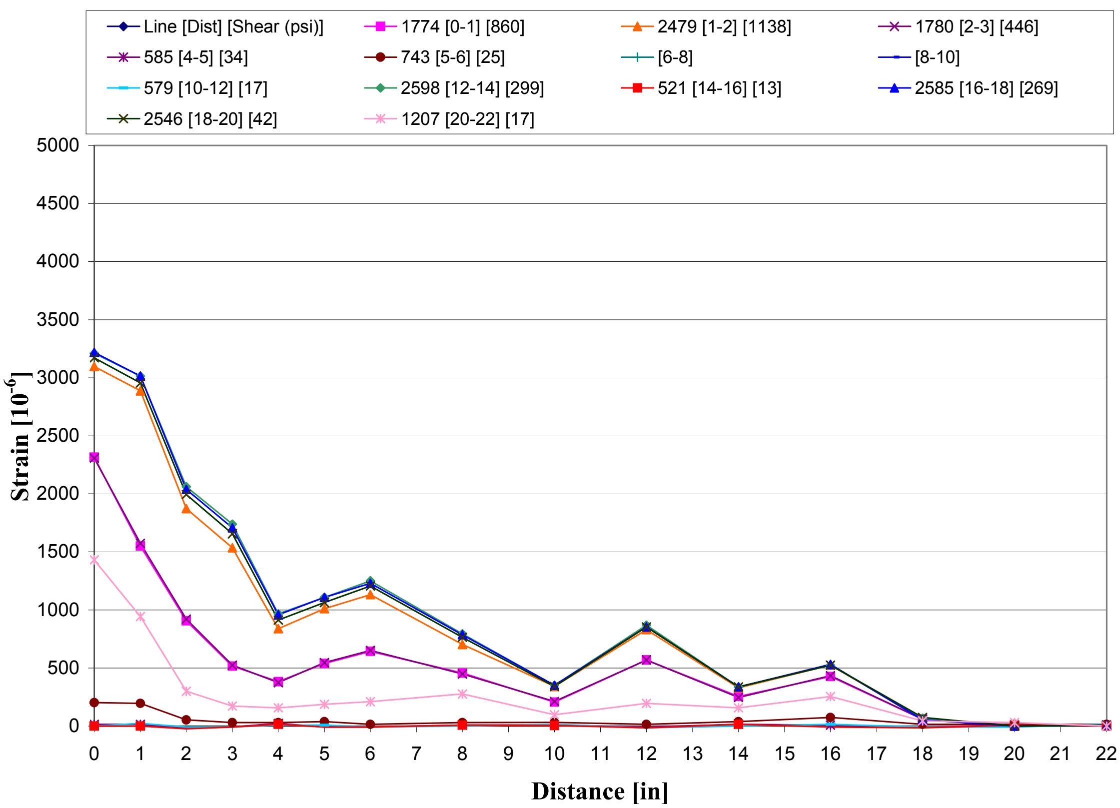

Figure 3.11: Strain vs. Distance from the Crack for Specimen DBL2

Figure 3.12 shows the shear stress peaks did not fully develop when debonding failure occurred in the non-instrumented strip. The maximum shear stress of 1138 occurred at 1-2 inches from the crack, c1-2. The shear stress 1 inch from the crack, c0-1, increased along with c1-2, two inches away, as the crack opened. Once c0-1 reaches the peak shear stress, it then begins to decrease. The decrease in shear stress indicates debonding of the first inch of the FRP strip. The shear stress continues to propagate the length of the strip, evident by the increase in c1-2. The delamination of the non-gage strip limited the ability to observe the peak shear stress throughout the strip.

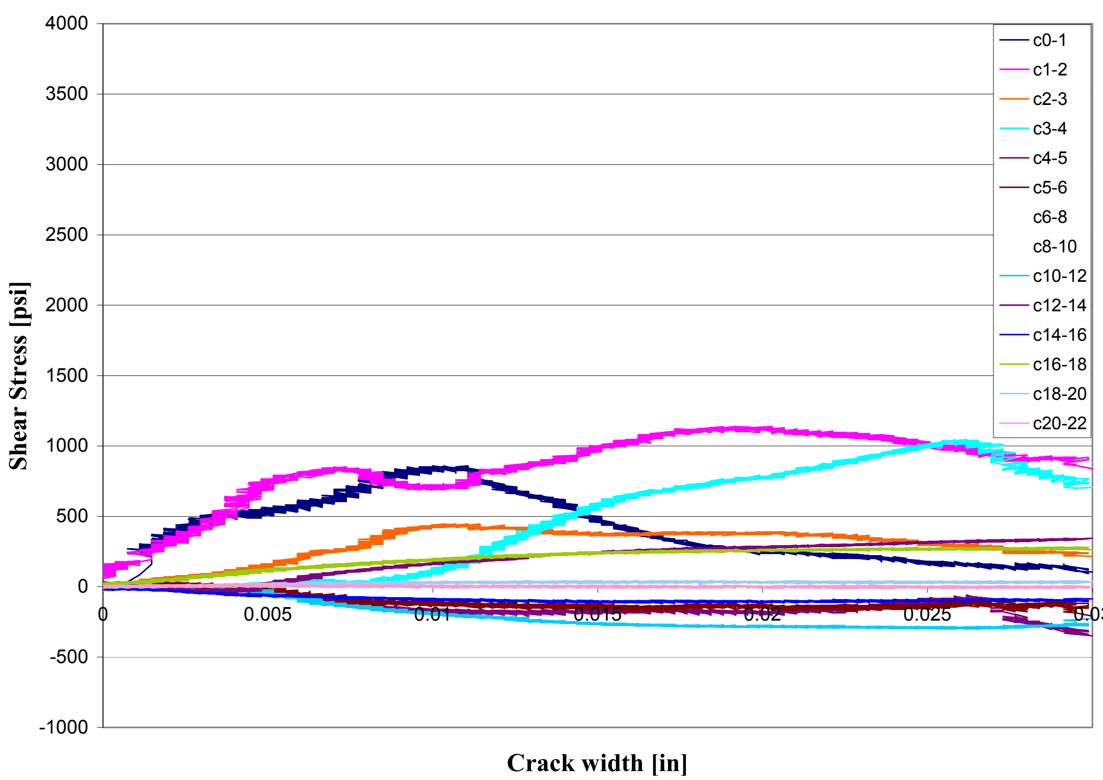

Figure 3.12: Shear Stress vs. Crack Width for Specimen DBL2

3.3.3 Test results for specimen DBL3

DBL3 was the only specimen in the group to debond on the instrumented strip. Figure 3.13 shows the strain gage measurements for the entire strip. Strain0, at the crack, increases followed by Strain1, one inch away, as the crack opens. The first debonding occurs with the first 3 inches of the strip completely debonded, subsequently, 8 inches of the strip to debonds at a crack width of 0.012 inches. The second debonding lead to complete debonding failure of the strip at a crack opening of 0.025 inches.

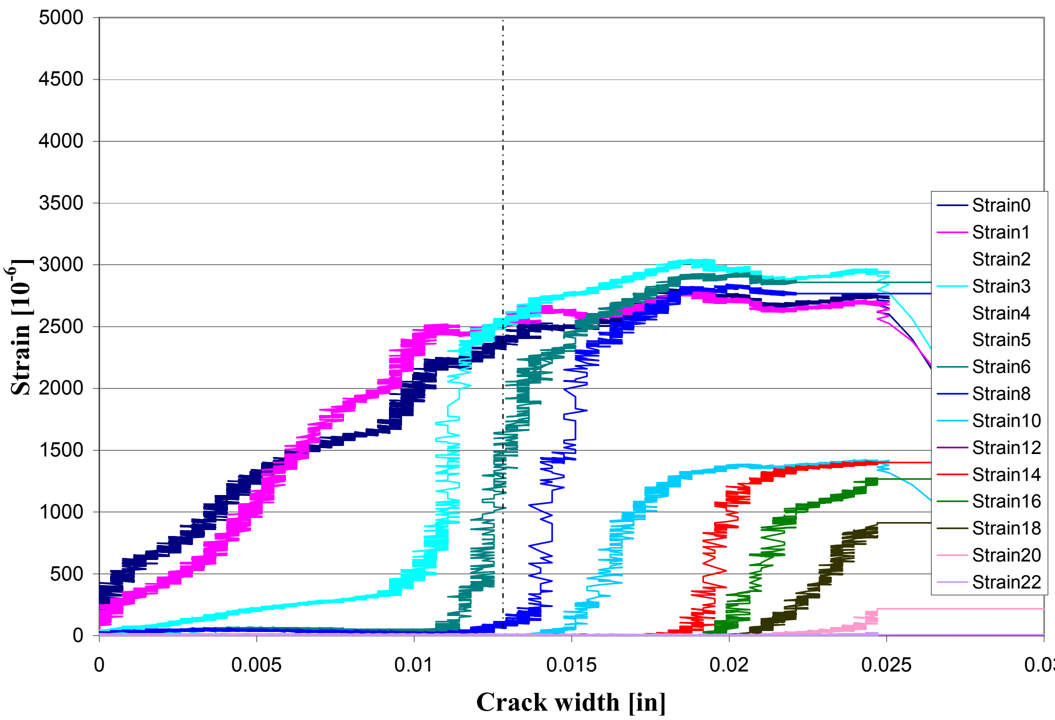

Figure 3.13: Strain vs. Crack Width for Specimen DBL3

Figure 3.14 shows the maximum load 13.27 kips occurred at an average crack width of 0.022 inches. The load continued to increase after the first debonding occurred at a crack width of 0.012 inches. The maximum load corresponds to the final debonding that failed the strip. The measurement of the crack gages demonstrated a relatively even crack opening as the specimen was tested.

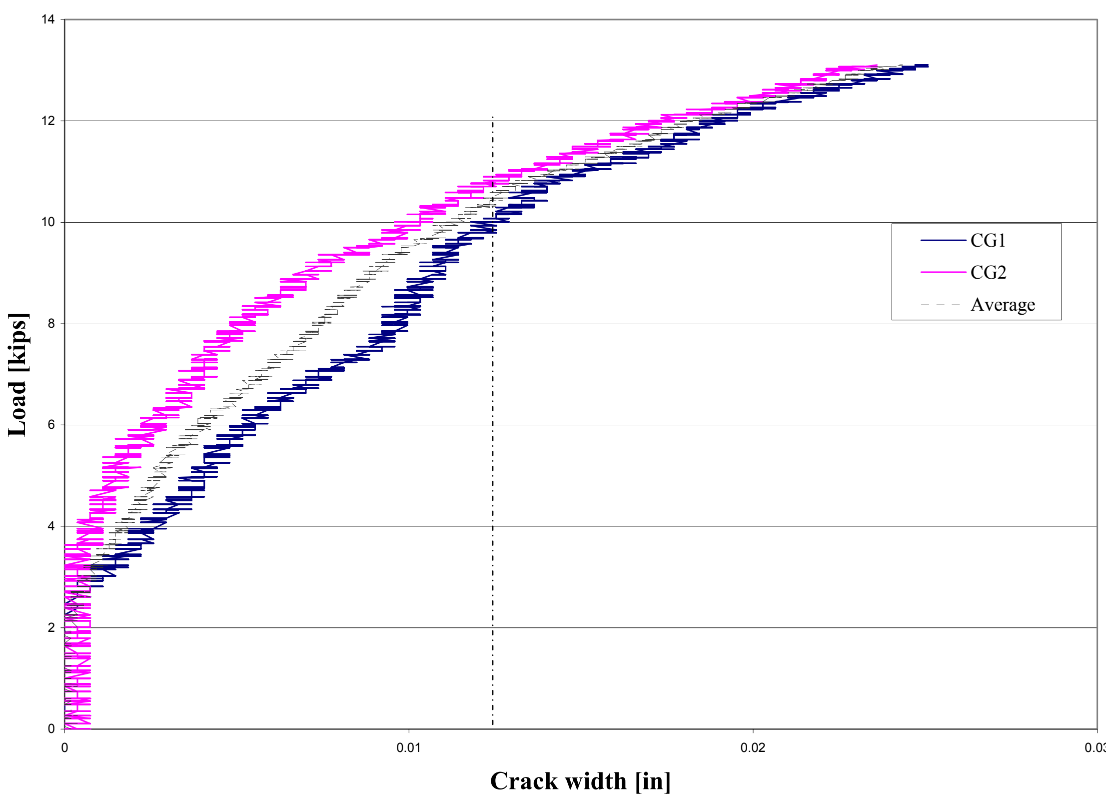

Figure 3.14: Load vs. Crack Width for Specimen DBL3

Figure 3.15 shows the strain profile along the FRP strip at selected intervals. The solid line profiles display the maximum shear stress in the bond between two gages. The maximum shear stress, 1141 psi, was observed between 6-8 inches from the crack. The first debonding is visible in the profiles when 8 inches of the strip from the crack all measure high strain, approximately 3000 microstrain. The second debonding causes complete failure of the strip.

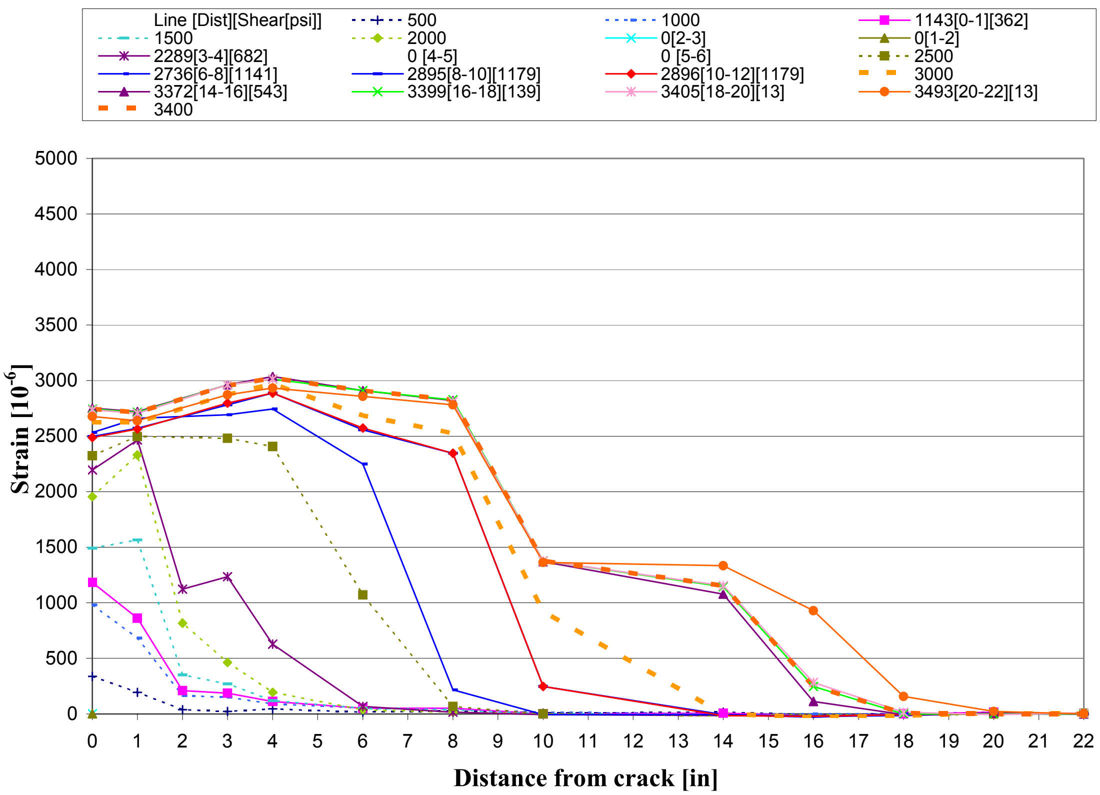

Figure 3.15: Strain vs. Distance for Specimen DBL3

Figure 3.16 shows the bond shear stress along the length of the strip. The maximum shear stress of 1141 psi occurs 6-8 inches away from the crack, c6-8. The shear stress one inch away from the crack, c0-1, increases as the crack width increases. Sections of the FRP strip debond before the first debonding failure occurs at a crack width of 0.015 inches. The shear stress propagates the strip, evident by the increase to a peak and then decrease, until total debonding failure occurs at 0.025 inches.

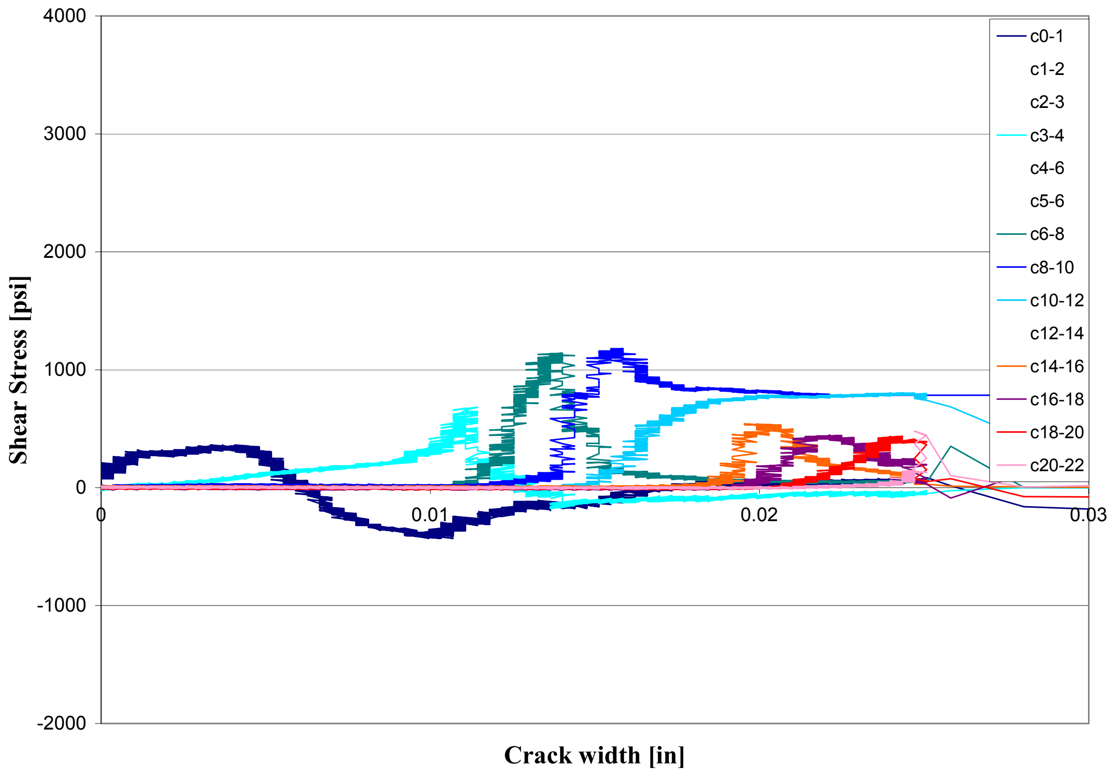

Figure 3.16: Shear Stress vs. Crack Width for Specimen DBL3

3.3.4 Test results for specimen DBL4

The DBL4 specimen debonded on the non-instrumented strip in the concrete-FRP interface. Figure 3.17 displays the strain gage measurements for the entire strip. The strain at the crack, Strain0, increased along with the strain 1 inch away, Strain1, as the crack opens. Strain2 and Strain3 debonded shortly after at a crack width of approximately 0.012 inches. Failure of the first 8 inches of the strip was caused by the debonding of the non-instrumented strip.

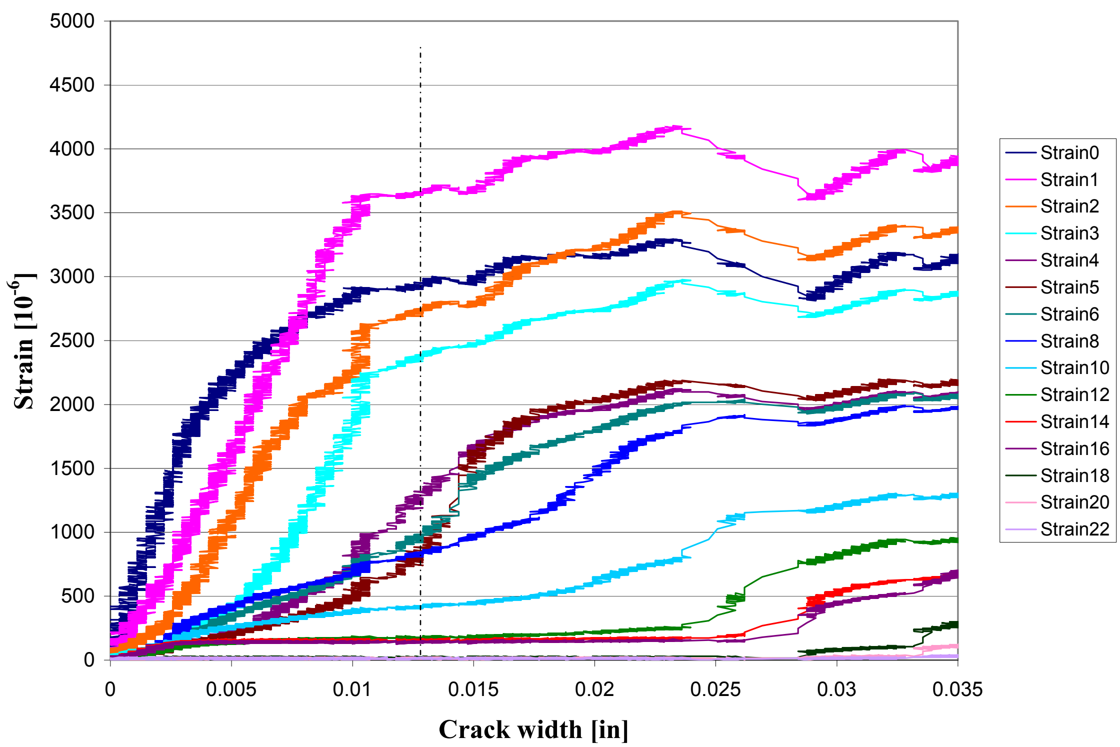

Figure 3.17: Reading vs. Strain for Specimen DBL4

Figure 3.18 shows the maximum load of 12.69 kips occurs a an average crack width of 0.012 inches. The maximum load corresponds to the failure of the non-instrumented strip. The applied load continues to increase after the first inch of the strip had debonded at a crack opening of 0.01 inches. The crack width opened evenly as the load was applied, however the displacement of the crack began to diverge. As more of the instrumented strip debonded, the crack gage measurements differ. The failure of the non-instrumented strip may have resulted from uneven loading of the specimen or a weaker bond strength of the non-instrumented strip.

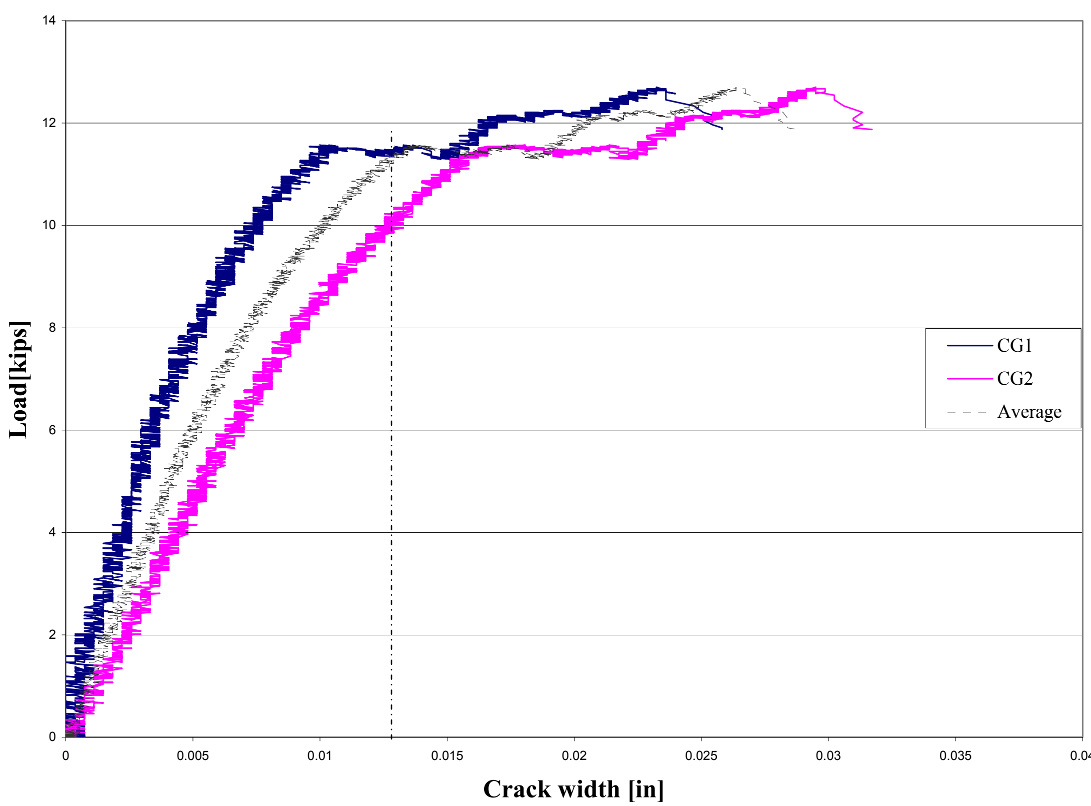

Figure 3.18: Load vs. Crack Width for Specimen DBL4

Figure 3.19 displays the strain profile along the FRP strip at selected intervals during the test of DBL4. The solid strain profiles indicate the maximum shear stress between two gages. The maximum shear stress, 1449 psi, was observed between 3-4 inches from the crack, at a crack width of 0.02 inches. The maximum occurs at the debonding failure of the non-instrumented strip.

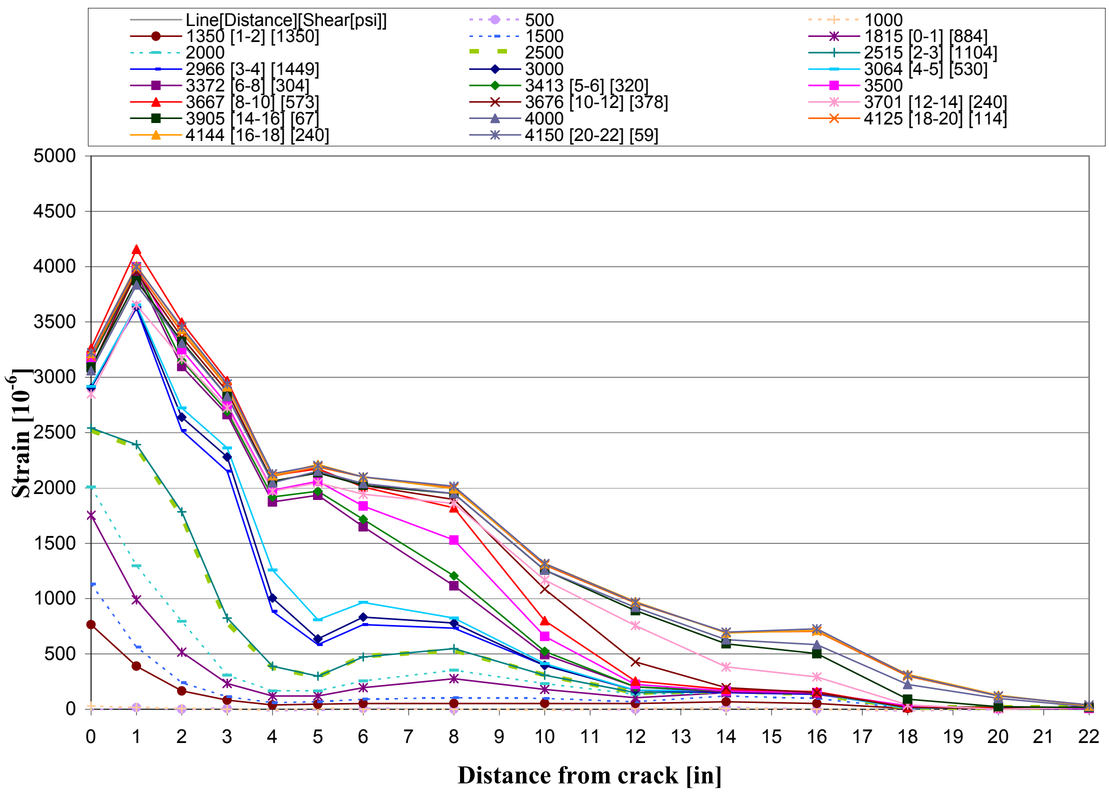

Figure 3.19: Strain vs. Distance from the Crack for Specimen DBL4

Figure 3.20 shows the maximum shear stress of 1449 psi occurs 3-4 inches from the crack, c3-4. The first peak, c0-1, displays the shear stress 1 inch from the crack, which increases as the crack opened and debonded as the bond shear stress c1-2, 1-2 inches away, increased. The delamination of the non-gage strip limited the ability to observe the increase and decrease in the peak shear stress throughout the strip. As the crack increases the first 8 inches of the FRP debonds at which time debonding failure of the non-instrumented strip occurs.

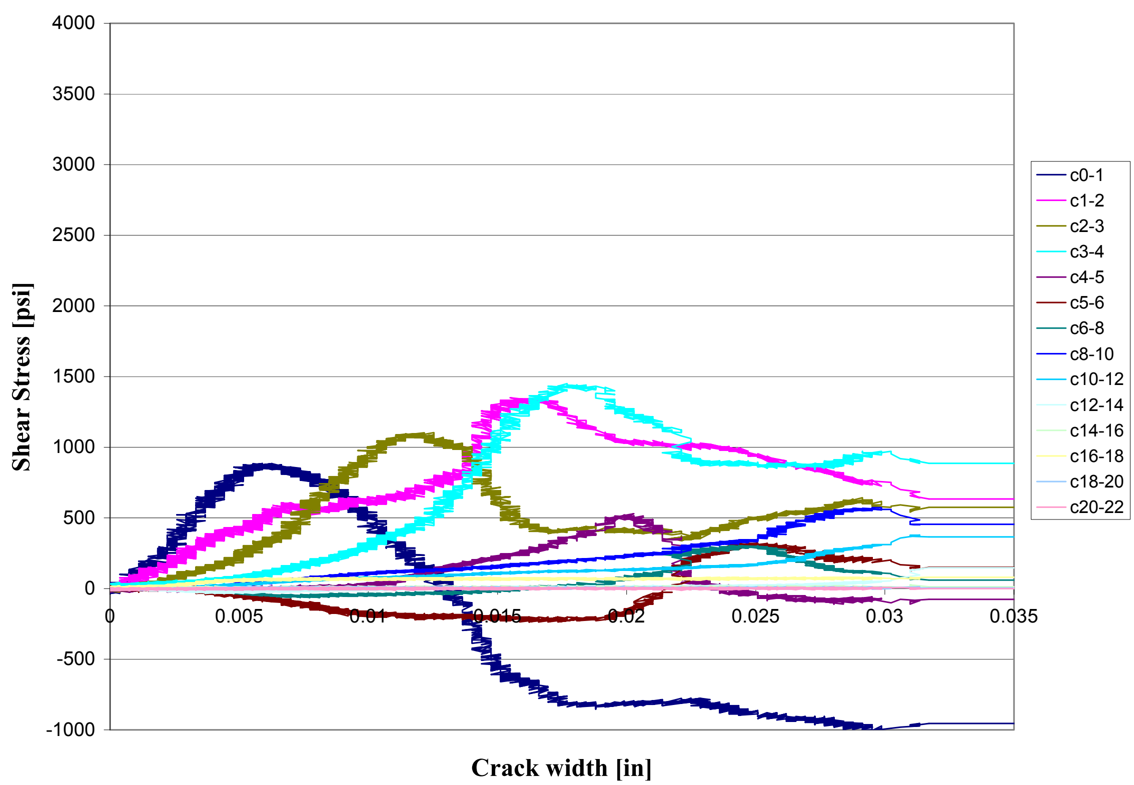

Figure 3.20: Shear Stress vs. Crack Width for Specimen DBL4

3.4 DBH Specimens

Of the four specimens tested, two delaminated in the non-instrumented FRP strip (DBH2 and DBH3) while DBH1 and DBH4 delaminated in the instrumented strip (Fig. 3.21). The dashed line indicates the initiation of debonding.

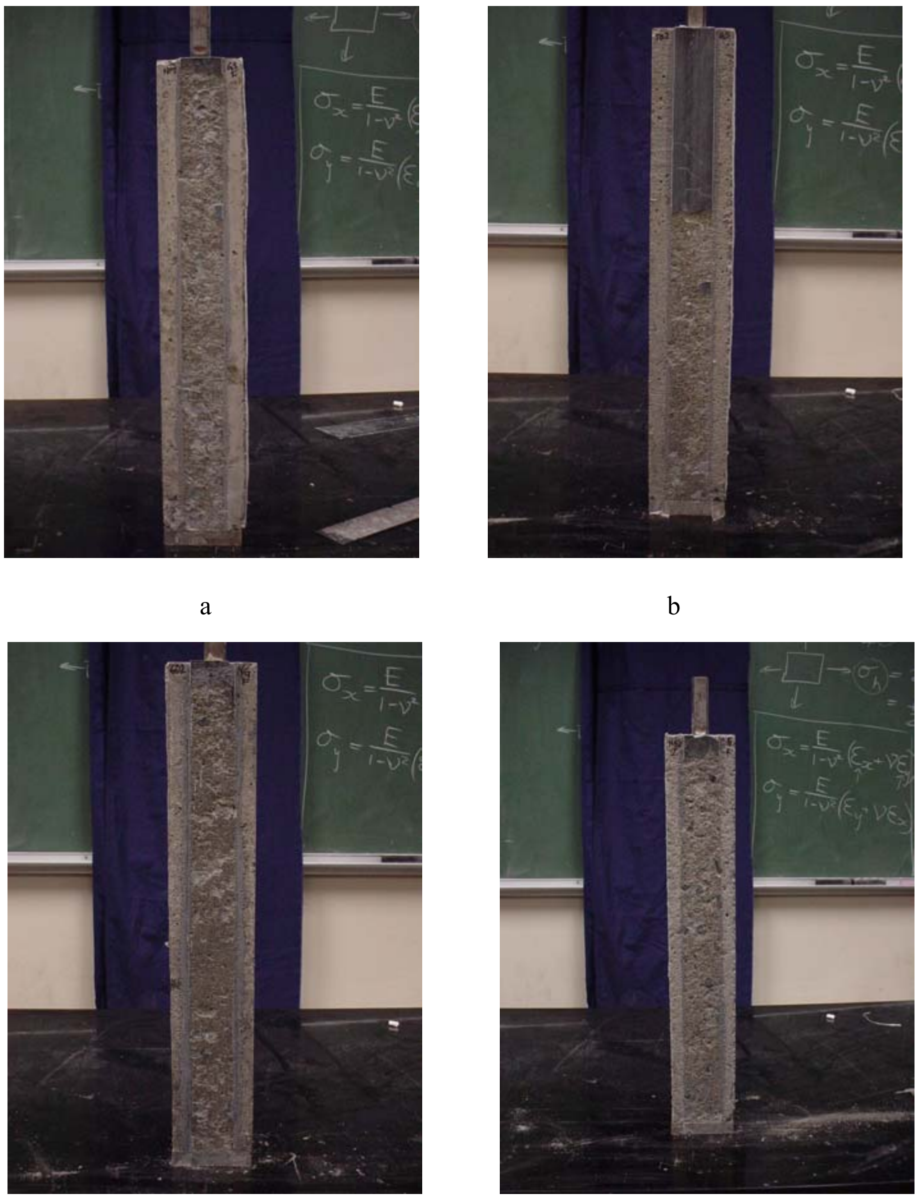

a b c d

Figure 3.21: Photo of Debonded DBH Specimens: (a) DBH1; (b) DBH2; (c) DBH3; (d) DBH4

3.4.1 Test Results for specimen DBH1

Figure 3.22 shows the strain gage measurements along the FRP strip for specimen DBH1. The debonding failure occurred in the instrumented strip in the concrete interface. The strain at the crack, Strain0, and one inch away, Strain1, increase as the crack opens. Strain2 and Strain3 debond shortly after at a crack width of approximately 0.005 inches. The first debonding occurs in the first 6 inches of the strip at a crack opening of 0.008 inches. Strain8, the strain in the FRP 8 inches away from the crack, shows partial debonding through a sudden increase in strain, however it continues to increase indicating the region between Strain8 and Strain12 was bonded. The second debonding led to complete debonding failure of the strip at a crack opening of 0.025 inches.

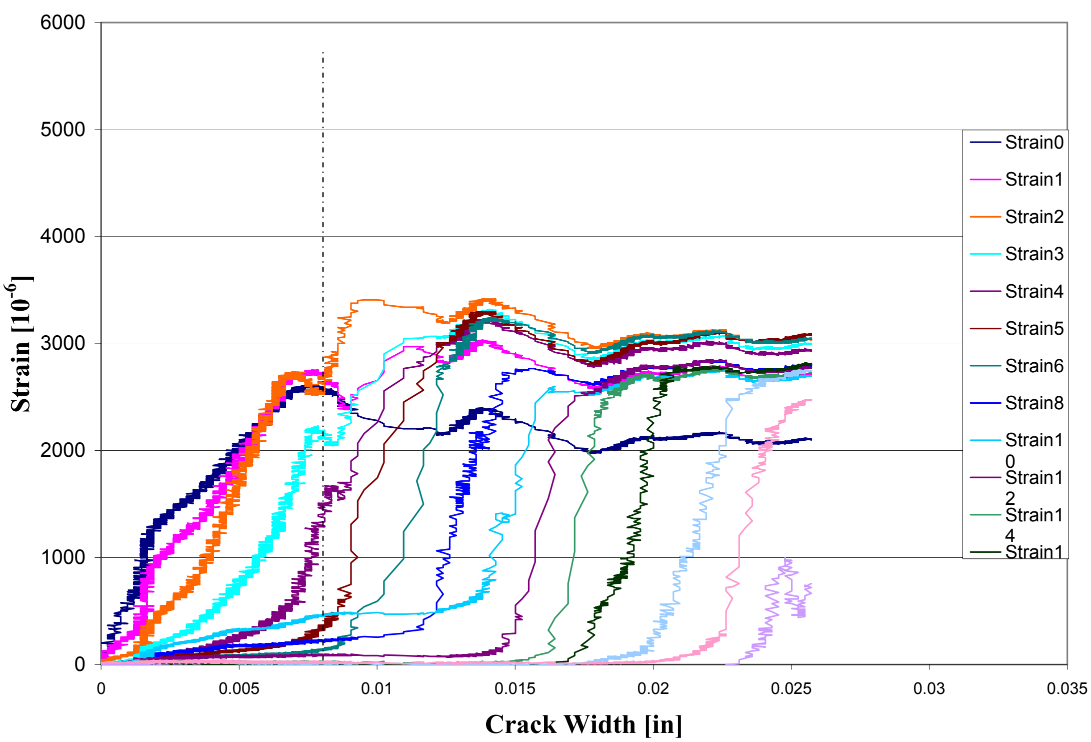

Figure 3.22: Strain vs. Crack Width for Specimen DBH1

Figure 3.23 shows the relationship between the applied load and the crack width. The maximum load, 10.45 kips, occurs at a crack width of 0.008 inches immediately prior to the debonding of the first 6 inches of the FRP strip. As the crack width increases, the FRP attempts to carry additional load, but fails with the second debonding failure at a crack width of 0.025 inches.

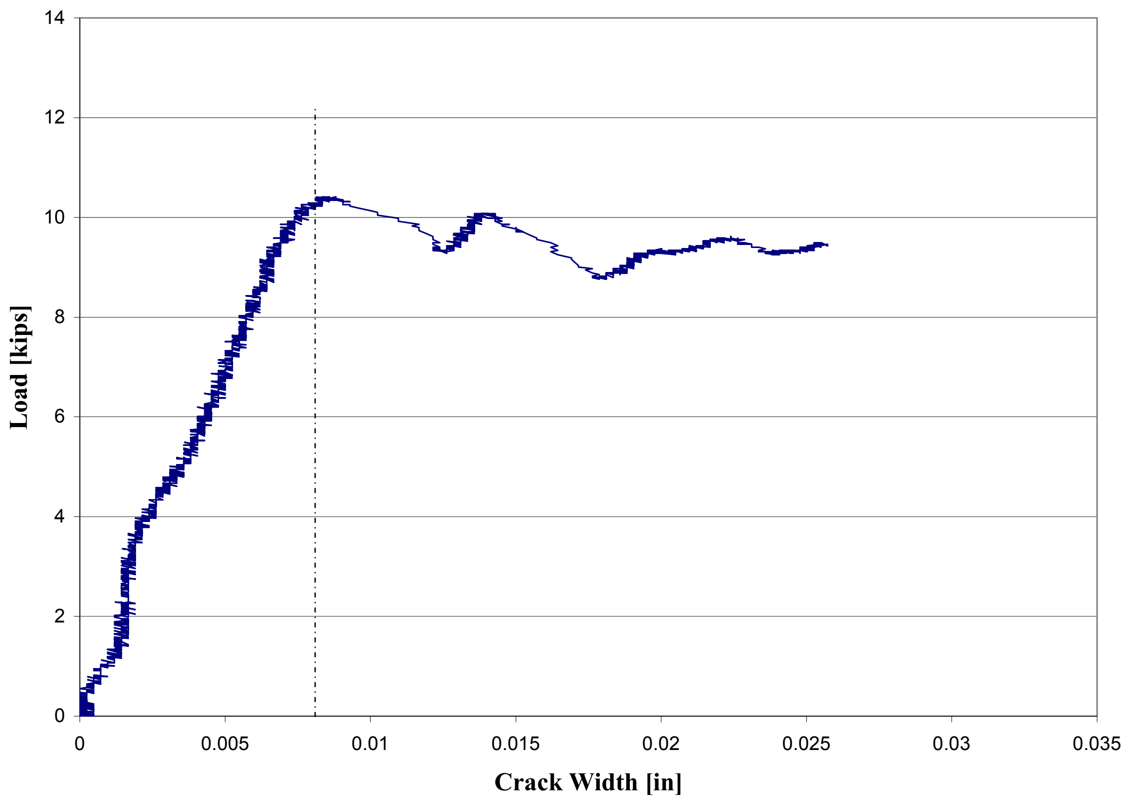

Figure 3.23: Load vs. Crack Width for Specimen DBH1

The two debonding events that occur in specimen DBH1 are observed in the strain profiles in Figure 3.24. The solid line strain profiles show the show the maximum shear stress in the bond observed between two gages. The maximum shear stress, 1449 psi, was observed between 5-6 inches from the crack. The first debonding failure of the first six inches from the crack is visible in the maintained high strain of approximately 3250 microstrain. The lack of preparation provided a good bond transfer for the high strength concrete. The lack of bond stiffness allowed for a more ductile failure of the strip.

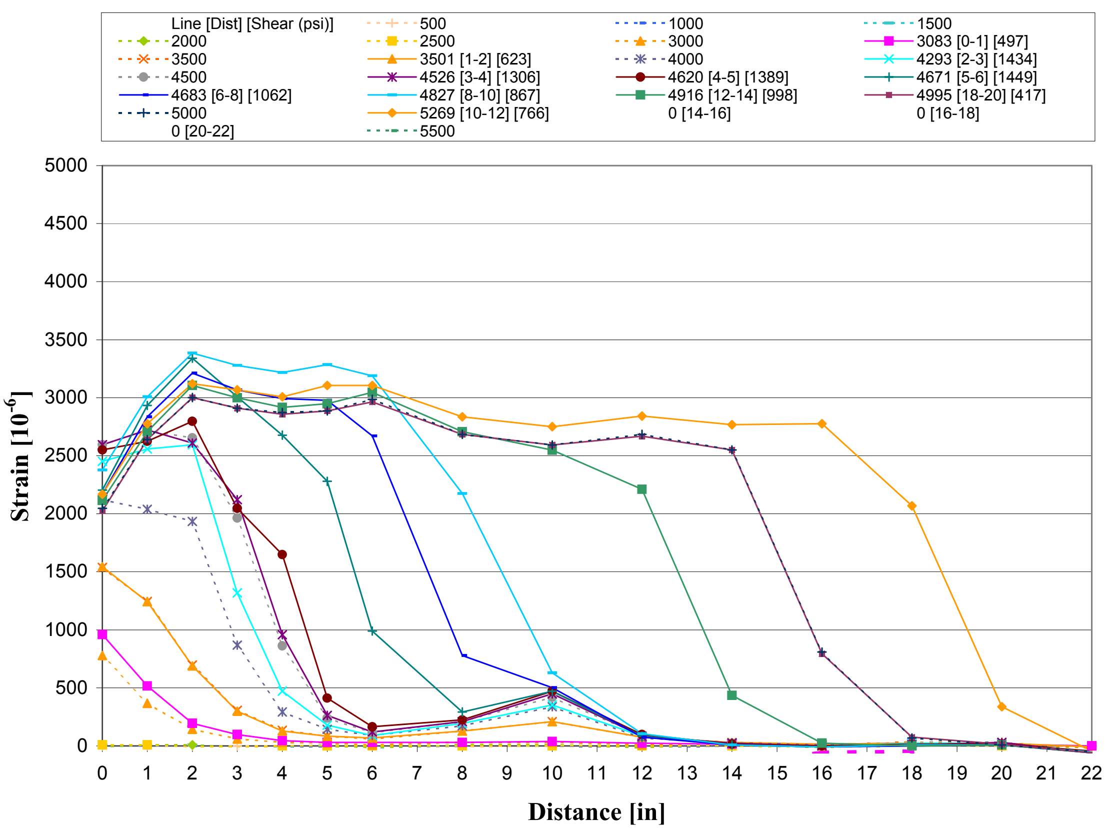

Figure 3.24: Strain vs. Distance from the Crack for Specimen DBH1

Figure 3.25 shows the peak shear stress of 1449 psi occurred 5-6 inches from the crack, c5-6. As the crack width increases the shear stress in the first inch of the bond begins to increase. Simultaneously the shear stress two inches away, c1-2 increases and surpasses c0-1. The development of shear stress in the bond propagates the length of the strip, visible in the increase and decrease along the length of the strip. The peaks in the first debonding, at a crack width of 0.008 inches, overlap which indicates a brittle fracture of the concrete interface. The remaining strip gradually fails with the clearly defined shear peaks increasing and decreasing, with segments of the FRP debonding.

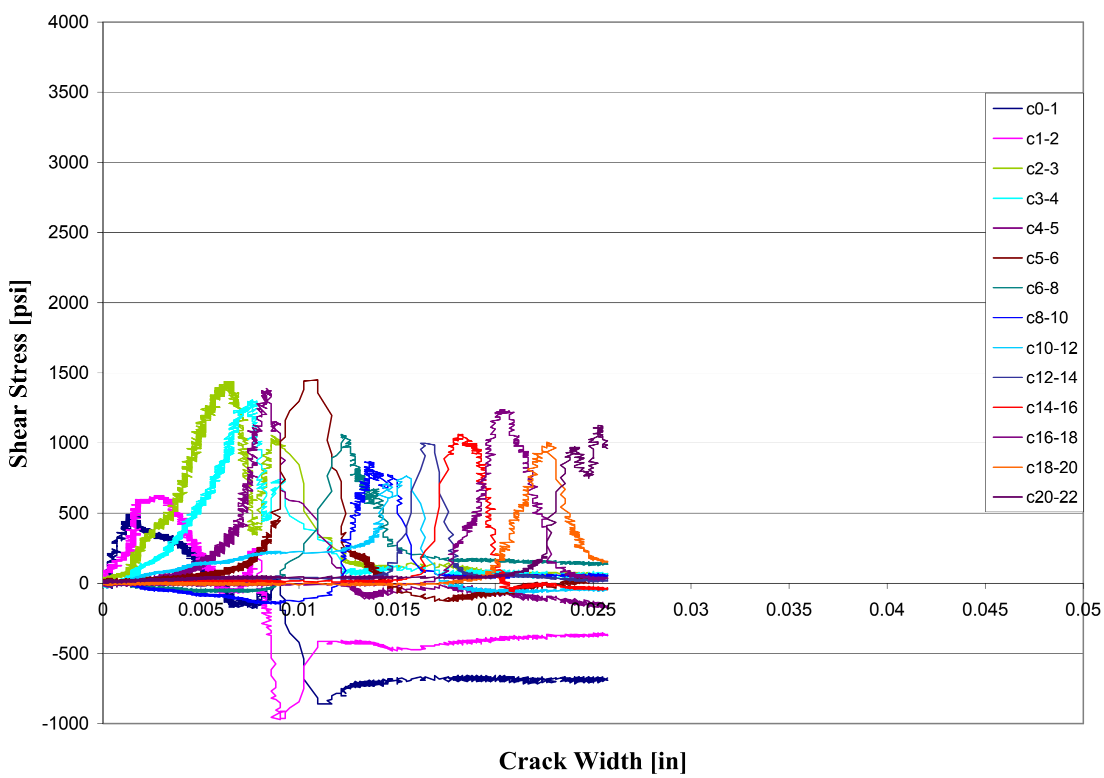

Figure 3.25: Shear Stress vs. Crack Width for Specimen DBH1

3.4.2 Test results for specimen DBH2

Figure 3.26 shows the strain gage measurements for the entire FRP strip. The DBH2 specimen failure was caused by delamination of the non-instrumented strip at a crack width of 0.015 inches. The strain at the crack, Strain0, begins to increase immediately as the crack opens. Strain1, one inch away, increases as well although at a slower rate, with the subsequent gages increasing as the crack opens. The first major debonding on the instrumented strip occurs in the first 8 inches of the strip at a crack opening of approximately 0.031 inches. The remaining bonded strip continues to carry the load as the crack width increases. The failure of the non-instrumented strip occurred at 0.049 inches, with subsequent failure of 16 inches of the FRP strip.

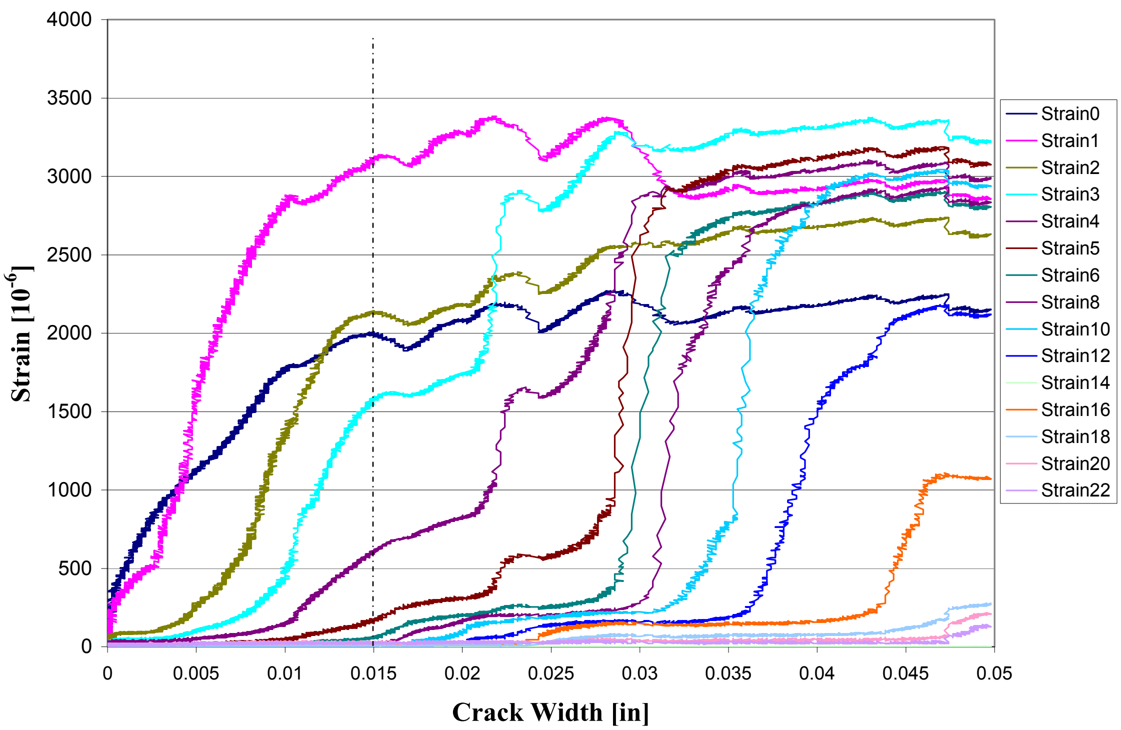

Figure 3.26: Strain vs. Crack Width for Specimen DBH2

Figure 3.27 shows the relationship between the applied load and the crack width. The maximum load of 10.05 kips occurs at a crack width of 0.049 inches. The fluctuations in the applied load indicate small debonding events on the non-instrumented strip before the first major debonding. The first decrease in the load occurs when the area one inch away from the crack debonds. The second decrease in the load, at a crack width of approximately 0.025 inches, occurs when the first two inches of the strip have debonded completely. The first major debonding event occurs at a crack width of 0.031 inches. The load continues to increase to the maximum until failure of the non-instrumented strip.

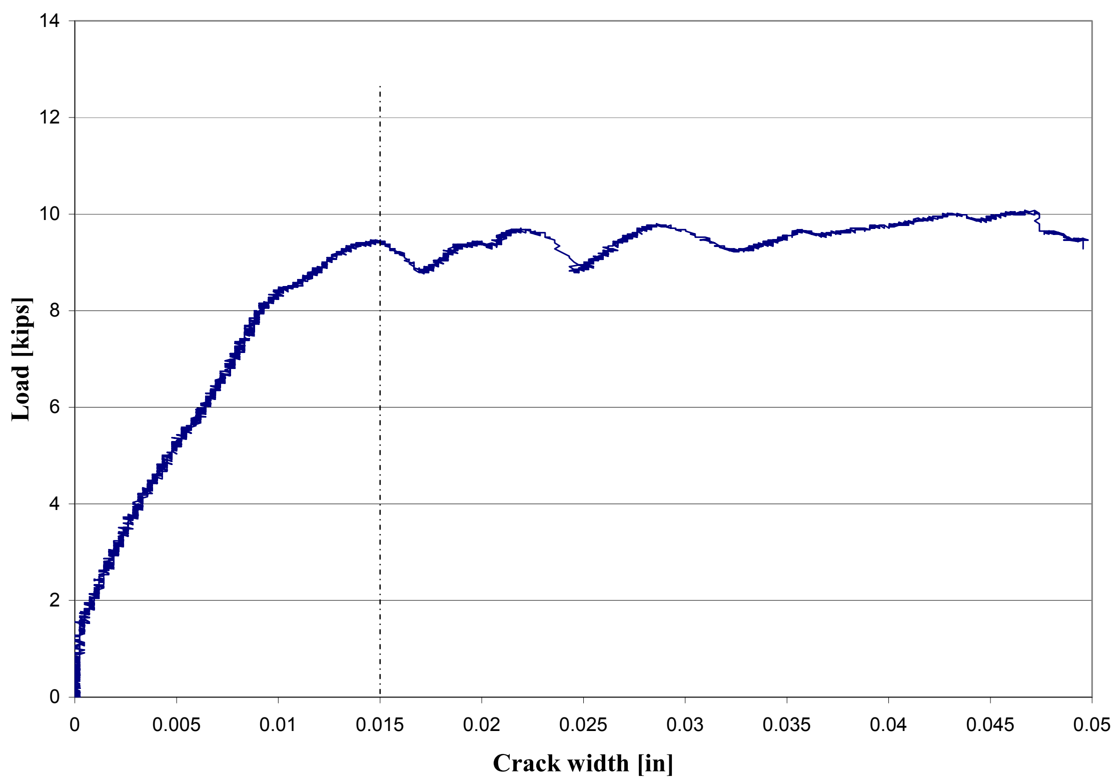

Figure 3.27: Load vs. Crack Width for Specimen DBH2

Figure 3.28 shows the strain profiles along the FRP strip at selected intervals during the test of DBH2. The solid line profiles display the maximum shear stress in the bond observed between two gages. The maximum shear stress, 2165 psi, was observed between 10-12 inches from the crack. The shear stress 1-2 inches away from the crack also was high at 2039 psi. The sandblasted surface increased the stiffness of the bond and provided a good bond transfer for the high strength concrete.

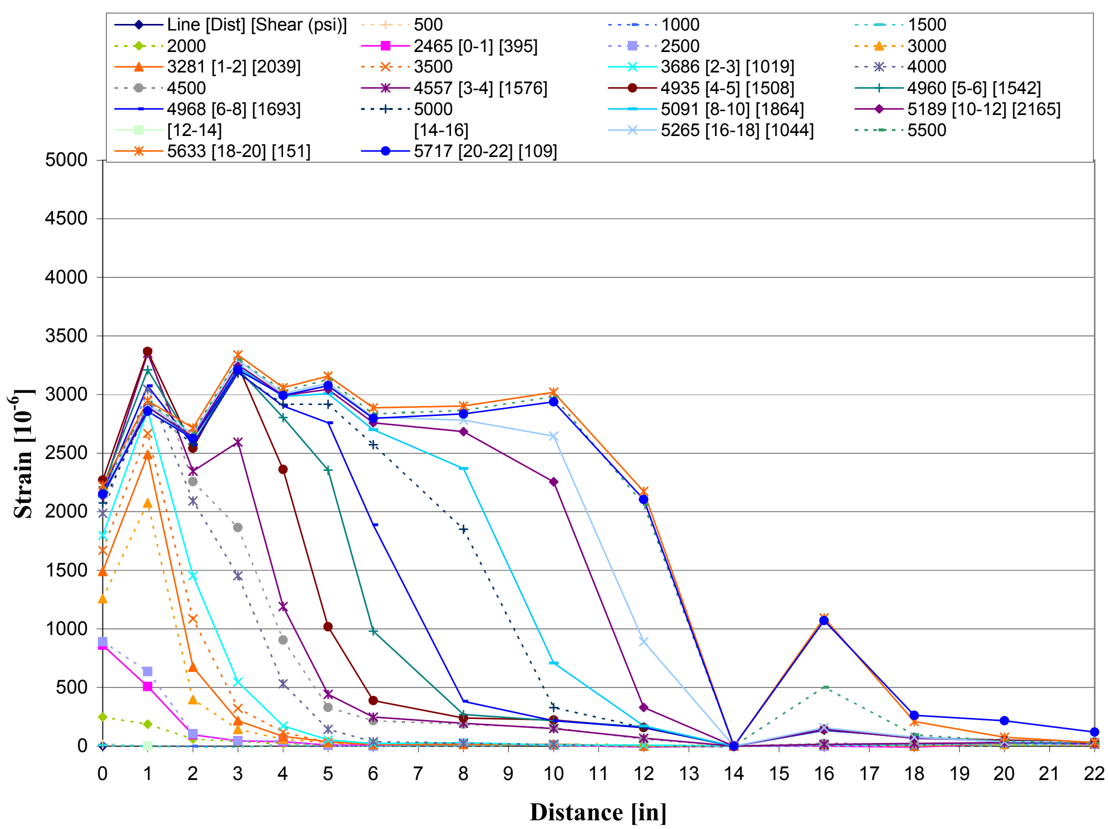

Figure 3.28: Strain vs. Distance from the Crack for Specimen DBH2

Figure 3.29 displays how the shear stress in bond developed throughout the FRP strip. The maximum shear stress of 2165 psi occurred 10-12 inches away, c10-12, almost equal to the shear stress 1-2 inches from the crack, which was 2039 psi. The shear stress one inch away from the crack c0-1 increased to the peak and then decreases becoming negative. The negative shear stress is attributed to the gage at the crack measuring less strain due to gage malfunction. The brittle fracture of the concrete surface is noted by the multiple peaks of shear stress that overlap. The overlapping signifies the fracture of the bond interface that propagates debonding failure of the strip.

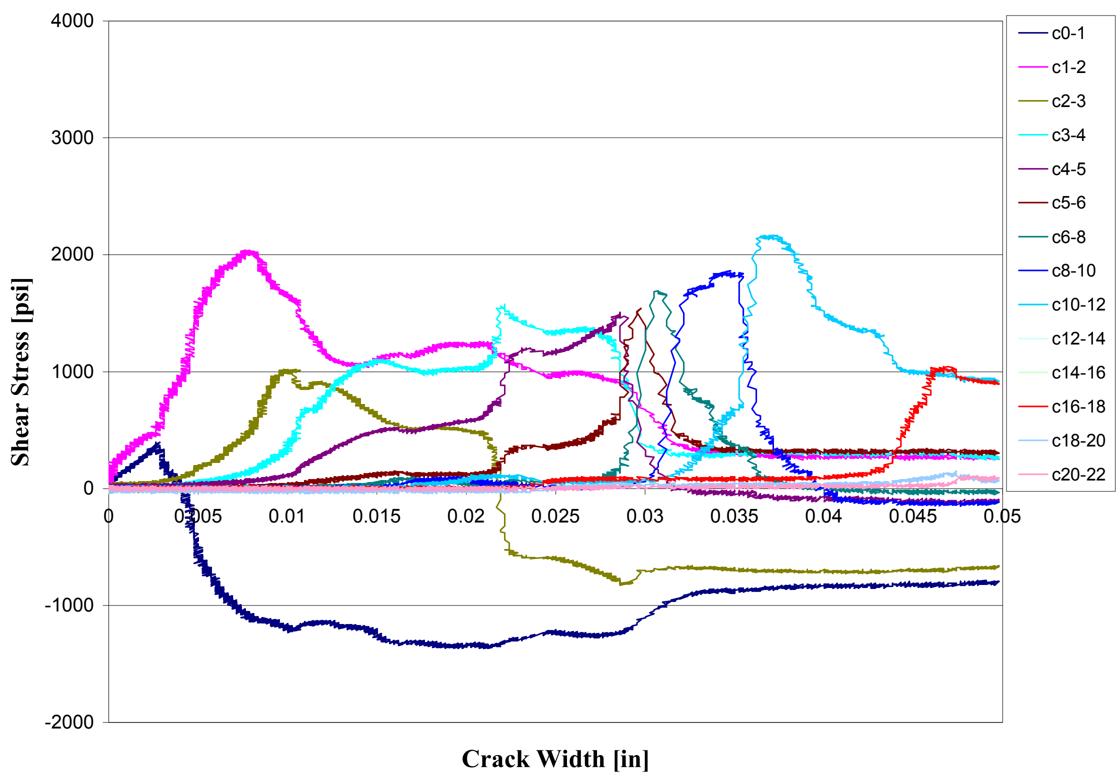

Figure 3.29: Shear Stress vs. Crack Width for Specimen DBH2

3.4.3 Test results for specimen DBH3

The premature debonding failure of the non-gage strip limited the results for DBH3. Figure 3.30 shows the strain measurements in the FRP as debonding of the non-instrumented strip initiated at approximately 0.018 inches. The strain at the crack, Strain0, beings to increase along with the strain one inch away, Strain1, before debonding failure of the non-instrumented strip at a crack width of approximately 0.034 inches.

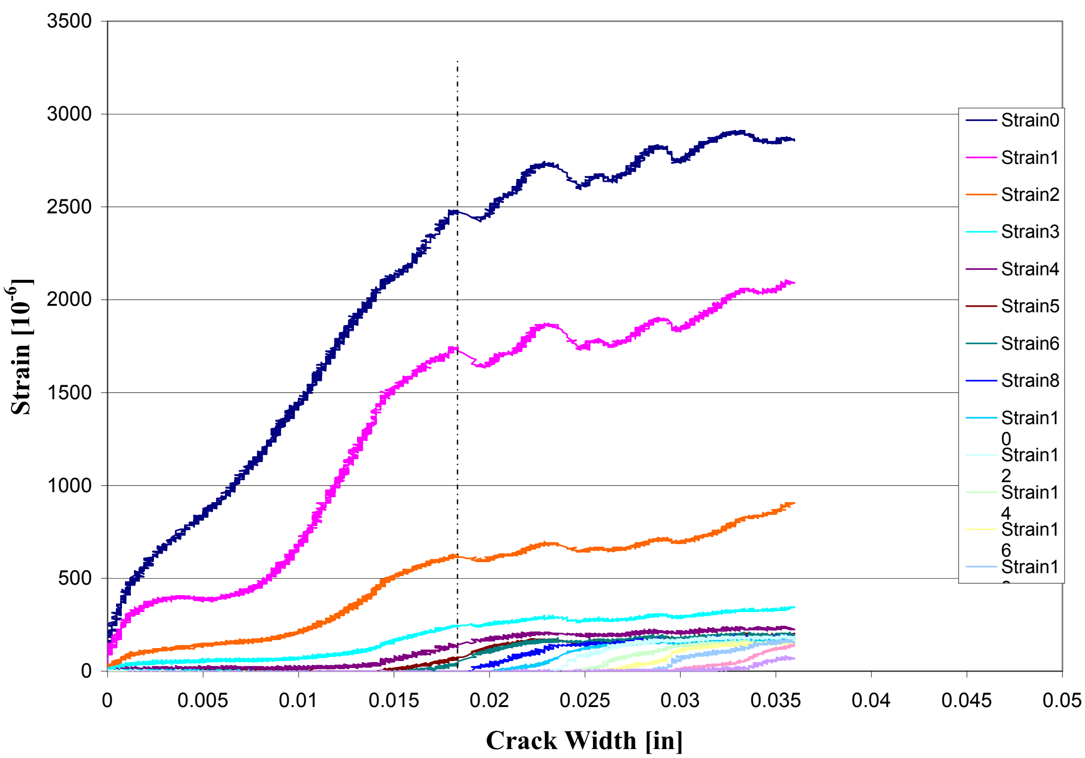

Figure 3.30: Strain vs. Crack Width for Specimen DBH3

Figure 3.31 shows the relationship between the applied load and the crack width. The maximum load of 8.72 kips occurs at a crack width of 0.034 inches. Fluctuations in the applied load do not indicate small debonding failure of the instrumented strip. The decreases in the applied load are attributed to the failure of the non-instrumented strip.

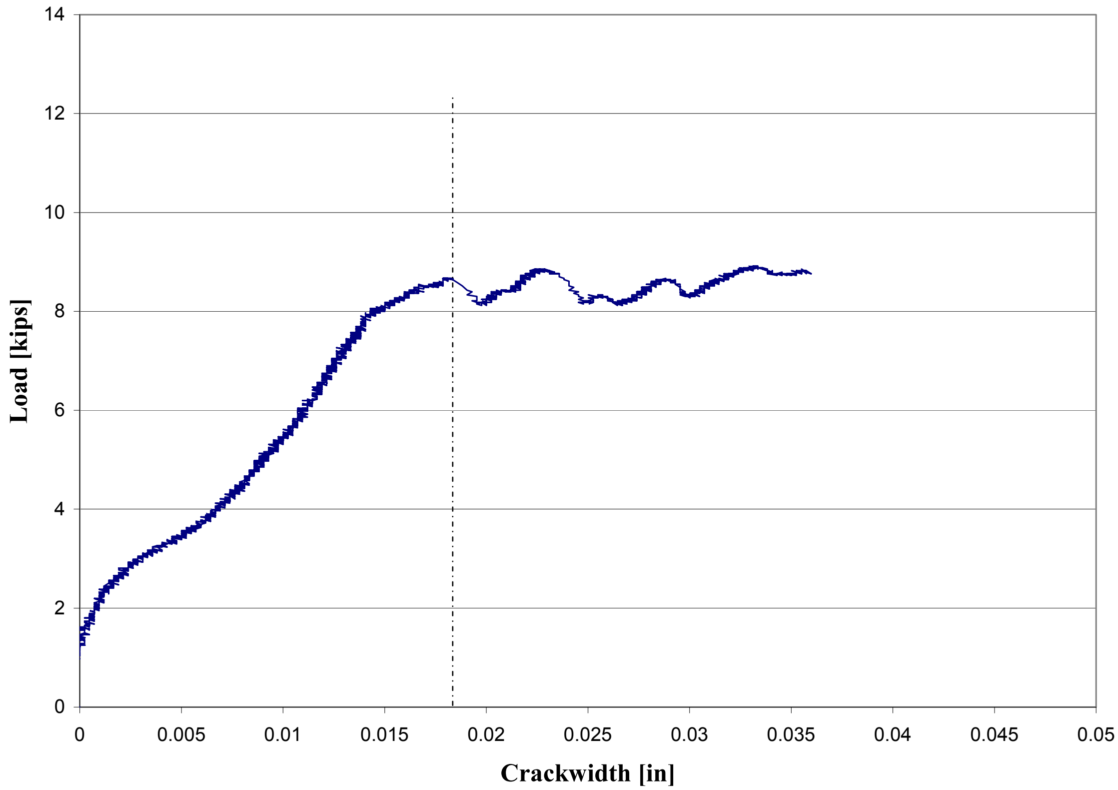

Figure 3.31: Load vs. Crack Width for Specimen DBH3

Figure 3.32 shows the strain profile for the entire FRP strip at selected intervals. The solid line profiles display the maximum shear stress in the bond observed between two gages. The maximum shear stress, 1390 psi, was observed between 1-2 inches from the crack. The low level of shear stress is attributed to the premature debonding of the non-instrumented strip.

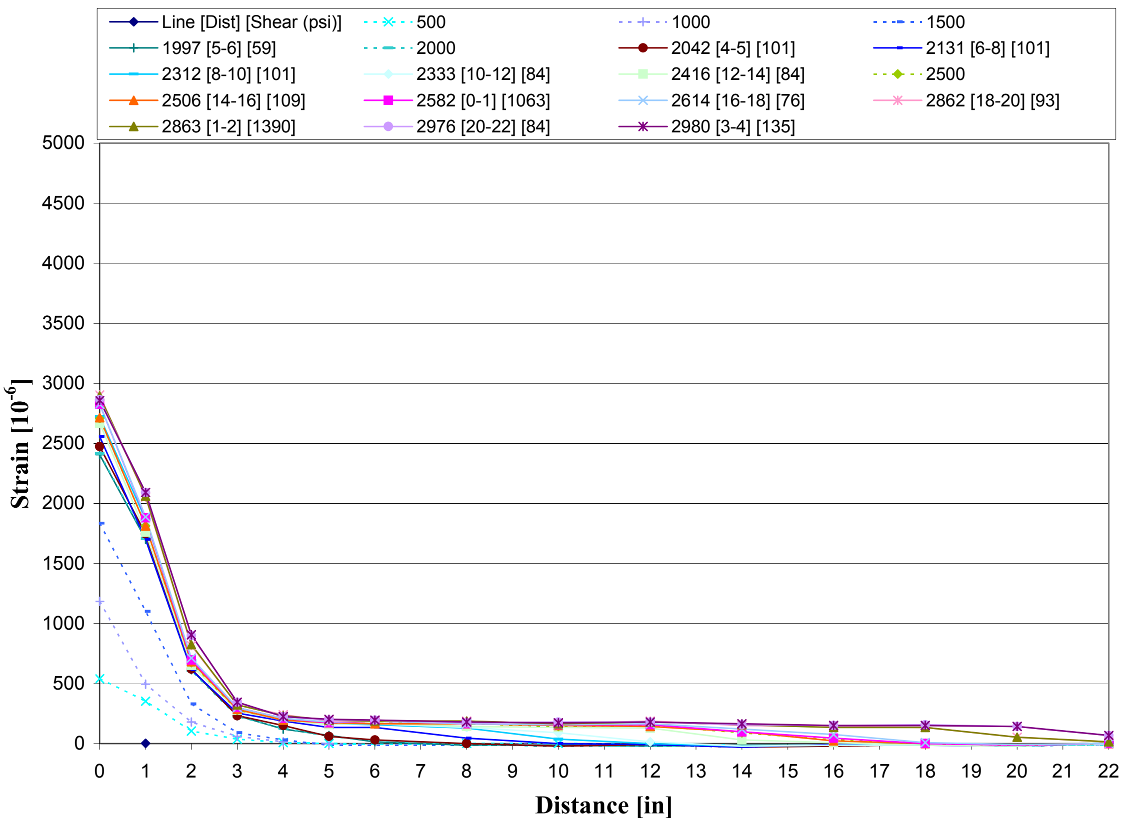

Figure 3.32: Strain vs. Distance from the Crack for Specimen DBH3

Figure 3.33 displays the shear stress in the bond. The maximum shear stress of 1390 psi occurred at a crack width of approximately 0.034 inches.

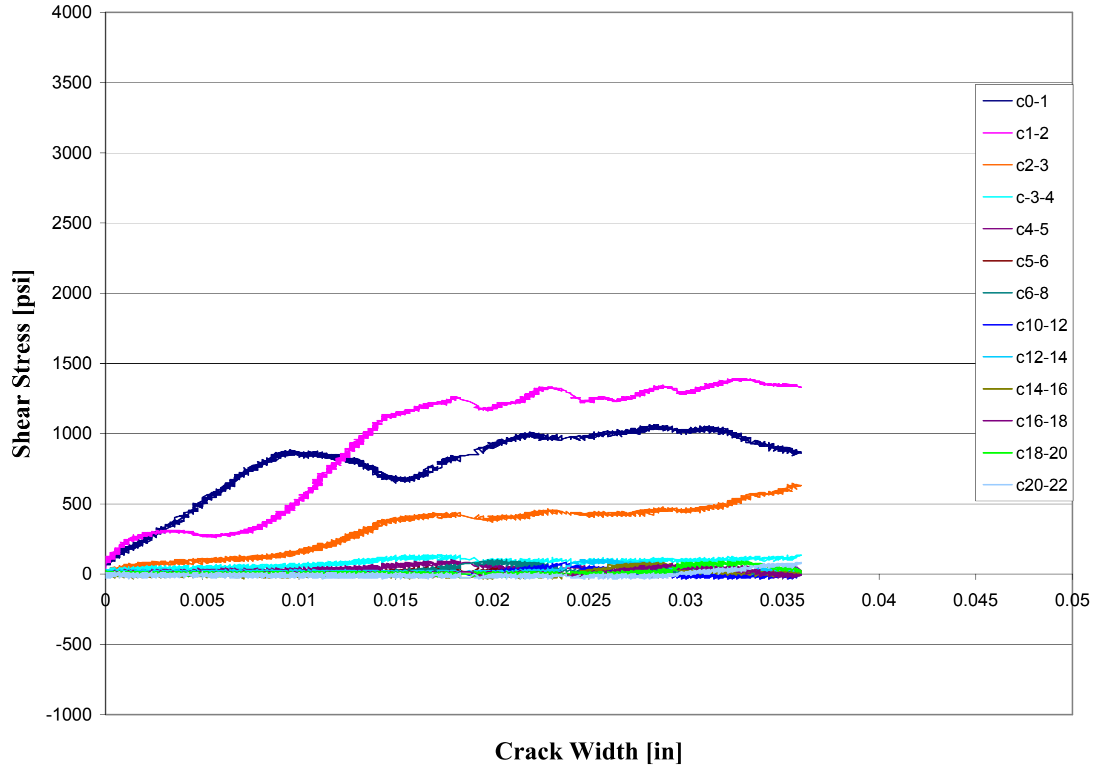

Figure 3.33: Shear Stress vs. Crack Width for Specimen DBH3

3.4.4 Test results for specimen DBH4

Figure 3.34 shows the strain measurements for all gages as the crack width increased. The debonding failure of specimen DBH4 occurred in the instrumented strip. The strain at the crack, Strain0, increased followed by the strain one inch away, Strain1. Strain2 also increased, however more gradually as the crack width increased. The first debonding failure occurred in the first 6 inches of the strip at a crack width of 0.015 inches. As the crack width increases, the remaining bonded FRP increases in strain. The failure of the FRP strip is evenly distributed, with single sections of the FRP increasing in strain, which indicates a peeling failure as opposed to the simultaneous fracture of the concrete interface, as found in the first six inches. The second debonding

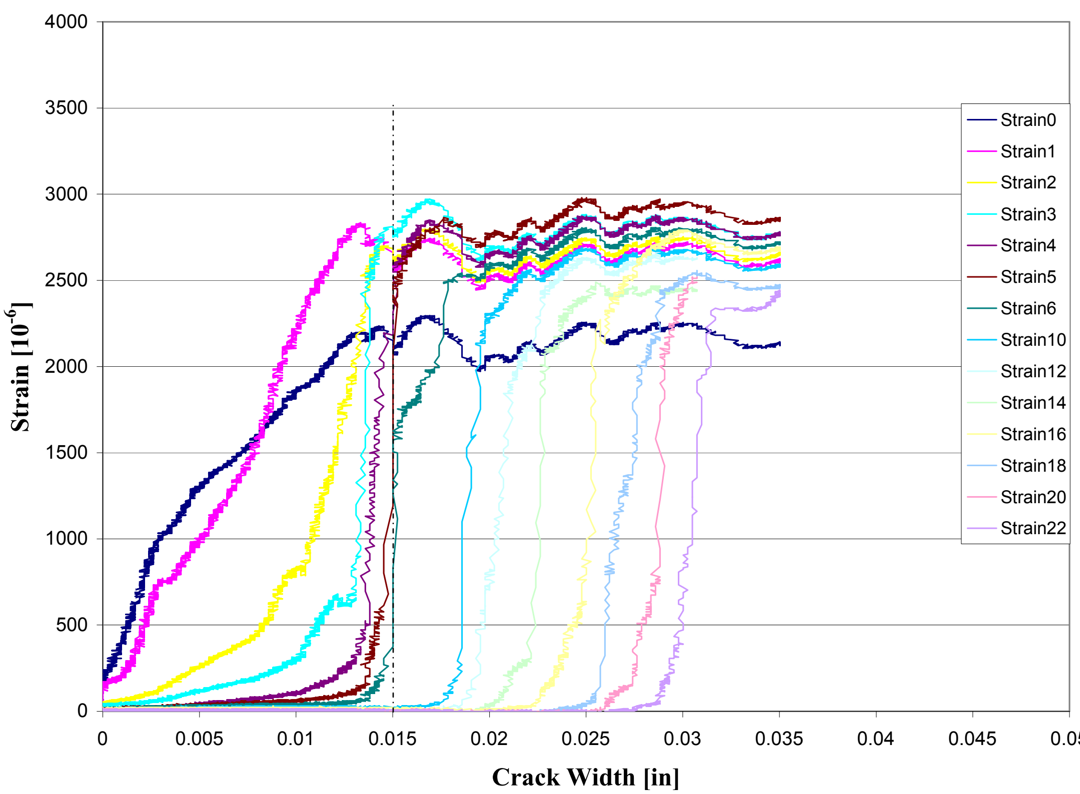

Figure 3.34: Strain vs. Crack Width for Specimen DBH4

led to complete failure of the FRP strip at a crack width of 0.035 inches.

Figure 3.35 shows the relationship between the applied load and the crack width. The maximum load of 9.32 kips occurs at a crack width of 0.035 inches. The first debonding failure occurs at approximately 8.5 kips and a crack width of 0.015 inches. The fluctuations in the applied load indicate small debonding events before the second major debonding failure. The load continued to increase to the maximum applied load, at which the final debonding failure occurred.

In figure 3.36, the strain profiles along the length of the FRP indicate the strain at selected intervals. The solid line strain profiles display the maximum shear stress in the

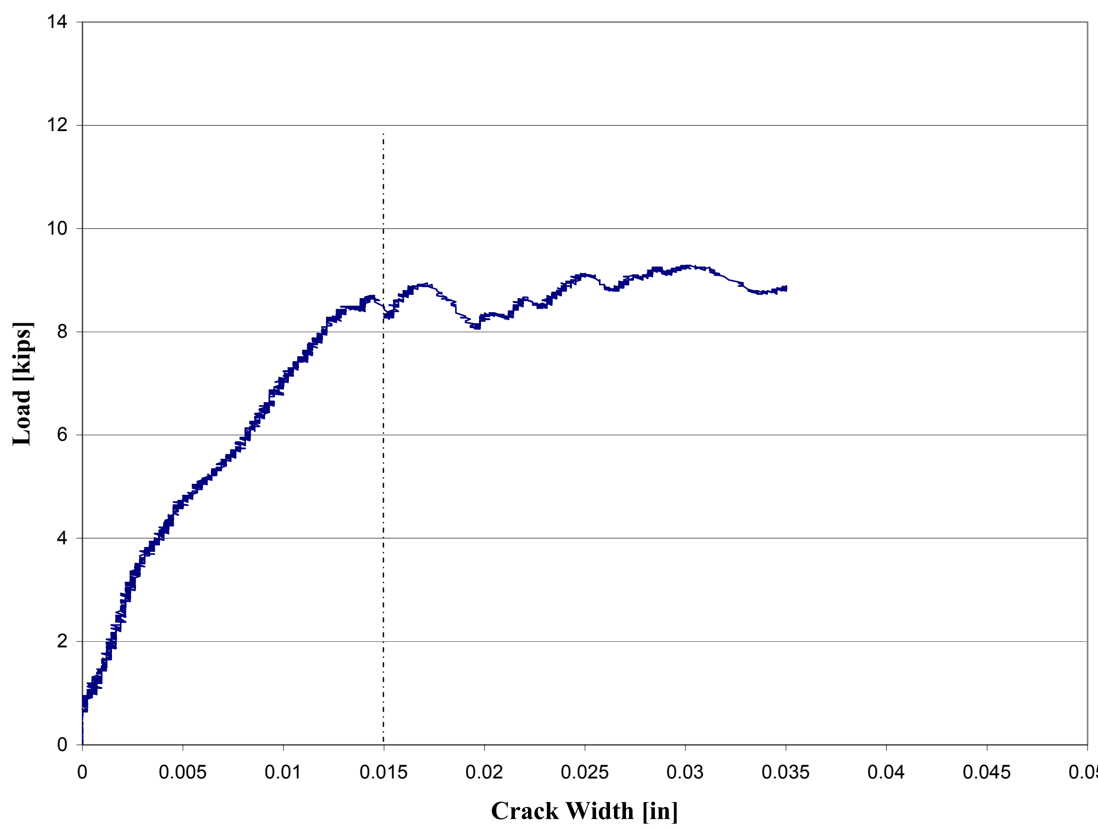

Figure 3.35: Load vs. Crack Width for Specimen DBH4

bond observed between two gages. The maximum shear stress, 2932 psi, was observed between 16-18 inches from the crack at a crack opening of 0.025 inches. High bond stresses were found throughout the specimen. The largest shear stress in the first six inches of the strip was found four inches away, 1938 psi at a crack opening of approximately 0.015 inches (during the first debonding failure). The surface preparation provided a good bond transfer for the high strength concrete. The strain profiles show the two debonding failures that occurred in the FRP strip.

Figure 3.37 shows that the shear stress peaks are clearly defined as the crack width increases. As the crack opening increases, the shear stress 1 inch from the crack, c0-1, reaches the maximum and then decreases, becoming negative. The negative value is

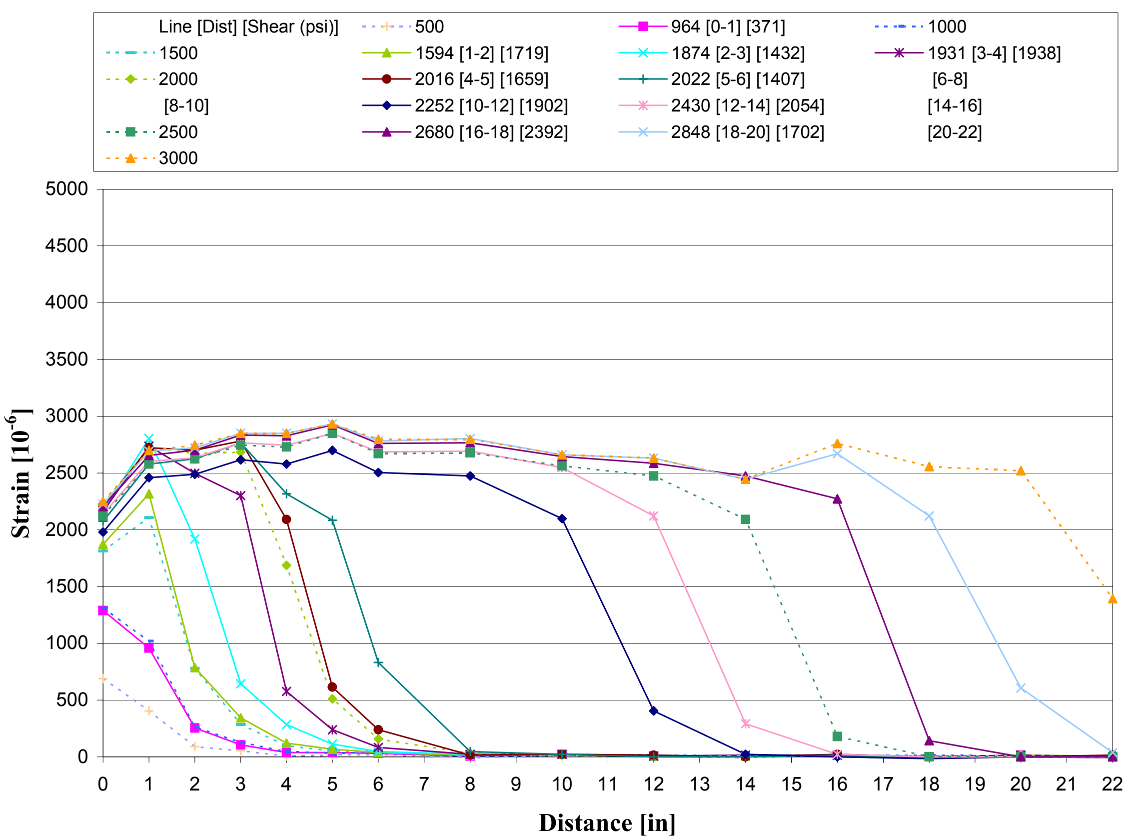

Figure 3.36: Strain vs. Distance from the Crack for Specimen DBH4

attributed to the lower strain reading, possibly due to the failure of the gage. The next segment, c1-2, increases simultaneously with c0-1, and continues to increase to the peak shear stress. As the area two inches away from the crack, c1-2, debonds, the shear stress in the next two one-inch segments increases. The first six inches of the strip display a brittle fracture of the FRP interface, illustrated by the overlapping peaks. The remaining peaks indicate a peeling failure, similar to the S1A and S1B specimens. The peaks increase and decrease without the overlapping found in the first six inches of the strip. The delamination is similar to the steel specimens S1A and S1B, due to the strong bond interface which is comparable to the FRP-steel bond interface.

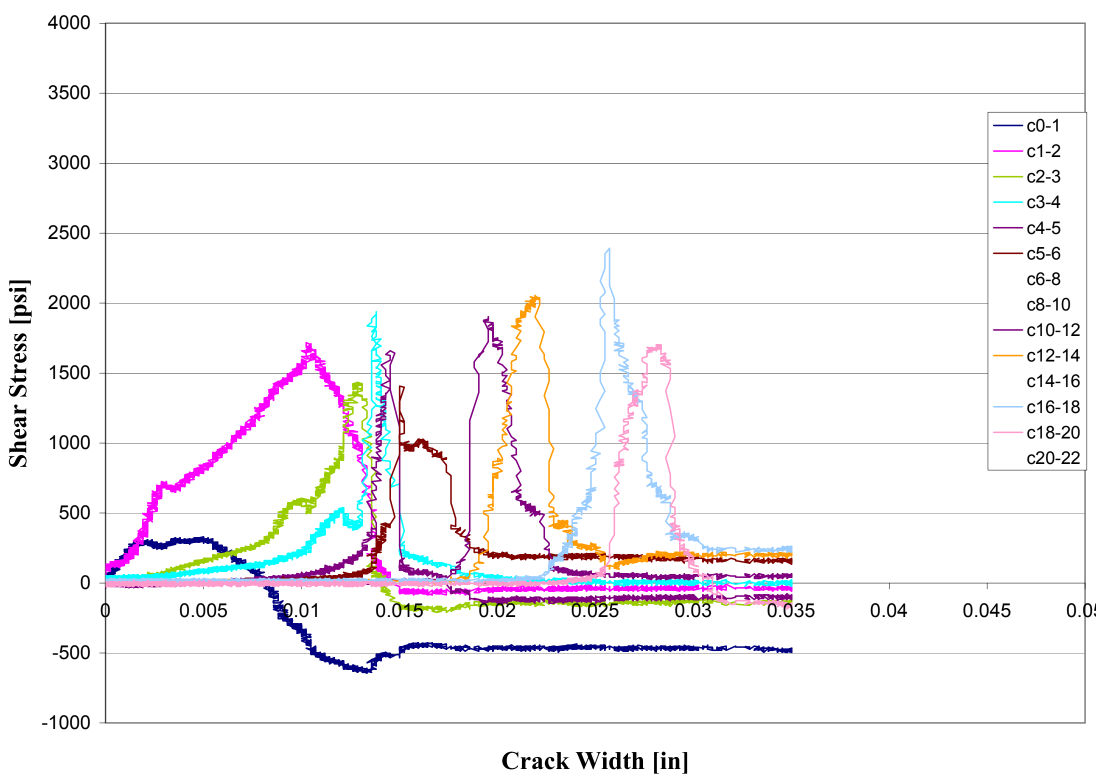

Figure 3.37: Shear stress vs. Crack Width for Specimen DBH4

3.5 Concrete Comparison

The results summary of the concrete specimens, DBL and DBH are found in Table 3.9a and 3.9b. Table 3.9a shows the total maximum load and corresponding crack width and Table 3.9b shows the results within the initial debonding failure for each specimen.

Table 3.9a. Maximum Load and Crack Width for DBL and DBH specimens

Specimens	Maximum Load [kips]	Crack width at Maximum Load [in]
DBL1*	12.62	0.009
2*	13.43	0.013
3	13.27	0.022
4*	12.69	0.012
DBH1	10.45	0.008
2*	10.05	0.049
3*	8.72	0.034
4	9.32	0.035

* Non-instrumented strip delaminated

3.5.1 Comparison of results on DBL Specimens

The performance of the DBL specimens did not provide any definitive results, which can partially be attributed to premature failure of the non-instrumented strip on all but one specimen. The experiments did provide information on the bond strength and the effect of the surface preparation. In the DBL1 specimen no preparation was used and the specimen had the lowest values for the ultimate load and the maximum bond shear stress. The values of bond stress, however, are similar to the SC1 specimen, with the maximum shear stress occurring in the first three inches of the crack (Fig. 3.8). Specimen DBL2 had the highest load and second highest crack width (Fig. 3.10 and

Table 3.9a). The bond stress in specimen DBL2 was greater than specimen DBL1 and was again located in the first three inches from the crack (Fig. 3.8 and 3.12). Specimen DBL3 had the largest crack width and the second largest load; however it was the only specimen to fail on the instrumented strip (Table 3.9a). The bond stress was largest eight inches from the crack (Fig. 3.15). The strain readings indicate the first delamination occurs with delamination of the first 8 inches from the crack and then a

Table 3.9b. Maximum values within initial debonding length for the DBL and DBH

	Maximum Values Within Initial Debonding Length					
Specimen	Maximum Load per FRP strip [kips]	Crack width [in]	FRP strain at the crack [$\mu\varepsilon$]	Debonding Length [in]	Average Shear Stress over debonding length [psi]	Maximum Shear Stress for limit ($\Delta\varepsilon/\Delta x_i$) [psi]
DBL1*	5.6	0.009	3000	8*	355*	715*
2*	6.72	0.013	3500	6*	569*	1138*
3	5	0.012	2500	8	317	1141
4*	6.35	0.012	3250	—*	—*	1449*
DBH1	5.23	0.008	2500	8	332	1449
2*	5.03	0.015	2750†	8*	319*	2039*
3*	4.36	0.018	2800	—*	—*	1390*
4	4.26	0.015	2250	6	360	1938

* Non-instrumented strip delaminated
† Strain1 reading

second delamination of the remaining strip (Fig. 3.13 and Table 3.9b). Specimen DBL4 performed almost equally to specimen DBL2. The highest bond shear stress values were located in the first four inches of the strip (Fig. 3.15), and were comparable to specimens DBL2 and DBL3.

The results of the DBL specimens suggest that with a lower strength concrete, surface preparation does help provide a good bond interface between the concrete and FRP. The shear stress in the bond indicates the surface preparations have comparable bond strengths for surfaces prepared by sandblasting, grinding and needle gun.

3.5.2 Comparison of results on DBH Specimens

The failure of the instrumented strip occurred in two specimens, DBH1 and DBH4. The DBH1 specimen performed well and reached the highest maximum load (Fig. 3.23 and Table 3.9a). The shear stress in the bond was highest at 6 inches from the crack, and measured high bond shear stress in the first six inches of the strip (Fig. 3.24). Delamination of the instrumented strip had almost occurred in DBH2 before the non-gage strip failed. The specimen achieved the second highest load and largest crack opening (Fig. 3.27 and Table 3.9a). The highest shear stress in the initial debond length was located 2 inches from the crack, with high values measured along the remaining delaminated strip, indicating a good bond. Specimen DBH3 had a partial failure of the instrumented strip with very little shear stress developed in the bond. The specimen had the third largest crack width and the lowest ultimate load (Fig. 3.31). The DBH4 specimen provided a good bond, with a crack width comparable to specimen DBH3. The maximum shear stress in the bond was located at 18 inches away from the crack (Fig. 3.36). The entire strip measured high values with the largest values in the center of the strip. The first delamination occurred with the first 6 inches of the strip failing, the second debonding fails the remaining strip (Fig. 3.34).

Overall, the DBH specimens performed poorly in contrast to the DBL specimens. The ultimate load was achieved by no surface preparation. The DBH results suggest that with a higher strength concrete, surface preparation does help provide a good bond interface between the concrete and FRP. The shear stress in the bond indicates the surface preparations have comparable bond stresses for surfaces prepared by sand blasting, needle gun and grinding.

3.5.3 Comparison of DBL and DBH Specimens

The results indicate the higher strength concrete (DBH specimens) produced a more brittle failure of the FRP at lower loads than the DBL specimens, at approximately the same crack width. All three surface preparations used in this study gave similar results.

The results show the concrete strength can help improve the bond strength and shear stress, which allows for a larger crack opening before failure, however the failure occurs at a lower ultimate load. In both the DBL and DBH specimens, the first six to eight inches of the strip delaminated at a crack width between 0.009 and 0.018 inches (Table 3.9b). The tests indicate that the first eight inches are part of the critical bond transfer length and once debonded, delamination continues to propagate along the remaining strip.

3.5.4 Comparison with other research

Additional research on the FRP debonding failure of double face shear-type specimens was conducted by Zhang (2005). The study found the maximum load for two specimens, with sandblasted surface preparation, varied from 7.2 to 9.8 kips. The concrete strength of the specimens was approximately 8000 psi, equivalent to the DBH specimens in this study. The maximum strain that occurred at debonding ranged from 1500 to 1750 microstrain. The approximate bond shear stress was obtained by averaging the maximum change in strain between two adjacent gages. The sandblasted surface provided a good bond transfer and the approximated shear stress range was 710 to 754 psi. In general the specimens in the Zhang (2005) study obtained lower values at the initiation of debonding. The load at debonding was approximately 3.25 to 4.1 kips per FRP strip. The crack width at the initiation of debonding was between 0.01 and 0.017 inches, corresponding to a strain at the crack of approximately 1400—1500 microstrain. The effective bond length, L_e, was 6-7 inches for both specimens.

The DBH2 specimen is comparable to the specimens in the Zhang (2005) study. The DBH2, or sandblasted higher strength concrete specimen, was able to achieve a higher load, 5.03 kips per strip, at approximately the same crack width, 0.015 inches (Table 3.9b). The strain at the crack before the initiation of debonding was also higher, and the debonding length was slightly larger, approximately 8 inches (Table 3.9b). The approximate average bond shear stress for specimen DBH2 was greater. The variation between the results presented in this study and the Zhang (2005) results are attributed to the loading rate of the experiment. In the study presented here, the loading rate for the concrete debonding specimens, DBL and DBH, was 1.68 mm/min. The experiments in the Zhang (2005) study were conducted at a slower loading rate, approximately 0.021 mm/min.

The effect of the loading rate on FRP debonding was investigated by White et al. (2001). The authors compared the effect of a slow loading rate, 0.0167mm/s (1.002mm/min), and a fast loading rate of 36mm/s (2160mm/min). The White et al. study showed the beams tested at a slower rate achieved a lower ultimate load and strain in the FRP. White et al. (2001) concluded that the specimens with the faster loading rate had a slight increase in flexural capacity and stiffness in comparison to the specimens loaded at a slower rate (White et al., 2001). The loading rate did not affect the failure mode of the FRP. The conclusions of the White et al. study agree with results presented here and in the Zhang (2005) study.

Prior research also has obtained maximum values for the strain in the FRP at debonding failure. Oehelers and Seracino (2004) presented a comparison of recommendations of FRP IC debonding resistances obtained from several different methods. The intermediate crack (IC) strain, at 95 % of the characteristic value, ranged from 2500 to 8500 microstrain. The maximum strain results from the DBL and DBH specimens in this study correspond to the lower values recommended.

The results from this study are also in agreement with the design limits obtained from ACI 440 guidelines (ACI440R-02). The ACI 440 recommended effective strain for two sided bonding for the lower strength concrete (DBL specimens) was approximately 2000 microstrain and 2400 microstrain for the higher strength specimens (DBH). These values are similar to the maximum strain at the crack prior to the initial debonding for both DBL and DBH specimens (Table3.9b).

Of the eight specimens tested in this study, three debonded on the instrumented strip, DBL3, DBH1 and DBH4. The maximum strain at the crack at initiation of debonding for these specimens was in a range from 2250-2500 microstrain. The crack width at the initiation of debonding was between 0.008 and 0.015 inches, and the debonding length was 6 to 8 inches.

Overall, the results presented in this study are in agreement with the maximum strain values indicated by the ACI guidelines and in other studies. Prior results also indicated the lack of significant difference in performance between the three concrete surface preparations. The effect of concrete strength on FRP debonding failure still is unclear, however the concrete strength does appear to improve the bond strength, while the increased concrete stiffness may result in a more brittle delamination failure.

Chapter 4: FRP Anchorage Specimens

4.1 Introduction

Debonding is the most common failure mechanism for externally applied FRP systems. Unless effective anchorage is provided at each end of the FRP, debonding represents failure of the entire system. Providing end anchorage can ensure structural integrity even after debonding. Anchorage of FRP systems can be achieved through effective mechanical anchorage or embedment into the concrete. In this series of tests, a wet lay-up anchorage system is compared to pre-cured anchorage system for a bridge shear retrofit application. The test materials and installation procedures were designed to replicate the actual bridge installation to determine feasibility as well as performance of both FRP systems.

4.2 Experimental Setup

4.2.1 Specimen Description

The specimens were constructed in a large reinforced concrete slab (Fig. 4.1). The slab was prepared with slots of varying widths from $^{1}/_{8}$ inch to ½ inch. A preliminary test

Figure 4.1: Photo of Concrete Slab for Anchorage Experiments

found the slots too narrow for proper installation of the FRP fabric anchor. Two slots were widened to approximately ¾ inch to 1 inch. The depth of the slots was approximately 4 inches.

4.2.2 Material Properties

The experiment utilized two types of FRP systems. The wet lay-up system employed SikaWrap Hex 103C (Table 4.1) with the Sikadur 300 epoxy (Table 4.2). The second system used pre-cured CarboShear-L plates (Table 4.3). Both of the FRP systems were anchored into the slot using Sikadur 30 epoxy that was mixed with silica sand in a 1:1 ratio (Table 4.4).

Table 4.1. SikaWrap Hex 103C Design Properties

Tensile Strength	5.5×10^5 psi (3,793 MPa)
Tensile Modulus	34×10^6 psi (234,500 MPa)
Elongation at Break	1.5%
Density	0.065 lbs/in^3 (1.8g/cc)
Width	25 in

Table 4.2. Sikadur 300 Design Properties

Tensile Strength	8,000 psi (55 MPa)
Tensile Modulus	2.5×10^5 psi (1,724 MPa)
Elongation at Break	3%
Recommended Surface Preparation	ICRI CSP 3

Table 4.3. Sika CarboShear-L Design Properties

Tensile Strength	2.83×10^4 lbf /1.57 in(126 kN/40 mm)
Modulus of Elasticity	17.4×10^6 psi (120 GPa)
Thickness	0.055 in (1.4 mm)
Width	1.57 in (40 mm)

Table 4.4. Sikadur 30 Design Properties

Tensile Strength	3,600psi (24.8 MPa)
Modulus of Elasticity	6.5 x 10^5 psi (4,482 MPa)
Elongation at Break	1%
Recommended Surface Preparation	ICRI CSP 3

4.2.3 Installation

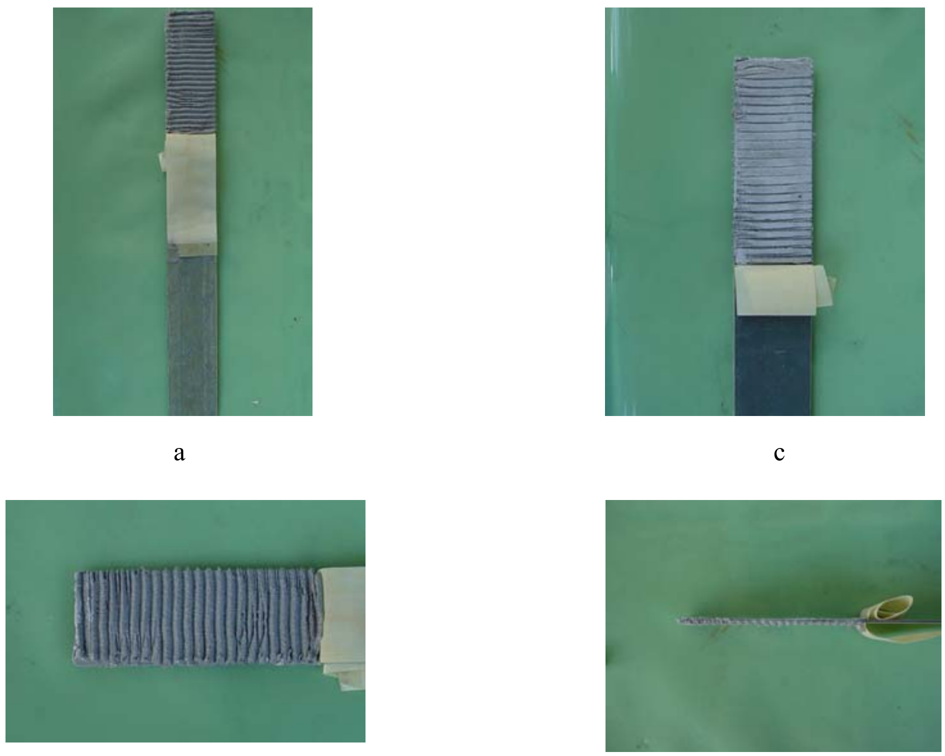

a c b d

Figure 4.2: Photo of CarboShear-L Specimens with Sikadur 30 Epoxy: (a-b) epoxy on both sides; (c-d) epoxy ground down

The procedure to install the anchorage was designed to replicate installation of anchors into the soffit of the bridge deck at the top end of shear stirrups on the actual bridge.

The preliminary installation used slots with varying widths, from $^1/_8$" to $^1/_2$". The slots were too narrow to install the FRP anchors. As the wet lay-up specimens were pushed into the slot the fabric began to curl and develop kinks in the wet fabric. The slot was also too narrow to place the nozzle of the epoxy cartridge into the slot without shifting the installed wet lay-up specimen. Although the thin cross-section of the CarboShear-L specimens was able to fit into the slot, the remaining slot width was too narrow for the epoxy nozzle. After the preliminary installation, the slots were widened to approximately ¾ " to 1", while maintaining the 4 inch depth of the slot.

The slots were first cleaned with water to remove loose pieces of concrete and then blown dry with an air hose removing loose dust and particles. The slots were primed using a sponge soaked in Sikadur 300 epoxy (Table 4.2). Four inches of the protective

Figure 4.4: Photo of SikaWrap Hex 103C with GFRP rod for anchorage

Figure 4.5: Photo of SikaWrap Hex 103C with plexi-glass sheet

sheet on the CarboShear-L FRP stirrups (Table 4.3) were removed for anchorage and then cleaned with MEK. Two strips were left bare, while three strips had pre-cured anchorage ends consisting of Sikadur 30 epoxy (Table 4.4) placed on both sides and combed using a $^{1}/_{8}$ inch trowel (Fig. 4.2a-b). To allow for installation flush against the girder web, one side of the anchorage strip was ground smooth on one of the anchorage specimens (Fig. 4.2c-d).

<u>Wet Lay-up Anchorage Installation</u>

The SikaWrap Hex 103C was impregnated with Sikadur 300 epoxy as per the manufacturer's instructions. The end of the two-ply 6 inch wide wet lay-up fabric was wrapped tightly around a $^{1}/_{4}$" square by 7" long bar of Glass FRP (GFRP) to help anchor the fabric at the base of the slot (Fig. 4.4). The fabric was kept straight and taut as a sheet of plexi-glass was used to press it into the slot (Figure 4.5). The plexi-glass was removed and placed the slot was filled with Sikadur 30 epoxy.

<u>CarboShear-L Anchorage Installation</u>

The slot was filled with Sikadur 30 epoxy and compacted until the slot was filled. The

Figure 4.3: Photo of Installed anchorage specimens

pre-cured FRP strip was then forced into the slot ensuring the strip remained straight. Epoxy was again compacted ensuring no air pockets were present. All anchorage specimens were cured for a minimum of 14 days, ensuring the FRP remained straight and perpendicular to the concrete surface (Fig. 4.5). The wet lay-up system was cured between sheets of Teflon plastic to prevent bonding with the support surfaces.

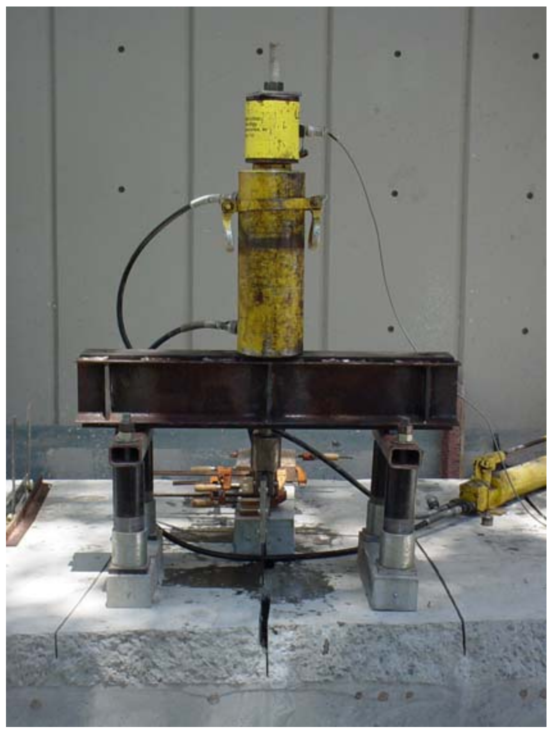

Figure 4.6: Photo of Initial test set-up

4.2.4 Test setup

The initial test setup used an I – beam resting on two adjustable supports placed on the concrete slab (Fig. 4.6). A clevis attached to clamping plates was used to grip the FRP, ensuring that the apparatus was plumb and level to reduce any bending effects. The clevis was attached to a threaded rod that ran through a hydraulic ram and load cell. A preliminary test showed a lack of clamping force and failure occurred in the clamping plate epoxy.

Figure 4.7: Photo of CarboShear-L final test set-up and detail of grip

Additional clamping of the loading plates was provided by a manual grip and larger bolts. The CarboShear-L plates were gripped using a manual grip attached to a threaded rod that was loaded by the hydraulic ram (Fig. 4.7). A preliminary test was run to ensure there was no rotation caused by the grip. During each pull-out test the applied load was recorded using a National Instruments data acquisition system.

4.3 Results

4.3.1 CarboShear-L Plates

The failure for all four specimens was a brittle failure of the fiber with no visible effect on the anchorage zone (Fig. 4.8). The failure loads were between 6.14 and 15.01 kips, all below the 28 kip tensile capacity of the CarboShear-L plate (Fig. 4.9). These premature failures are attributed to weakness introduced by predrilled holes in the FRP for the initial test set-up (Fig. 4.10). The loading responses for all four specimens are shown in Figure 4.9.

Figure 4.8: Photo of the Failure of CarboShear-L Plates

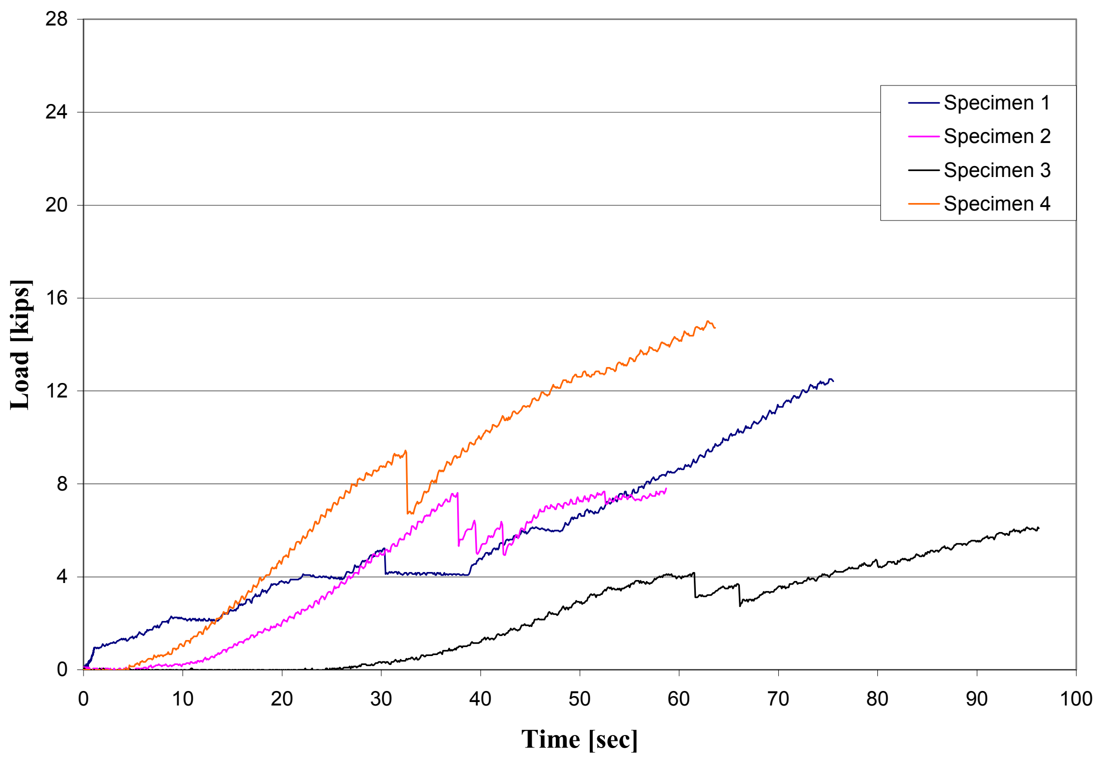

Figure 4.9: Load vs. Time for CarboShear-L Anchorage Specimens

a

b

c

d

Figure 4.10: Photo of CarboShear-L Plates Failed with Anchorage zone detail: (a) Double Grout; (b) Single Grout; (c) No Grout; (d) No Grout

4.3.2 Wet lay-up Anchorage System

Figure 4.11 shows the results from the wet lay-up anchorage specimen tests. Specimen 1 developed a kink in the fabric during curing and had a tearing failure at that point. The specimen reached 16.12 kips before failure. Specimen 2 failed at the edge of the anchorage zone in the fabric. The load at failure was 27.37 kips. Specimen 3 was unable to be tested due to bending of the clamping apparatus. The specimen reached 15.2 kips before the test was stopped. Specimen 2 was the only experiment tested to failure and the anchorage zone remained undamaged (Figure 4.12). None of the specimens developed the full fracture capacity of the CFRP fabric (approximately 50 kips). The premature failures are attributed to misalignment of the applied load.

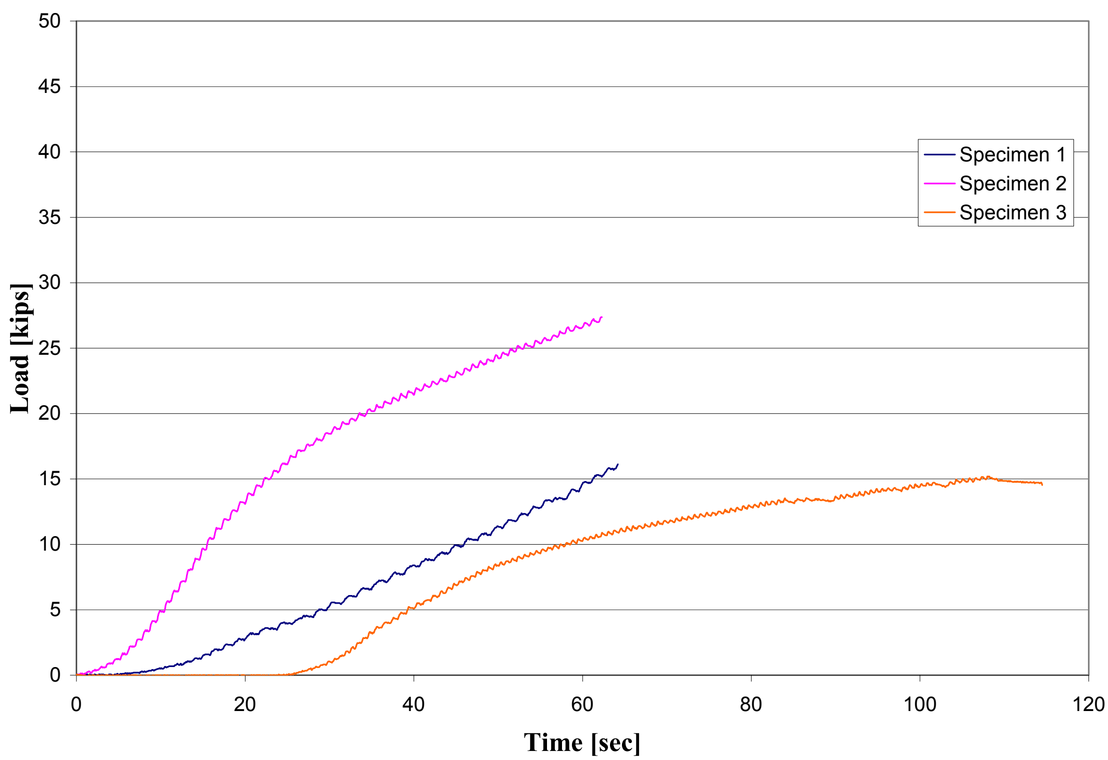

Figure 4.11: Load vs. Time for Wet Lay-up Anchorage Specimens

Figure 4.12: Wet lay-up Anchorage zone Specimen 2

4.4 Comparison of FRP Anchorage Systems

4.4.1 CarboShear-L Anchorage System

The results from the CarboShear-L plates demonstrated that the anchorage system was effective and remained undamaged. The comparison of the pull-out tests, however were inconclusive due to the varying loads and premature failure of the strips (Figure 4.9). The failure mode of the plates was a shear fracture of the fibers and not failure of the anchorage zone. The results indicated that damage of the laminate caused a premature shear failure in the CFRP plate. An undamaged laminate and a test set-up which would place a direct force on the anchorage zone could better demonstrate the design tensile strength and performance of the anchorage system.

4.4.2 Wet lay-up Anchorage System

The results from the wet lay-up specimens also showed the effectiveness of the anchorage system. The results, however were not repeated in the other specimens due to premature failure of the fiber and malfunction of the test set-up. The failure in the fiber along the edge of the anchorage zone, at 27.37 kips (Figure 4.11) was well below the expected load of 50 kips for the specimen. The discrepancy in the loads is attributed to the test set-up, which needs to be improved.

Chapter 5: Summary and Conclusions

5.1 Summary

The research objectives were to conduct experiments which varied the factors that were controlled in the field, such as concrete strength and surface preparation. The bond interface of the FRP-concrete interface is complicated by these factors. Through use of a steel substrate, the effects of the concrete were eliminated and additional information regarding the behavior of the bond interface was found. The steel tests illustrated the increase and decrease in shear stress as the debonding failure of the strip propagated the length of the strip. The critical, or peak shear stress corresponded to the maximum strain limit at which debonding of the strip occurs. The results showed that the shear stress develops in the bond interface and keeps form until total failure of the strip. The failure of the interface was in the adhesive and not the substrate. The results indicate the shear stress develops in the material in the system that is poor in shear, i.e., the adhesive in S1A and S1B. The concrete paste interface in SC1 was the weakest link in the system and the debonding failure occurred in the interface. The results did suggest that a potential limit for debonding could be discerned and provide a benchmark for remotely monitored FRP. The strain limit, however, is affected by other factors, such as concrete strength and surface preparation.

The concrete prism tests demonstrated the effect of surface preparation and concrete strength. Although the results were not definitive, the experiments did reveal a variation in the performance of the FRP due to the different factors. The concrete strength has an effect on the bond interface, adding stiffness to the FRP-concrete bond. The high concrete strength (DBH specimens) created a stiff bond, which caused a premature failure of the FRP-concrete bond at a lower load than the low strength concrete. The various surface preparations all improved bond performance compared with no preparation, and added stiffness to the bond interface. In the lower strength specimens (DBL), the surface preparations improved the bond, while allowing the interface to remain ductile. The ductile bond interfaces allowed the specimen to reach a higher load and strain in the FRP. Overall, the sandblasted surface preparation performed the most consistently, however the ground and needle-scaling surface preparation also performed well.

The significance of the concrete strength in the bond interface is still unknown. The results suggest that the strength of the substrate does improve the total crack width before failure, however the failure of the FRP-concrete bond occurs at a lower strain and load. Additional research is needed to understand the impact of the concrete strength on FRP debonding failure.

Overall, the results presented in this study are in agreement with the results presented in other studies, and consistent with the ACI 440 design guidelines. Prior results also indicated the lack of significant difference in performance between the three concrete surface preparations. The effect of concrete strength on FRP debonding failure still is unclear, however the concrete strength does appear to improve the bond strength, while the increased concrete stiffness may result in a more brittle delamination failure.

The anchorage zone experiments verified that both the wet lay-up and pre-cured FRP anchorage systems could withstand serviceability loads without failure. The experiments, however, were not able to develop the full tensile strength of the material. The installation of both systems was feasible when adequate slot width is provided.

5.2 Conclusions

The experimental study presented in this thesis led to the following conclusions:

- For the two specimens with a FRP-to-steel interface, the maximum strain in the FRP prior to debonding was between 3500 and 4250 microstrain. Initial debonding occurred at a crack width between 0.006 and 0.016 inches.
- For the eight debonding specimens with a FRP-to-concrete interface, the maximum strain limit observed in the FRP prior to debonding was between 2250 and 3500 microstrain. Initial debonding occurred at a crack width between 0.007 and 0.018 inches.
- Sandblasting, grinding and needle gun scaling surface preparations showed no significant difference in the specimen performance.
- The higher strength concrete appeared to lead to a more brittle delamination failure of the DBH specimens.
- The effective bond length prior to initiation of delamination was approximately 6 to 8 inches for all concrete specimens.
- Both the wet lay-up and pre-cured slotted anchorage systems exceeded serviceability loads without failure of the anchorage zone.

5.3 Future Research

Further experiments are needed to establish a strain limit for early detection of debonding and monitoring of the FRP. Repeatable results would create a range of strain limits, based on surface preparation and concrete strength.

Development of a test set-up that was able to fully develop the FRP tensile strength would provide further information on the ultimate failure of the slotted anchorage.

References

ACI (2002), "Guide for the Design and Construction of Externally Bonded FRP Systems for Strengthening Concrete Structures". ACI 440R-02, American Concrete Institute, Farmington Hills, MI.

Alfano, G., Rosati, L, and Simonelli, G. (2005), "Modeling of Failure Mechanisms in RC Beams Retrofitted with FRP in Flexure," VIII International Conference on Computational Plasticity, COMPLAS VIII, CIMNE, Barcelona, 2005.

Arduini, M. and Nanni, A. (1997). "Behavior of Pre-cracked RC Beams Strengthened with Carbon FRP Sheets," *Journal of Composites for Construction*, 1(2), 63-70.

Bizindavyi, L. and Neale, K.W. (1999). "Transfer lengths and Bond Strengths for Composites bonded to Concrete," *Journal of Composites for Construction*, 3(4), 153-160.

Brena, S.F., Benouaich, M.A., Kreger, M.E., and Wood, S.L. (2005). "Fatigue tests of Reinforced Concrete Beams Strengthened using Carbon Fiber-Reinforced Polymer Composites," *ACI Structural Journal*, 102(2), 305-313.

Buyukozturk, O. and Hearing, B. (1998). "Failure behavior of pre-cracked concrete beams retrofitted with FRP," *Journal of Composites for Construction*, 2(3), 138-144.

Chajes, M.J., Januszka, T.F., Mertz, D.R., Thomson Jr., T.A., and Finch, W.W. (1995). "Shear strengthening of reinforced concrete beams using externally applied composite fabrics," *ACI Structural Journal*, 92(3), 295-303.

Chajes, M.J., Finch Jr., W.W., Januska, T.F., and Thomson Jr., T.A.(1996) "Bond and force transfer of composite material plates bonded to concrete," *ACI Structural Journal*, 93(2), 208-217.

Chen, J.F. and Teng, J.G. (2003), “Shear Capacity of Fiber-Reinforced Polymer-Strengthened Reinforced Concrete Beams: Fiber Reinforced Polymer Rupture,” *Journal of Structural Engineering*, 129(5), 615-625.

De Lorenzis, L., Miller, B. and Nanni, A. (2001), “Bond of fiber-reinforced polymer laminates to concrete,” *ACI Materials Journal*, 98(3), 256-264.

Harmon, T.G., Kim, Y.J., Kardos, J. Johnson, T. and Stark, A. (2003).”Bond of Surface mounted fiber reinforced polymer reinforcement for concrete structures,” *ACI Structural Journal*, 100(5), 557-564.

ICRI (1997), “Guide for Selecting and Specifying Materials for Repairs of Concrete Surfaces”. ICRI 03733, International Concrete Repair Institute, Sterling, VA.

Kanakubo, T., Wu, Z., and Ueda, T. (2005), “Influence of Local Bond Characteristics in FRP-Concrete Bond Behavior,” Japan Concrete Institute Technical Committee on Retrofitting Technology for Concrete Structures.

Lau, K.T., Dutta, P.K., Zhou, L.M. and Hui, D. (2001). “Mechanics of bonds in an FRP bonded concrete beam,” *Composites: Part B*, 32, 491-502.

Lee, Y.J. et al. (1999). “Slip modulus of FRP sheets bonded to concrete,” *Journal of Composites for construction*, 3(4), 161-167.

Leung, C.K.Y. (2001).“Delamination failure in concrete beams retrofitted with a bonded plate,” *Journal of Materials in Civil Engineering*, 13(2), 106-113.

Leung, C.K.Y. (2004). “Fracture mechanics of debonding failure in FRP-strengthened concrete beams,” Fracture Mechanics of Concrete Structures, Ia-FraMCos, 41-52.

Nakaba, K., Kanakubo, T. Furuta, T., and Yoshizawa, H. (2001), "Bond behavior between Fiber-reinforced polymer laminates and concrete," *ACI Structural Journal*, 98(3), 359-367.

Oehlers, D.J. and Seracino, R. (2004) Design of FRP and Steel Plated RC Structures: Retrofitting Beams and Slabs for Strength, Stiffness, and Ductility. Elsevier, Amsterdam.

Oehlers, D.J., Liu, I.S.T., and Seracino, R. (2005), "Shear deformation debonding of adhesively bonded plates," *Proceedings of the Institution of Civil Engineers. Structures & Buildings*, 158(SB1), 77-84.

Rasheed, H.A. and Pervaiz, S. (2002), "Bond Slip Analysis of Fiber-Reinforced Polymer-Strengthened Beams," *Journal of Engineering Mechanics*, 128(1), 78-86.

Riggs, H.R., Robertson, I.N., and Park, S.H. (2002), Instrumentation and Monitoring the Performance of the FRP Shear Strengthening of the Salt Lake Boulevard Bridge, Department of Civil and Environmental Engineering, University of Hawaii at Manoa.

Ueda, T. and Dai, J.G. (2005), "Interface bond between FRP sheets and Concrete substrates: properties, numerical modeling and roles in member behaviour," *Prog. Struct. Engng. Mater.,* 7, 27-43.

White, T.W., Soudki, K.A., and Erki, M. (2001), "Response of RC beams strengthened with CFRP laminates and subjected to a high rate of loading," *Journal of Composites for Construction*, 5(3), 153-162.

Wu, Z. and Yin, J. (2003), "Fracturing behaviors of FRP-strengthened concrete structures," *Engineering Fracture Mechanics*, 70, 1339-1355.

Yuan, H., Teng, J.G., Seracino, R., Wu, Z.S., and Yao, J. (2004), "Full-range behavior of FRP-to-concrete bonded joints," *Engineering Structures*, 26, 553-565.

Zhang, H. (2005), Shear Strengthening of Reinforced Concrete Beams using CFRP and Bonding Behavior between CFRP and Concrete, Master's Thesis, University of Hawaii.